東海大学大学院　平成 30 年度博士論文

Vector control of two-phase inverter-fed three-phase induction motor drive
（二相インバータのベクトル制御による三相誘導電動機駆動）

指導　稲森真美子　准教授

東海大学大学院　総合理工学研究科

総合理工学専攻

EKONG UFOT UFOT

Vector control of two-phase inverter-fed three-phase induction motor drive

Ph.D. Dissertation

Graduate School of Science and Technology
Tokai University

Supervisor Associate Professor Mamiko Inamori

EKONG UFOT UFOT

2018

Abstract

In recent years, advances in power electronics have led to an increase of three-phase motor drive systems controlled by three-phase inverters. However, a fault in the inverter results in a shutdown of the motor drive system. In specific applications such as electric vehicles, the inverter failure leads to a loss of the vehicle's propulsion ability, causing safety issues like traffic accidents and many other consequences. Therefore, there is a need for emergency strategies for inverter failure in electric vehicles. In this dissertation, a two-phase inverter is presented as an emergency strategy for inverter failure in motor drive systems.

The conventional three-phase inverter composes of six switching devices and has three-phase outputs. On the other hand, the two-phase inverter composes of four switching devices and also has three-phase outputs. For this reason, over the years, research has been conducted on two-phase inverters as low-cost inverters to drive three-phase motors. However, from their working principle, two-phase inverters have a low voltage utilization factor (ratio of output voltage to power supply voltage), thus, they cannot be utilized in applications that efficiency is essential such as home appliances. Nevertheless, research continued on the application of two-phase inverters as an emergency strategy for inverter failure.

In this emergency strategy, when one-leg of the three-phase inverter fails, the two-phase inverter is configured from the remaining healthy two-legs of the three-phase inverter. Regarding implementation, when inverter failure occurs, the wiring of the damaged phase is disconnected and reconnected to the neutral point of the DC power source, and by changing the control software, the two-phase inverter can drive the three-phase motor. In the emergency strategy, although the maximum speed and output of the motor reduce, the electric vehicle can propel, and move to a safe place or back home.

In the present research, a new vector control method is proposed for the two-phase inverter which is an emergency strategy for inverter failure in motor drive systems. This dissertation focuses on the enhancement of the vector control method of two-phase inverter-fed induction motor drives and improvements on the motors operating performance. The reported works on the vector-controlled two-phase inverter-fed AC motor drives derived the output voltage references by subtraction from the output voltage references of the conventional three-phase inverter. This subtraction method has some disadvantages. These disadvantages are slow speed response, unbalanced motor currents, and difficulty in implementation of two-phase inverters as an emergency drive for the conventional three-phase inverter. In terms of implementation, depending on the inverter phase U, V, or W that a fault occurs, the subtraction procedure to derive the output voltage references for the two-phase inverter is different. Hence, three different subtraction programs must be prepared.

In this dissertation, a transformation matrix that can instantaneously derive the output voltage references for vector-controlled two-phase inverters is proposed. The power invariance of the proposed transformation matrix is verified, which indicate that it can be used in motor control. The proposed transformation matrix is applicable irrespective of the damaged inverter phase U, V, or W of the three-phase inverter that fails. The effectiveness of the proposed transformation matrix to derive voltage references for vector-controlled two-phase inverter-fed AC motor drives is verified by simulation and experiment. The results showed that the instantaneous generation of voltage references and instantaneous speed response is achievable using the proposed transformation matrix

A comparison of the performance characteristics of both the vector-controlled two-phase and three-phase inverter-fed induction motor drives was performed. The results showed that the torque-speed characteristics, maximum output voltage and motor efficiency of the two-phase inverter drive reduces. Furthermore, a comparison between the experimental results of the vector-controlled two-phase inverter-fed induction

motor drive using the proposed transformation matrix and the previous method in literature was performed. From the results, it is clear that although both methods can generate the required output voltages, better torque-speed characteristics, three-phase motor current, and higher motor efficiency were obtained using the proposed transformation matrix.

In the conventional three-phase inverter-fed induction motor drive, the output voltage reaches its limit at a certain speed which is called the base speed. Above this base speed, the flux of the induction motor cannot be controlled as a constant, which leads to a loss of current control and eventually low performance in the high-speed region. In the conventional three-phase inverter-fed induction motor drive, a method to improve the performance of the drive in the high-speed region is to apply a field weakening control strategy. However, in the two-phase inverter-fed induction motor drive, because the base speed and maximum utilizable voltage are different, the conventional field weakening control strategy for three-phase inverter-fed induction motor drives cannot be directly applied.

Therefore, in this dissertation, a field weakening control strategy was proposed for two-phase inverter-fed induction motor drives. The proposed field weakening control enables precise current control in the high-speed region. The effectiveness of the proposed field weakening control was verified by simulation and experiment. The results showed that by applying the proposed field weakening control, the torque-speed characteristics, motor efficiency, and overall performance are improved in the high-speed region.

In this dissertation, a transformation matrix is proposed to generate voltage references and facilitate easy implementation of the vector-controlled two-phase inverter as an emergency strategy. Furthermore, a field weakening control strategy is proposed to improve the performance of the two-phase inverter-fed induction motor drive in the high-speed region.

The progress achieved in the dissertation will enable further developments in the application of vector-controlled two-phase inverter as an emergency drive for the conventional three-phase inverter-fed induction motor used in electric vehicles and other AC motor drives.

Acknowledgments

First and foremost, I would like to express my sincere gratitude to my wife and children who have endured through this latter part of the struggle to fulfill this goal. I would also like to express gratitude to Prof. Masayuki Morimoto, for his support that he has given in the last five years under his tutorage. In this period, I have grown from a teenager to a man, I could not have wished or hoped for a better experience. Many Thanks to my supervisor from Ph.D. degree, Associate Prof. Mamiko Inamori, for all the support, encouragement and advice.

My sincerest appreciation to the rest of my dissertation committee, Prof. Kiyoteru Kobayashi, Prof. Kunio Okimura, Prof. Shigeru Yamaguchi and Prof. Yukihiko Sato for their valuable comments, advice, and guidance that has shaped and improved this dissertation.

Sincerely, I am grateful to all the lecturers at the Japanese language school of Tokai University, for they are the foundation of all the successes I have achieved since I arrived in Japan. Indeed, a ten years' journey that started on a good foundation. My profound gratitude to all the scholarship organizations that supported along this journey. Rotary Yoneyama scholarship, Japan Gas Cooperation (JGC), Honjo international scholarship foundation, Japan Student Services Organisation (JASSO), Akwa Ibom State Government (AKSG) and Tokai University. Your support was the catalyst to all my achievements.

I am grateful to all the 12 students that I researched with in the last five years, I specifically thank Mr. Tomoyuki Nakade and Mr.Takuya Shirashi for being the best team players in the last three years. I also like to express my gratitude to Mr. Hisashi Yoneoka for his advice and assistance on our experimental apparatus, your depth of knowledge in electrical equipment's was more than helpful to me but an exciting relationship. I thank all the staff of Tokai University who have assisted me in one way or the other in the last ten years.

Many thanks to all my friends, acquaintances, comrades, Shibusawa Presbyterian Church, Akwa cross association Japan, Nigerian Embassy Tokyo, Nigerian Union Japan, Chigasaki-cyuo rotary club, McDonald's staffs, and my in-laws for all their support.

Finally, I thank my mother and siblings for pushing to achieve this childhood dream, even when I considered quitting because the struggle was more than I could ever imagine. Your prayers, support, and encouragement have always kept me going.

Contents

List of Tables

List of Figures

List of Abbreviations

Abbreviation	Description
DC	Direct Current
AC	Alternating Current
VFD	Variable Frequency Drives
VSD	Variable Speed Drives
ASD	Adjustable Speed Drives
IM	Induction Motor
OC	Over Current
OV	Over Voltage
CW	Clockwise
CCW	Counter Clock Wise
PWM	Pulse Width Modulation
DSP	Digital Signal Processor
AD	Analog Digital
SPWM	Sinusoidal Pulse Width Modulation
SVPWM	Space Vector Pulse Width Modulation
VVVF	Variable Voltage Variable Frequency
IGBT	Insulated Gate Bipolar Transistor
DCG	Direct Current Generator
TS	Torque Sensor
FW	Field Weakening
EMF	Electromotive Force
CT	Constant flux
PI	Proportional Integral
FOC	Field Oriented Control
IFOC	Indirect Field Oriented Control
E	Identity Matrix

List of Symbols

Symbol	Description
V_{dc}	DC power voltage
V_{smax}	Maximum voltage of inverter
I_{smax}	Maximum current of inverter
I_{rated}	Rated current of the motor
ω_{base}	Base speed of three-phase inverter-fed motor drive
$\omega_{base[Two\text{-}phase]}$	Base speed of two-phase inverter-fed motor drive
ω_{rated}	Rated speed of the motor
ω_{smax}	Maximum slip
ω_s	Slip frequency
ω_r	Rotor speed
$I_{smax[FW]}$	Maximum current for field weakening in region 2
I_a	Armature current
I_f	Machine field current
I_d	Flux component current
I_q	Torque component current
L_m	Magnetizing inductance
R'_1	Stator resistance
L'_1	Stator leakage inductance
R'_2	Rotor resistance
L'_2	Rotor leakage inductance
P	Poles of motor
φ	Magnetizing flux
θ	Rotor angle
T_r	Rotor time constant
V_d^*, V_q^*	Voltage references in dq axis
V_α^*, V_β^*	Voltage references in αβ axis
V_A^*, V_B^*	Voltage references for two-phase inverter
I_u, I_v, I_w	Three-phase motor current
V_u, V_v, V_w	Motor terminal voltage
V_{un}, V_{vn}, V_{wn}	Phase voltage of three-phase load

Chapter 1

Introduction

1.1 Inverters and their applications

Inverters are devices that convert Direct Current (DC) to Alternating Current (AC). Depending on their application, the function of inverters may differ, from supplying of constant AC power, varying of the frequency of AC power, to precise control of speed and torque of electric motors. Inverters are widely used from home appliances to industrial applications. Inverters play an essential role in our everyday lives because they drive most of the equipment we need for business and pleasure. Examples of home appliances are washing machines, refrigerators, air conditioners and so on as shown in Fig. 1.1. Examples of industrial applications are Variable Frequency Drives (VFD), pump motors, trains, electric cars and so on [(1)-(3)].

Industrial motor applications have been reported to consume more than 50% of all the energy produced in the world [(4)-(6)]. However, industrial motors driven by inverters reduce the energy consumption of the systems. Although inverters may not be easily seen on the outer components of home appliances or industrial equipment, they play a vital role in our society.

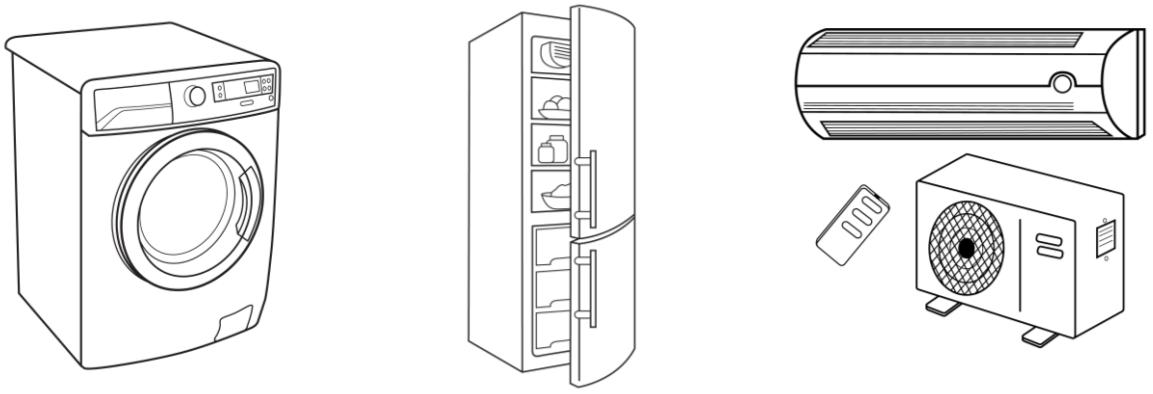

Fig. 1.1 Home appliances

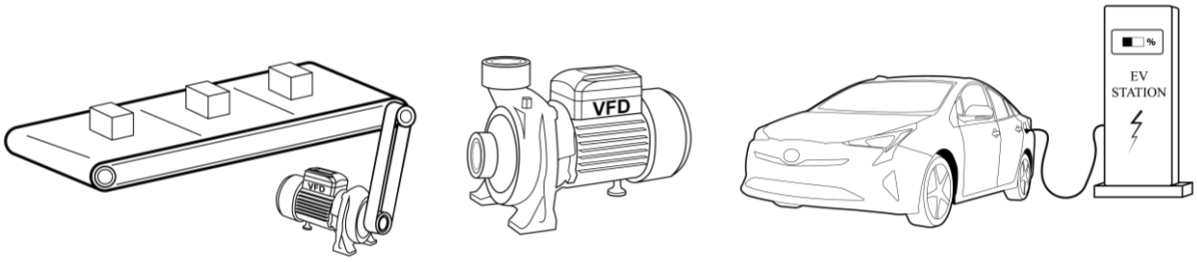

Fig. 1.2 Industrial applications

1.2 Inverter-fed AC motor drives

Inverter-fed AC motor drives can be explained as a system where the inverter is the controller or driver of the motor. Inverter-fed AC motors are used in many industries like textile, steel, oil and gas, electric vehicles and many more [7]-[9]. These inverter-fed motor drives are used in ratings from tens up to hundreds of kilowatts.

Without inverters, much energy is wasted which is not good for business. Furthermore, apart from inverters, there is no other method today that provides efficient control of AC motors, which are responsible for more than 50% of the power consumption in industry [10]-[12]. In order to reduce energy waste and consumption, the speed and torque of the motor should match what is required by the process/application. Using inverters is also the best method to improve productivity and reduce maintenance costs of motor drives. Inverter-fed AC motor drives are also called AC drives, VFD, Variable Speed Drives (VSD), inverter drives and Adjustable Speed Drives (ASD).

There are two types of AC motors, induction motors (asynchronous) and synchronous motors. Induction motors are more widely used in various industrial applications because of its ruggedness, cost, low maintenance and reliability [13]. Furthermore, compared to other motors, induction motors can be used in a volatile environment and aggressive industrial processes because they have no problems with spark and corrosion.

The schematic of the inverter-fed AC motor drive system is shown in Fig. 1.3. In this example, the main power supply is an AC source, thus, using a rectifier AC is converted to DC which is fed to the inverter. However, in applications like electric vehicles where the power source is a DC source, the rectifier is eliminated. The structure of the conventional three-phase inverter which is the most commonly used inverter is shown in Fig. 1.4. The three-phase inverter consists of three-legs and six semiconductor switching devices and one-leg for each phase is connected to the motor.

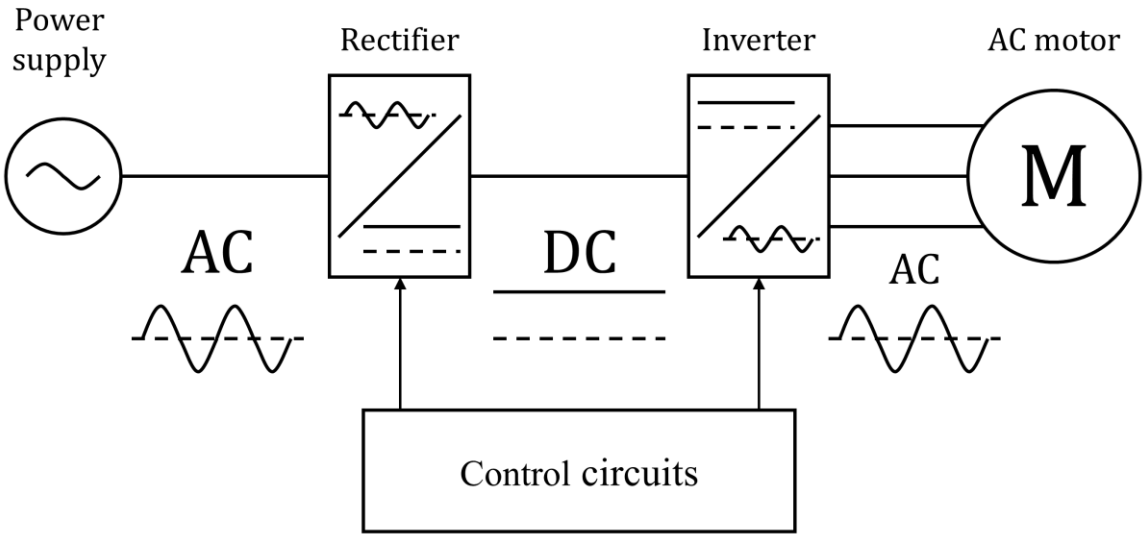

Fig. 1.3 Inverter-fed motor drive

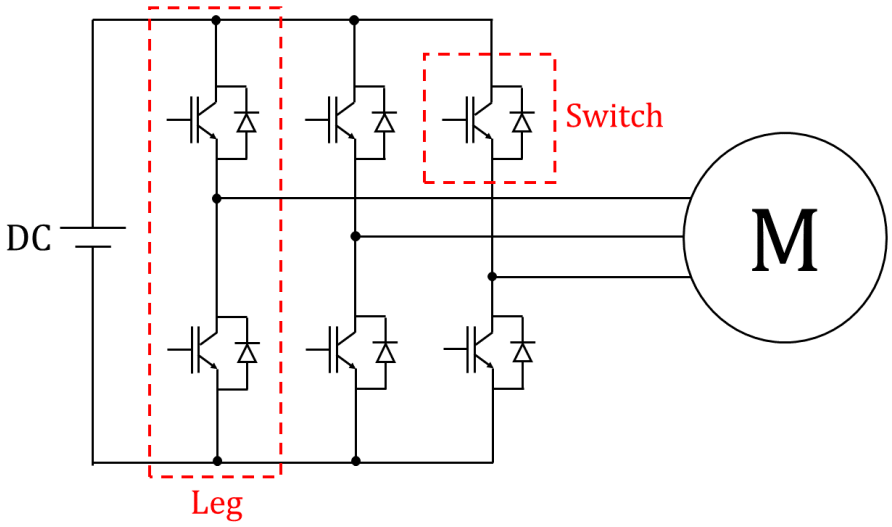

Fig. 1.4 Structure of three-phase inverter-fed induction motor drive

1.3 Emergency and fault-tolerant strategies for three-phase inverter-fed motor drives

A fault or failure of components of the inverters results in shutdown in operation of the drive. In industrial applications like conveyor systems, electric trains and vehicles and so on, a stop in operation due to inverter failure can lead to economic losses, traffic accidents, and many other consequences [14][15]. The use of inverter-fed AC motor drives in various applications is increasing daily [16]. Hence, research on emergency and fault-tolerant strategies for inverter-fed motor drives has gained much attention over the years. This dissertation focuses on the utilization of a two-phase inverter as an emergency strategy for inverter failure.

1.3.1 Category of faults in inverters

The faults and the causes of failure in power electronics inverters can be classified into four levels as shown in Fig. 1.5 [14] [17]. 1) Switch-level; 2) Leg-level; 3) Module-level; 4) System-level. Many emergency strategies have been proposed for these different fault levels in inverters [18]-[25]. Reported works and surveys on faults in inverters showed that switch-level failure is the most common and rampant [26]. Furthermore, the main reason for switch-level failure is a breakdown of semiconductor switches used in the inverters. [14] [27].

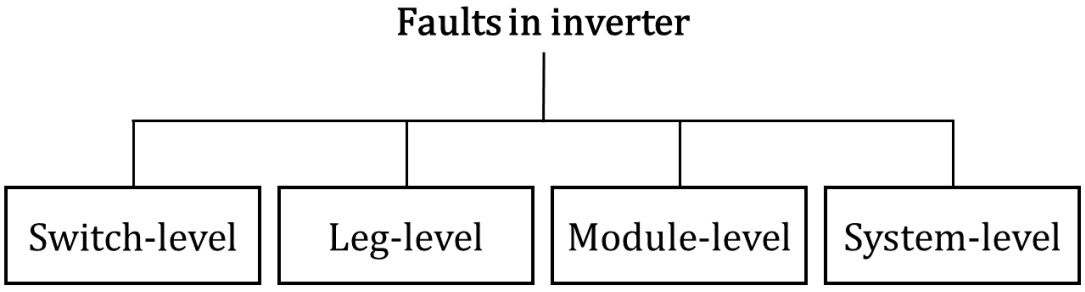

Fig. 1.5 Category of faults in power electronic inverters [14]

A general survey on the causes of inverter failure irrespective of fault level reported that 38% of inverter failures are caused by damages in semiconductors [28]. Thus, there is a need for emergency strategies for switch-level failure in inverter-fed motor drives. Moreover, when the switch of the inverter fails, one-leg (phase) of the inverter is lost, and the operation of the entire drive stops. Therefore, the failure of the switch can also be said to be a leg-level failure or system-level failure.

1.3.2 Life span and reliability of semiconductor switches

As explained in the previous section, faults in semiconductor switches are the main reasons for the breakdown of inverter-fed motor drives. In this section, the reliability and lifespan of the semiconductor switches used in inverters are discussed. The failure rate of semiconductor switches used in inverters can be expressed using the bathtub curve shown in Fig. 1.6 [29]-[31]. The failure rate of semiconductor switches can be classified into three periods: the initial failure period, the random failure period and wear out failure period. Figure 1.6 shows that the failure rate of semiconductor switches used in inverters is high in the initial failure period and the wear out failure period.

Initial failure or early failure could be as a result of incompatibility between the inverter and its load or wrong connections during installation. Random failure is mostly caused by external factors, conditions of usage such as Over Current (OC) and Over Voltage (OV). Wear out failure occurs after many hours or years of usage.

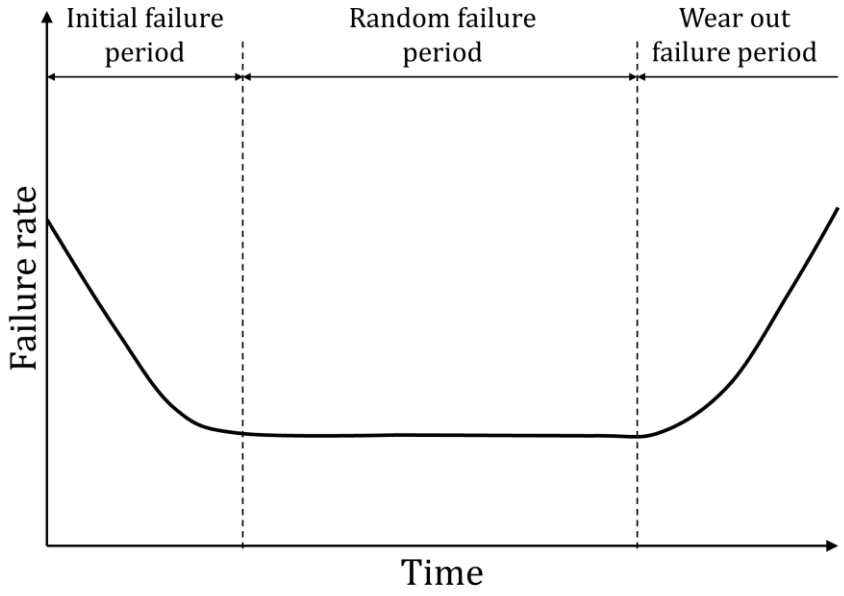

Fig. 1.6 Failure rate of semiconductor switches vs. time

1.3.3 Emergency and fault-tolerant strategies for switch-level failure

There are three main emergency strategies for switch-level faults in inverter-fed motor drives as shown in Fig. 1.7. 1) **Redundant switching state** method which can only be applied to multilevel inverters that have additional switches, due to their structure. In addition, this method can only be implemented using space vector modulation technique [32]-[36]. 2) **DC-bus midpoint connection** method where the phase of the damaged switch is reconnected to the midpoint of the DC source [37]-[40]. 3) **Redundant series or parallel switch** method where extra switches are placed in parallel to the main switches and are used to replace faulty switches when a switch-level failure occurs [41].

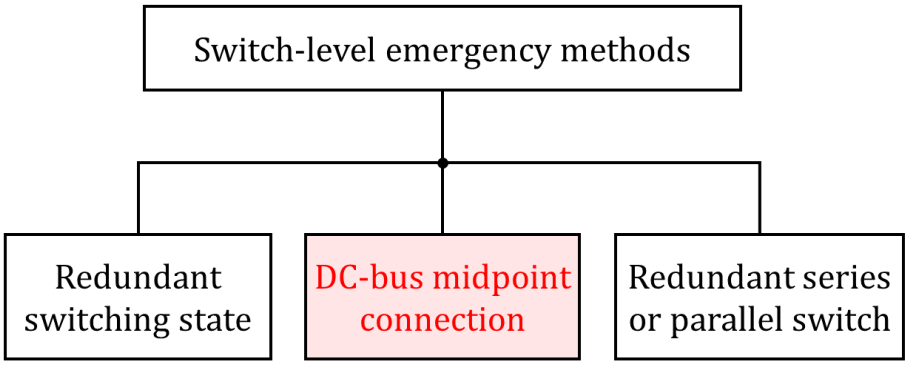

Fig. 1.7 Emergency methods for switch-level faults

In terms of cost and implementation, the DC-bus midpoint connection method is the most feasible as an emergency strategy because it does not require any additional component or complex algorithms to facilitate its application [42]. In the DC-bus midpoint method, when a fault occurs in the inverter, the faulty switch or leg is identified, and the wiring from the motor to that phase is disconnected and reconnected to the midpoint of the DC power source. After this reconnection, the inverter consists of only four switches. Hence, this topology is also called four-switch three-phase inverter, four-switch inverter, two-leg inverter, and two-phase inverter.

1.4 Two-phase inverter

1.4.1 Two-phase inverter as an emergency strategy

In this dissertation, the utilization of two-phase inverter as an emergency strategy for the conventional three-phase inverter-fed motor drive is presented. This emergency strategy can be utilized in several types of inverter-fed motor drives applications like electric vehicles, conveyor drives, pump motor drives and so on.

As earlier explained in this chapter, inverter failure is often caused by faults in switches or one-leg of the inverter. When a switch or leg failure occurs in inverter-fed motor drives, the entire operation of the drive stops. In this situation, the two-phase inverter can be constructed with a circuit modification to enable its application as an emergency strategy. First, the damaged phase of the inverter is identified and the wiring to the damaged phase is removed and reconnected to the midpoint of the DC source. With this simple re-wiring, the hardware of the two-phase inverter can be constructed.

Figure 1.8 shows the *V*-phase of the inverter drive is damaged, here the wiring to the *V*-phase is disconnected from point ① and is reconnected to point ②, which is the midpoint/neutral of the DC source. The control software is then changed and the constructed two-phase inverter can drive the three-phase motor. The advantage of this emergency strategy is no additional components or parts are required, only a change in the circuit wiring and control software enables the application of the two-phase inverter as an emergency strategy.

Therefore, the two-phase inverter can be said to be an effective emergency strategy for the conventional three-phase inverter drive because of its simplicity in construction.

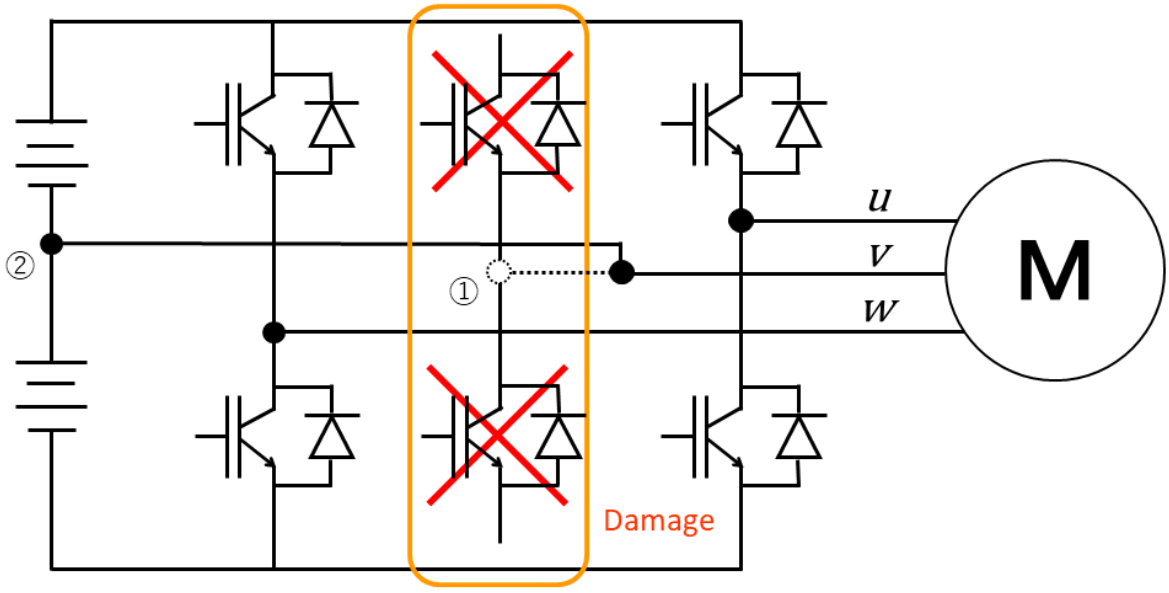

Fig. 1.8 Implementation process of two-phase inverter as an emergency drive

1.4.2 Structure of two-phase inverter

The circuit of the two-phase inverter-fed motor drive is shown in Fig. 1.9. The two-phase inverter consists of four switches also known as two-legs. For comparison, the circuit of the three-phase inverter is shown in Fig. 1.10. It can be seen that the number of switching devices in the two-phase inverter are less than that of the conventional three-phase inverter. In order to supply power from the two-phase inverter to a three-phase load (motor), the wiring of one-phase of the motor is connected to the midpoint of the DC source as shown in Fig. 1.9.

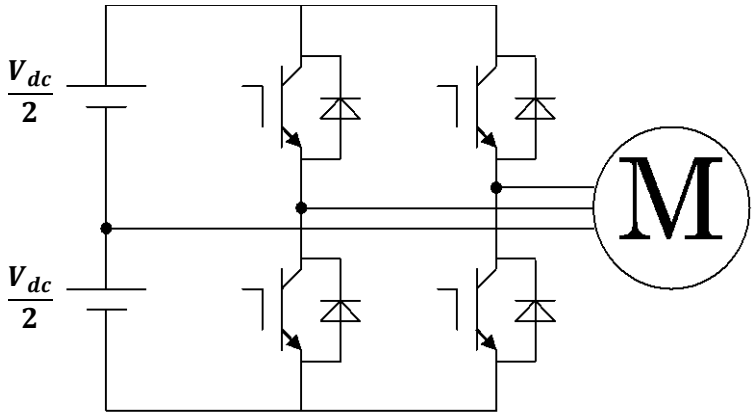

Fig. 1.9 Two-phase inverter-fed motor drive

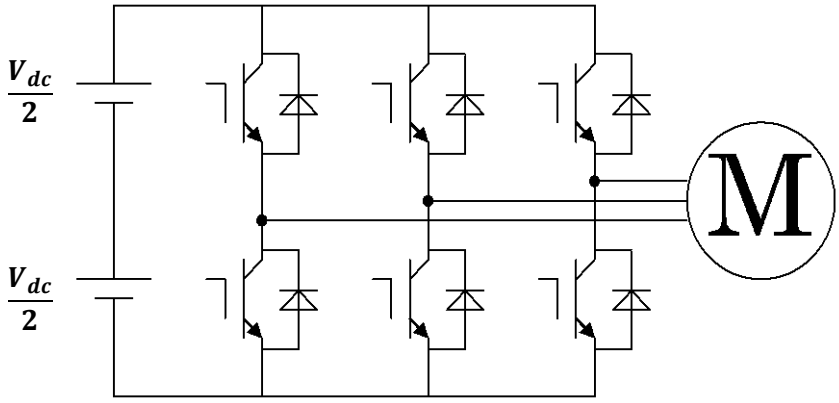

Fig. 1.10 Three-phase inverter-fed motor drive

1.4.3 Working principle of two-phase inverter

The working principle of the two-phase inverter-fed AC motor drive can be described using Fig. 1.11. Figure 1.11 shows a two-phase power supply connected to a three-phase load. V_A and V_B are AC power sources that have a phase difference of $\pi/3$ as given by equation (1.1). When two-phase power supply voltages V_A and V_B are applied to the three-phase load, three-phase balanced voltages, V_{un}, $V_{vn,}$ and V_{wn}, are

generated as shown in equation (1.2). Therefore, it can be seen that a two-phase AC power supply with a phase difference of π/3 can drive the three-phase AC motor. This is the basic working principle of the two-phase inverter-fed three-phase AC motor drive. However, it is important to note that the three-phase balanced voltages reduce by a factor of $1/\sqrt{3}$. This reduction in the phase voltage indicates that the maximum output of the two-phase inverter reduces compared to the conventional three-phase inverter drive. The details on derivation procedure of equation (1.2) is written in Appendix A.

Furthermore, as shown in Fig. 1.12, if the direction of the two-phase power supply (V_A ,V_B) is reversed, the rotating direction of the three-phase voltage is reserved.

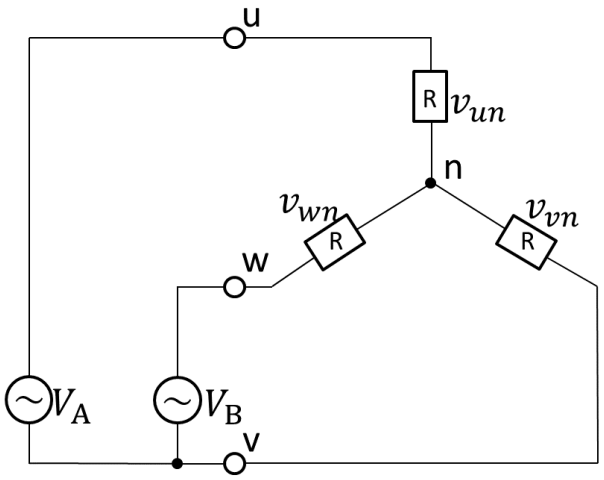

Fig. 1.11 Two-phase power circuit

$$V_A = V \cdot \sin \omega t$$
$$V_B = V \cdot \sin\left(\omega t + \frac{\pi}{3}\right) \tag{1.1}$$

$$V_{un} = \frac{1}{\sqrt{3}} V \cdot \sin\left(\omega t + \frac{\pi}{2}\right)$$
$$V_{vn} = \frac{1}{\sqrt{3}} V \cdot \sin\left(\omega t - \frac{\pi}{6}\right)$$
$$V_{wn} = \frac{1}{\sqrt{3}} V \cdot \sin\left(\omega t - \frac{5\pi}{6}\right) \tag{1.2}$$

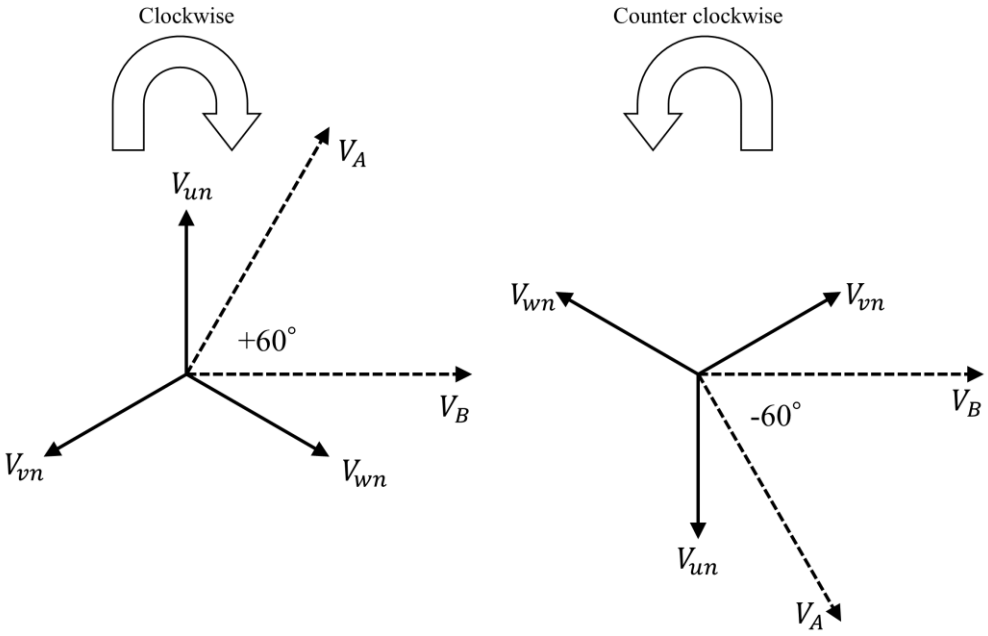

Fig. 1.12 Phasor diagram of three-phase voltage

1.4.4 Control methods of inverter-fed AC motor drives

In the conventional three-phase inverter-fed induction motor drive, there are several control methods. These control methods can be categorized into scalar and vector control methods [43] - [45]. The scalar method is a well-known control method used for applications that do not require full torque at starting or low-speed region such as fans, blowers and so on. Vector control is used in applications where full torque or rated torque is required from zero speed and precise control of speed and torque is required such as electric vehicles, spindle drives and so on.

These control methods can also be utilized in the two-phase inverter-fed AC motor drives. However, two-phase output voltage references that have a phase difference of π/3 are required.

1.5 Earlier reported literature on two-phase inverter

In this section, an overview of the earlier reported literature on the two-phase inverter-fed motor drive, using various control strategies and their results are discussed. This review focuses on factors that determine the performance of inverter-fed induction motor drives. Furthermore, some challenges of the two-phase inverter drive and their proposed compensation methods are discussed.

1.5.1 Maximum output voltage

In the conventional three-phase inverter-fed motor drive, depending on the control strategy and the adopted Pulse Width Modulation (PWM) strategy, the maximum utilizable voltage of the drive differs. However, this difference is between 5 to10 percent of the maximum available voltage.

Previous literature reported that the voltage utilization factor of the two-phase inverter-fed induction motor drive compared to the conventional three-phase inverter reduces by approximately 50% [(46)-(49)]. As shown in Fig. 1.13, in the low-speed region, the output voltage of both the two-phase and three-phase inverter-fed motor drives are similar. However, the maximum output voltage of the two-phase inverter drive is attained at a lower speed compared to the three-phase inverter drive. This implies that the two-phase inverter drive experiences some challenges in the high-speed region because of a reduction of voltage that can be utilized irrespective of the adopted PWM strategy [(47)(48)].

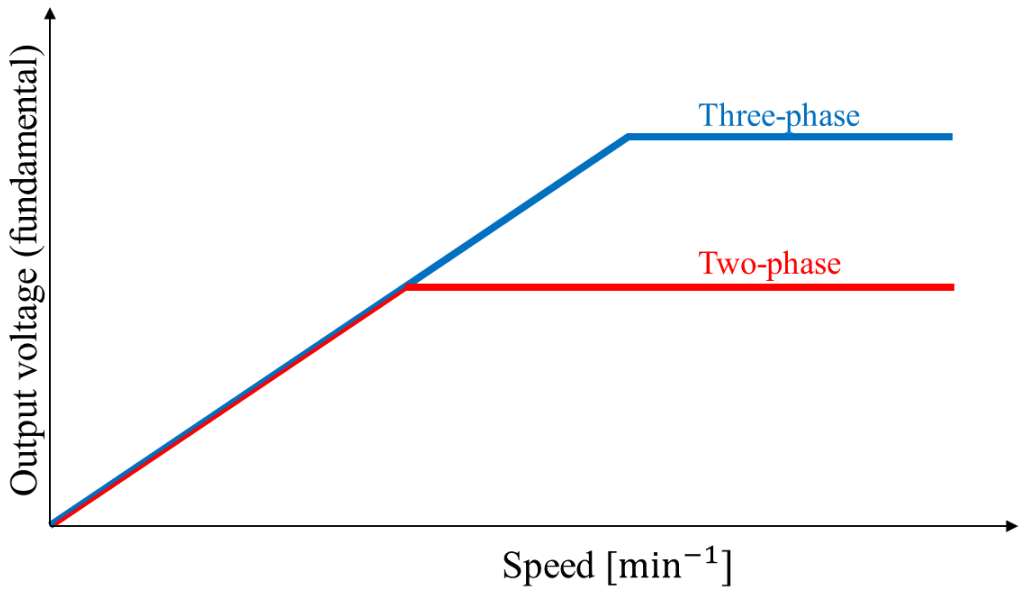

Fig. 1.13 Maximum output voltage

1.5.2 Torque-speed characteristics

The torque-speed characteristics of the inverter-fed induction motor drive is one of the main criteria that determines the type of application where the drive can be utilized. In the conventional three-phase inverter-fed motor drive, the rated torque of the motor can be achieved up to its rated speed and above reduces inversely. Maximum output voltage of the drive is one of the main factors that affect the torque-speed characteristics of the drive. As explained in section 1.5.1, the maximum output voltage of two-phase inverter drives is low. For this reason, the torque-speed characteristics of the two-phase inverter drive differ similarly to the conventional three-phase inverter drive.

Earlier reported literature showed the reduction of the maximum output voltage of the two-phase inverter drive has an adverse effect the torque-speed characteristics compared to the three-phase inverter drive [51]-[55]. Ishikawa *et al.* investigated the torque-speed characteristics of the two-phase inverter-fed induction motor drive using the Variable Voltage Variable Frequency (VVVF) control method. For comparison purposes, they conducted the same experiment on the three-phase inverter drive. Their results showed the maximum torque attainable speed and the maximum speed of the two-phase inverter drive reduced [49].

Figure 1.14 shows the comparison of the torque-speed characteristics. Ishikawa *et al.* further insisted that although the two-phase inverter drive experiences a reduction in performance characteristics, it is good enough for an emergency operation after inverter failure [49]. Furthermore, in the VVVF control strategy, because voltage and frequency are the controllable variables when the voltage reaches its maximum output value in the two-phase inverter, the current is not enough to drive the motor. Hence, the maximum attainable speed also reduces.

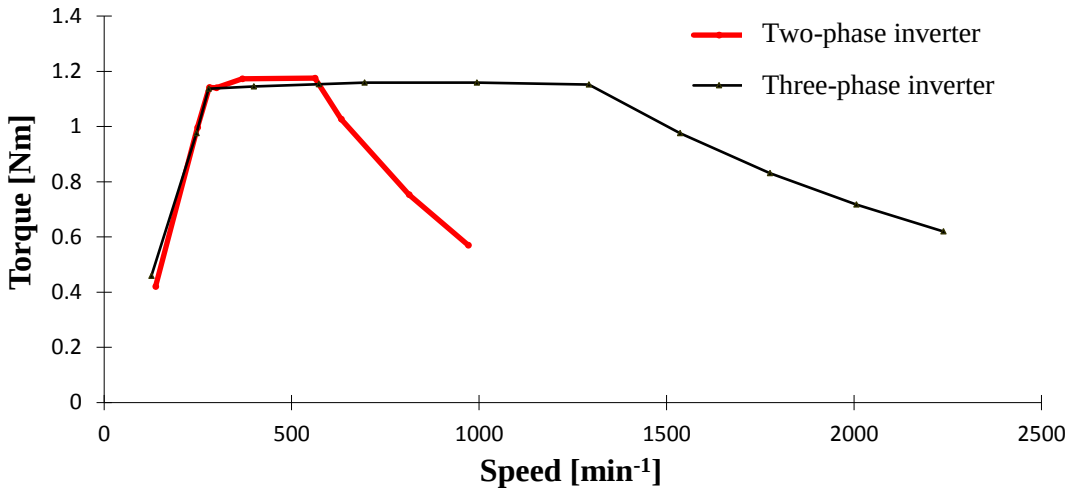

Fig. 1.14 Comparison of speed-torque characteristics (two-phase vs. three-phase) [46]

1.5.3 Thermal behavior and performance

Thermal performance of the inverter-fed AC motor drive is a feature that must be considered when designing drives for specific applications. Overheating of motors and components of the inverter may increase the possibility of failure of the entire drive. Furthermore, there is a need to study and verify the thermal behavior of the three-phase motor driven by the two-phase inverter.

Mendes *et al.* performed an investigation on the thermal performance of the two-phase inverter-fed induction motor drive by focusing on the temperature rise [50]. They applied the two-phase inverter as an emergency strategy and also conducted the same experiment on the conventional three-phase inverter drive. Their results showed that the stator temperature of the motor and overall thermal behavior of the two-phase and three-phase inverters were similar. Furthermore, they concluded that as far as the motor's thermal characteristics are concerned, there is no need to reinforce the motor insulation properties to protect the motor or increase heat dissipation techniques when the motor is driven by two-phase inverters.

1.5.4 Voltage imbalance and current ripple compensations

As earlier explained in section 1.4, one-phase of the motor is connected to the midpoint of the DC source in the two-phase inverter. In most cases, in order to achieve the neutral/midpoint, two capacitors of the same capacity are used to split the DC source into two voltage sources as shown in Fig. 1.15. Hence, the current from the motor flows through the capacitors (C_1, C_2). This connection causes fluctuation in the voltage of the two capacitors (C_1, C_2). This fluctuation leads to imbalance in the output voltage and the motor phase currents and increases the motor current and torque ripples [51]-[65].

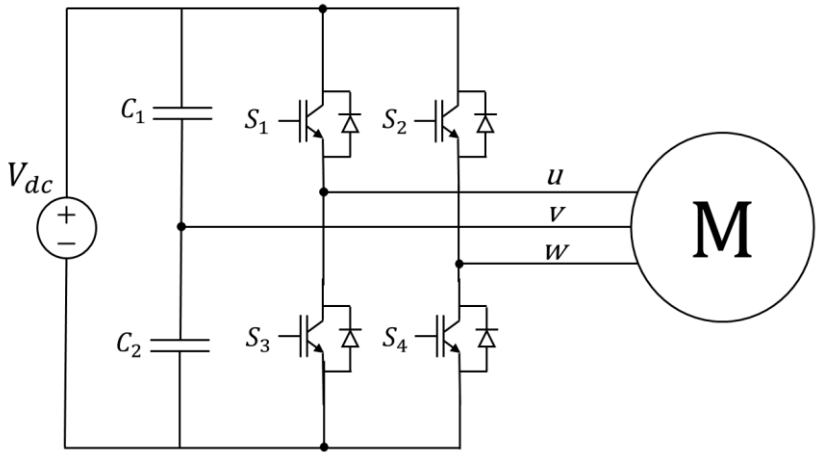

Fig. 1.15 Two-phase inverter-fed motor drive

In order to correct the voltage fluctuations and current imbalances, several methods and topologies have been proposed using both scalar and vector control strategies [54]-[65]. These methods can be classified into two categories; (i) PWM techniques (ii) Voltage and current compensation schemes.

(i) **PWM techniques** involve compensation methods using space vector PWM methods and new PWM techniques [51]-[60]. Some of these strategies focused on selecting the appropriate switching time and periods, while others focused on modulation techniques. Broeck and Wyk proposed an asymmetric pulse width modulation [46], Blaabjerg *et al.* proposed three kinds of space vector modulation techniques that made the voltage vector track a desired circular trajectory and a voltage error compensation [52].

(ii) **Voltage and current compensation schemes** involve the use of a feedback control loop of either voltage or current into the control circuit. These feedback values are compared with their ideal values and their errors are processed by PI controllers. The outputs are then applied to proposed algorithms for compensations and finally added to the output voltage references [61]-[64]. J.Kim *et al.* investigated the main reason that caused the imbalance of the motor current, and their investigation showed that the source impedance and the voltage fluctuation from the capacitors were the two main reasons [47]. They proposed a compensation method based on their analysis, and their results showed that the motor current imbalance was eradicated and the compensation control was effective in the low-speed region of the two-phase inverter-fed induction motor drive.

The voltage and current compensation methods are seen to be more effective compared to the proposed PWM techniques because they can be applied to more control strategies (VVVF, vector control, direct torque control, and so on) used in the inverter-fed motor drives. Furthermore, most of the proposed space vector PWM methods are complicated in terms of calculation and implementation.

In addition, Matsuse *et al*. investigated and reported that by increasing the capacity of the capacitor used, the voltage fluctuation could be reduced [65]. There are several proposed methods to eradicate the voltage fluctuation and current imbalance in the two-phase inverter-fed motor drive. It is necessary to investigate which method best fits the control strategy adopted for the two-phase inverter.

1.5.5 Motor efficiency and loss

The motor efficiency of the two-phase inverter-fed induction motor has earlier been examined and evaluated [66]. Ishikawa *et al*. performed experiments on both the two-phase and three-phase inverter-fed induction motor drives using VVVF control strategy [66]. They evaluated the motor efficiency using a motor efficiency map, their results showed that the efficiency of the motor driven by both the two-phase and three-phase inverters was the same in the low-speed region [66]. It is important to note that in this region the voltage and speed had not yet reached its maximum output value.

The motor loss of the two-phase inverter-fed induction motor drive has also been investigated [67]. Ma *et al.* measured the motor loss at no-load and load conditions. They further analyzed the losses of each phase of the motor into copper loss and iron core loss and their results showed the copper losses were balanced but the iron core losses were unbalanced [67]. Finally, Ma *et al.* compared the total losses of the two-phase and three-phase inverter-fed motor drive and concluded that the losses of both the two-phase and three-phase inverter drives were the same in the low-speed region but different in the middle-speed region.

1.5.6 Inverter efficiency

Low inverter efficiency leads to a waste of energy and an increase in the probability of inverter failure. Inverter efficiency is usually calculated as the ratio of the input DC power and to the inverter output power.

The efficiency of the two-phase inverter-fed induction motor drive has been investigated. Ishikawa *et al.* conducted the same experiment on both the two-phase and three-phase inverter-fed induction motor drives. In their experiment, the speed was set a constant (approximately 780 min^{-1}), and the load was increased from its minimum value to its maximum value. Their evaluation results showed that regardless of the magnitude of the load, the efficiency of the two-phase and three-phase inverter drive was similar. They further added that there is no problem concerning the heat generation and dissipation of the two-phase inverter drive.

1.6 Vector control of AC motor drives

1.6.1 History and principles

Over the years, due to advances in power electronics, the utilization of inverter-fed AC motor drives in industrial applications has increased. However, in the past, DC motor drives dominated AC motor drives in industrial applications because of their ability to smoothly vary speed over a wide range, generate full torque from zero speed, and achieve high dynamic performance [68] [69].

In terms of motor comparison, AC motors have some advantages over DC motors like reliability, low maintenance and cost and so on. These advantages prompted continual attempts to find better control strategies for AC motors [70]. The advent of vector control in the early 1970s was a breakthrough for AC motors. Vector control opened avenues and opportunities for AC drives to be a competitive alternative to DC drives [71][72]. Vector control enables AC motor drives to precisely control speed and torque from zero speed to high-speed regions and to attain energy efficient operations at all speeds and fast dynamic response [73][74].

Vector control was invented in the early 1970s by K.Hasse and Siemens' Blaschke [75]. Vector control is also known as field oriented control because of its structure. Initially, vector control was implemented using several observer and sensors to feedback signals and values needed for the field orientation technique. Soon after, field orientation techniques with slip frequency that does not require flux sensors called indirect vector control or indirect field orientation control were developed. Since then, various methods and types of vector control that improved the original idea have been suggested and published as shown in Fig.1.16.

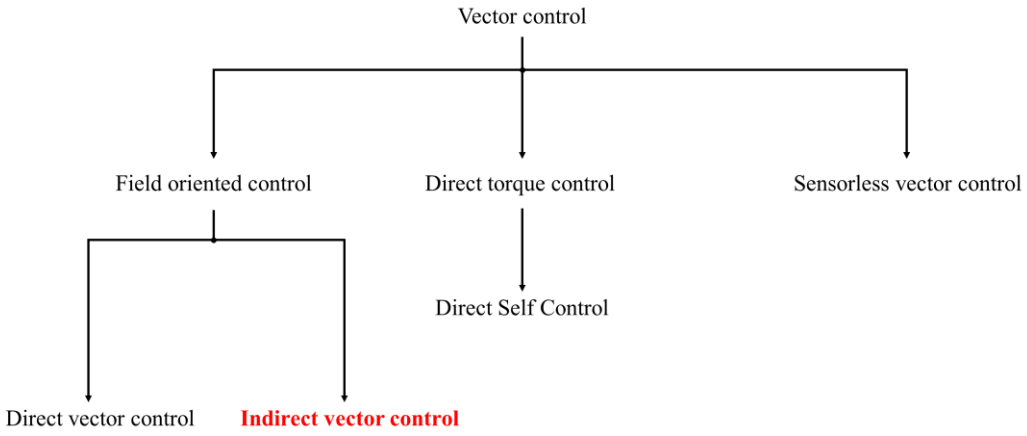

Fig. 1.16 Vector control methods of AC motor drives

The principle of vector control can be explained from the torque generation and control of a DC motor. The torque generation mechanism of a DC motor is shown in Fig. 1.17 (a). As shown in Fig. 1.17 (a), the armature current I_a and the field current I_f of the DC motor are orthogonal. This implies that the currents are decoupled in nature and can be controlled separately. Here, the magnetic flux is generated by the field current I_f and the armature flux is generated by the armature current I_a. Force is generated and the motor rotates. The torque of the DC motor has a relation of $T = K_T I_f I_a$. The torque can be controlled by controlling the armature current I_a only since I_f is the field current which only affects the field flux and K_T is a constant.

Hence, the special property of the DC motor is that torque is directly proportional to the armature current I_a[76] [77].

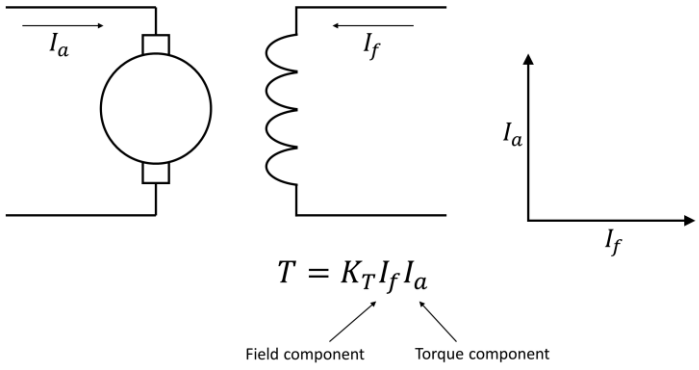

(a) Separately excited DC motor

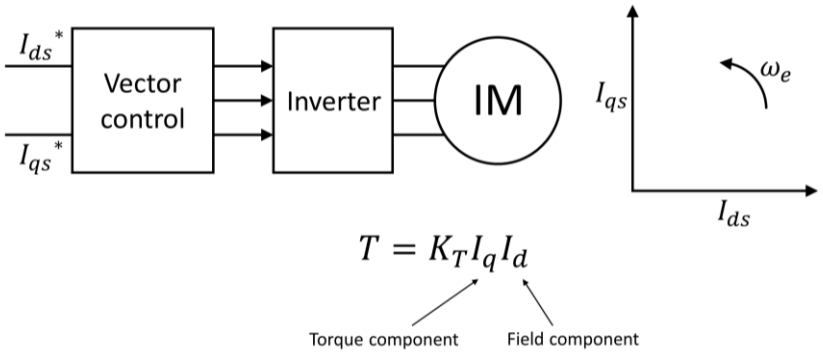

(b) Vector controlled induction motor

Fig. 1.17 Torque generation mechanism and control

This kind of precise torque control is achievable in AC motors by applying vector control. As shown in Fig. 1.17 (b), in vector control, the stator (primary) current of the induction motor is decoupled into flux (magnetizing) component current I_d and torque component current I_q. Therefore, I_d is equivalent to the field current I_f and I_q is equivalent to the armature current I_a of the DC motor as shown in Figs. 1.17 (a) and 1.17 (b). Thus, the same performance of the DC motor drive can be achieved if the flux current I_d is aligned in the direction of the flux and the torque component I_q is perpendicular to it [78] [79]. Hence, the generated torque of the AC motor can be controlled by adjusting the torque component current (I_q) just as in a separately excited DC motor.

The indirect vector control is one of the most popular and frequently used vector control method in induction motors drives [80]. This popularity is because it has better dynamic performance, eliminates the need for flux sensors and has no drift problems. In this research, indirect vector control was selected as the control method for the two-phase inverter-fed induction motor drive.

1.6.2 Overview of indirect vector control method

In this section, the overview of indirect vector control method is described. Indirect vector control is also known as indirect field oriented control. The block diagram of the indirect vector-controlled three-phase inverter-fed induction motor drive is shown in Fig. 1.18. Vector control accomplishes instantaneous commutation with velocity feedback ω_r from the motor via an encoder and a calculated feedforward slip command ω_s. The stator current of the motor is decoupled into flux (magnetizing) component current I_d and torque component current I_q. These components are then controlled independently. The flux component current I_d, varies slowly and is usually kept constant for fast response [(81)-(84)].

Indirect vector control begins by monitoring the currents that drive the motor. The signals for that sensor are the inverter outputs I_u, I_v, and I_w. Since the amplitudes of the signals I_u, I_v, and I_w are very small, they are amplified by an amplifier and input to an AD converter. The three-phase signals I_u, I_v, and I_w are converted into digital current values I_a, I_b, and I_c by the AD converter, and then converted into two-phase current values I_α and I_β using Clarke transformation (for details, refer to 1.6.3-1).

Next, these two-phase currents I_α and I_β are transformed from stationary coordinates to rotating coordinates using Park transformation to obtain the currents I_d and I_q (for details, refer to 1.6.3-2). The reference values of the flux component current I_d^* and the torque component current I_q^* are then compared with feedback values I_d and I_q and their errors are processed through Proportional Integral (PI) controllers to eliminate deviation from the referenced values. The corrected values and outputs of the PI controller are not current but voltage references V_d^* and V_q^*.

Next, voltage references V_d^* and V_q^* are transformed from rotating coordinates back to stationary coordinates using inverse Park transformation to obtain voltage references V_α^* and V_β^*. This voltage references V_α^* and V_β^* are then transformed using inverse Clarke transformation to sinusoidal three-phase voltage references V_u^*, V_v^*, and V_w^*, which are used to generate PWM signals for the inverter and finally to drive the motor. This is one complete cycle of an indirect vector control method.

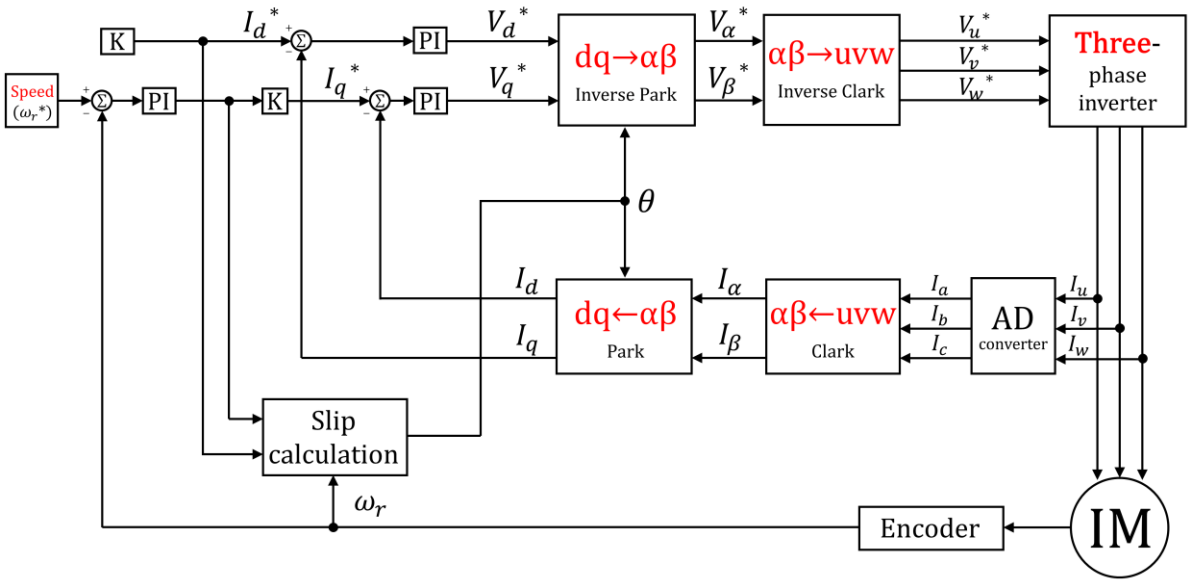

Fig. 1.18 Indirect vector control method

1.6.3 Transformation matrix and voltage signals for vector control of three-phase inverter

Vector control consists of four coordinate transformations, Park, Clarke, inverse Park and inverse Clarke transformations as shown in Fig. 1.18. These transformations are complicated processes that require mathematical knowledge to comprehend. In this section, these mathematical coordinate transformations are explained in detail.

1.6.3-1 Clarke transformation (*UVW → αβ*)

In general, it is difficult to handle three signals simultaneously because the three signals change with some relation to each other and computation in a three-dimensional space becomes necessary. Therefore, in order to simplify the calculation, the three-phase currents I_a, I_b, and I_c are transformed into two-phase currents I_α and I_β by a process called Clarke transformation.

In Clarke transformation, the property of an ideal three-phase alternating current is utilized, where the sum of three sine waves is equal to zero as shown in equation (1.3).

$$I_a + I_b + I_c = 0 \tag{1.3}$$

Based on this condition, the three-phase currents are transformed into two-phase currents which are assumed to be perpendicular to each other. The magnitudes of the three-phase currents are shown in equation (1.4).

$$\begin{aligned} I_a &= \sqrt{2} I \cos \omega t \\ I_b &= \sqrt{2} I \cos\left(\omega t - \frac{2}{3}\pi \right) \\ I_c &= \sqrt{2} I \cos\left(\omega t - \frac{4}{3}\pi \right) \end{aligned} \tag{1.4}$$

Clarke transformation is represented by

$$\begin{bmatrix} I_\alpha \\ I_\beta \end{bmatrix} = \sqrt{\frac{2}{3}} \begin{bmatrix} \cos 0^\circ & \cos \frac{2}{3}\pi & \cos \frac{4}{3}\pi \\ \sin 0^\circ & \sin \frac{2}{3}\pi & \sin \frac{4}{3}\pi \end{bmatrix} \begin{bmatrix} I_a \\ I_b \\ I_c \end{bmatrix}. \tag{1.5}$$

Here, $\sqrt{2/3}$ is a transformation coefficient used to retain the same power before and after the transformation. As shown in equations (1.6), the two-phase currents I_α and I_β can be derived by applying Clarke transformation to the three-phase currents.

$$I_{\alpha} = \sqrt{3} I \cos \omega t$$

$$I_{\beta} = \sqrt{3} I \sin \omega t \tag{1.6}$$

1.6.3-2 Park transformation ($\alpha\beta \rightarrow dq$)

The second transformation in vector control is a coordinate transformation from stationary coordinates to rotating coordinates which is called Park transformation. By performing Park transformation computation is simplified. In addition, the value of the rotation angle of the rotor θ is required for the transformation from stationary coordinates to rotating coordinates. In other words, without the knowledge of how far the rotor has rotated, it is impossible to transform values from stationary coordinates to rotating coordinates. Therefore, information on the rotation angle is acquired by some other means. In indirect vector control, the rotation angle of the rotor θ can be derived from an incremental encoder and the slip frequency calculation.

Park transformation can be expressed in matrix as shown in equation (1.7). Here $\theta = \omega t$.

$$\begin{bmatrix} I_d \\ I_q \end{bmatrix} = \begin{bmatrix} \cos\theta & \sin\theta \\ -\sin\theta & \cos\theta \end{bmatrix} \begin{bmatrix} I_{\alpha} \\ I_{\beta} \end{bmatrix} \tag{1.7}$$

$$I_d = \sqrt{3} I$$

$$I_q = 0 \tag{1.8}$$

1.6.3-3 Inverse Park transformation ($dq \rightarrow \alpha\beta$)

In vector control, the input of the PI controllers are current values and the output are voltage values V_d^* and V_q^*. The voltage values are used instead of the current values because the input signal of the inverter is voltage.

The two-phase voltage references V_d^* and V_q^* obtained through the PI controllers are transformed back to the stationary coordinates from the rotating coordinates. This transformation is called the inverse Park transformation. In this case, the rotation angle θ which is already known at the time of Park transformation (1.6.3.2) is required. The transformation matrix for inverse Park transformation is shown in equation (1.9) and the two-phase voltage references V_{α}^* and V_{β}^* is given by equations (1.10).

$$\begin{bmatrix} V_{\alpha}^* \\ V_{\beta}^* \end{bmatrix} = \begin{bmatrix} \cos\theta & -\sin\theta \\ \sin\theta & \cos\theta \end{bmatrix} \begin{bmatrix} V_d^* \\ V_q^* \end{bmatrix} \tag{1.9}$$

$$V_\alpha^* = \sqrt{3}V\cos\omega t$$

$$V_\beta^* = \sqrt{3}V\sin\omega t \tag{1.10}$$

1.6.3-4 Inverse Clarke transformation ($\alpha\beta \rightarrow UVW$)

The control in the two-phase axis is completed and must be transformed back into three-phase voltage references V_u^*, V_v^*, and V_w^* that have a phase difference of $2\pi/3$ for the inverter. The two-phase voltage references V_α^* and V_β^* are transformed to the three-phase voltage references V_u^*, V_v^*, and V_w^* by the process called inverse Clarke transformation. These three-phase voltage references are then transmitted to the PWM inverter to drive the three-phase motor.

The transformation matrix for inverse Clarke transformation is expressed by equation (1.11) and the final three-phase output voltage references V_u^*, V_v^*, and V_w^* of vector control is shown in equations (1.12).

$$\begin{bmatrix} V_u^* \\ V_v^* \\ V_w^* \end{bmatrix} = \sqrt{\frac{2}{3}} \begin{bmatrix} \cos 0^\circ & \sin 0^\circ \\ \cos\frac{2}{3}\pi & \sin\frac{2}{3}\pi \\ \cos\frac{4}{3}\pi & \sin\frac{4}{3}\pi \end{bmatrix} \begin{bmatrix} V_\alpha^* \\ V_\beta^* \end{bmatrix} \tag{1.11}$$

$$\begin{aligned} V_u^* &= \sqrt{2}V\cos\omega t \\ V_v^* &= \sqrt{2}V\cos\left(\omega t - \frac{2}{3}\pi\right) \\ V_w^* &= \sqrt{2}V\cos\left(\omega t - \frac{4}{3}\pi\right) \end{aligned} \tag{1.12}$$

1.6.4 Derivation of voltage references for a vector controlled two-phase inverter

In section 1.6.3, the transformations method to derive output voltage references V_u^*, V_v^*, and V_w^* for the conventional three-phase inverter-fed motor drive was explained in detail. A block diagram of these output transformations is shown in Fig. 1.19 (a). In this section, the previous method in literature used to derive the two-phase output voltage references V_A^* and V_B^* for the vector of two-phase inverter-fed AC motor drives is explained.

As earlier explained in section 1.4.3, two-phase inverters require two-phase output voltage references V_A^* and V_B^* that have a phase difference of $\pi/3$ to drive three-phase motors. Previous literature on vector control of two-phase inverter drives derived the output voltage references V_A^* and V_B^* by subtraction from the three-phase output voltage references V_u^*,V_v^*,and V_w^* used in the conventional three-phase inverter drive as shown in Fig. 1.19 (b) [62]–[65]. Figure 1.19 (b) illustrates the derivation process when the *V*-phase of the motor is connected to the midpoint of the DC source.

The two-phase output voltage references V_A^* and V_B^* that have a phase difference of $\pi/3$ are derived from the three-phase output voltage references V_u^*, V_v^*, and V_w^* that have a phase difference of $2\pi/3$ as shown in equations (1.13) and (1.14) respectively.

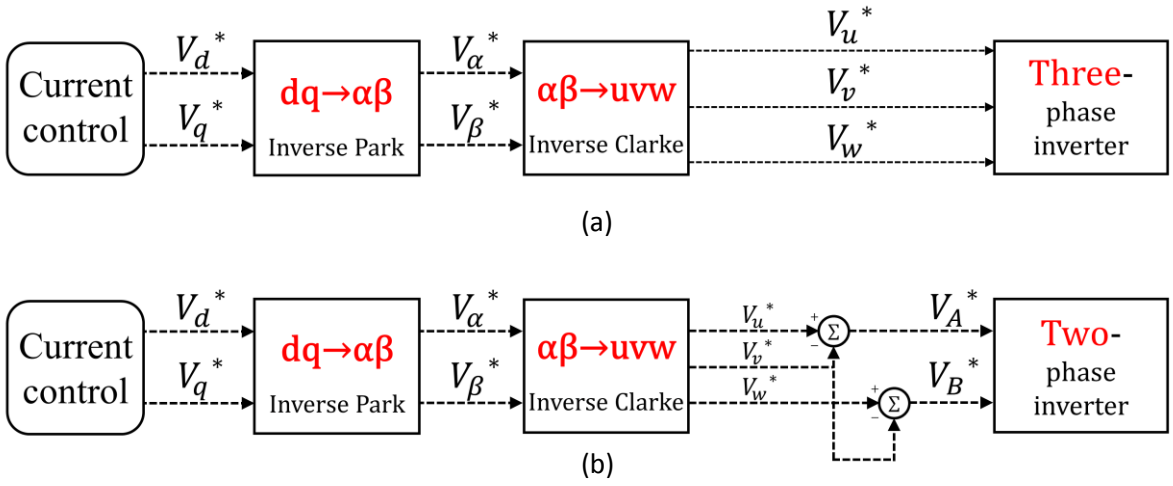

(a) Three-phase inverter (b) Two-phase inverter (Previous method)

Fig. 1.19 Derivation method of final voltage references

$$V_A^* = V_u^* - V_v^*$$

$$= \sqrt{6}V\cos\left(\omega t + \frac{\pi}{6}\right) \tag{1.13}$$

$$V_B^* = V_w^* - V_v^*$$

$$= \sqrt{6}V\cos\left(\omega t + \frac{\pi}{2}\right) \tag{1.14}$$

Although, the subtraction method can achieve the voltage references V_A^* and V_B^* that have a phase difference of $\pi/3$, it has three main disadvantages.

(i) If the two-phase inverter is applied as an emergency strategy for the conventional three-phase inverter drive, depending on the inverter phase *U*, *V* or *W* that is damaged, the phases of the three-phase voltage references from which subtraction is performed is different as shown in Fig. 1.20.
(ii) Due to the subtraction process, instantaneous speed control and response is unachievable.
(iii) This method affects the balance of motor currents in high load and high-speed regions.

Therefore, a transformation matrix that can instantaneously generate two-phase voltage references V_A^* and V_B^* that have a phase difference of $\pi/3$ for vector control of two-phase inverter in time domain is required. Furthermore, a transformation matrix that is applicable irrespective of the damaged inverter phase U, V, or W is required.

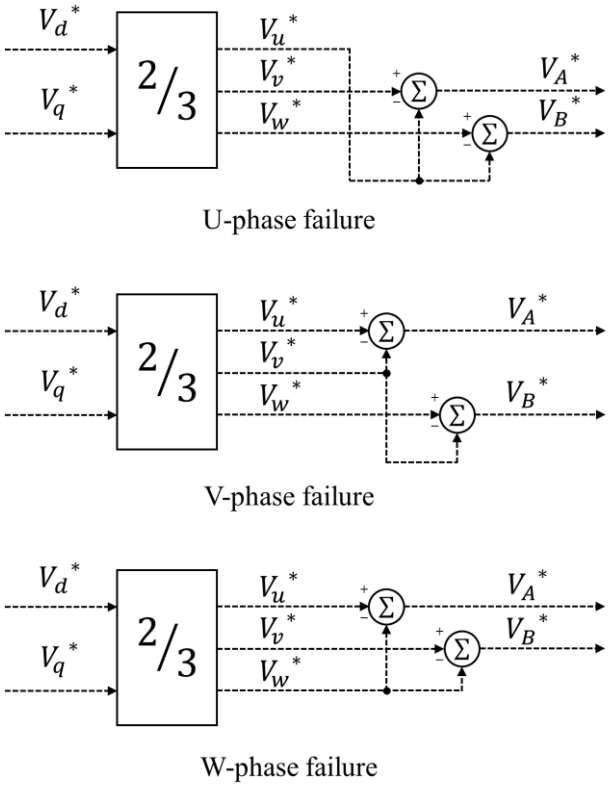

Fig. 1.20 Derivation of voltage references by subtraction method

1.7 Problem statement and research objectives

This dissertation presents the vector-controlled two-phase inverter-fed induction motor drive as an emergency strategy for switch/leg-level failure in three-phase inverter-fed induction motor drives.

1.7.1 Transformation matrix for instantaneous vector control of two-phase inverter

Vector control is known to achieve instantaneous control of speed and torque. In order to achieve instantaneous vector control of the conventional three-phase inverter, the three-phase motor current is fed back into the control system and transformed into to a two-phase axis using basic vector mathematics. Then, the two-phase currents are then controlled independently and thereafter transformed back to three-phase voltage references V_u^*,V_v^*, and V_w^* that have a phase difference of $2\pi/3$. These transformations are carried out using the well known Park, Clarke, inverse Park and inverse Clarke transformations, which are only applicable to the conventional three-phase inverter drives.

From the working principle of two-phase inverter-fed AC motor drives, two-phase output voltage references V_A^* and V_B^* that have a phase difference of $\pi/3$ are required. The previous method in literature on vector control of two-phase inverter-fed AC motor drives derived the output voltage references $V_A^*$and V_B^* by subtraction from the output voltage references V_u^*, V_v^*, and V_w^* of the conventional three-phase inverter. The previous method in literature has three main disadvantages as explained in section 1.6.4.

In order to achieve instantaneous vector control of two-phase inverter-fed AC motor drives, an instantaneous method to derive the output voltage references V_A^* and V_B^* that have a phase difference of $\pi/3$ from voltage references V_d^* and V_q^* is required. In this dissertation, an instantaneous transformation matrix is proposed to derive the voltage references V_A^* and V_B^* that have a phase difference of $\pi/3$ for vector control of two-phase inverter-fed AC motor drives.

1.7.2 Performance evaluation

Vector control is well known to have a good dynamic response and high-performance characteristics from zero speed to the high-speed region. In the high-speed, one main factor that affects the performance of a motor drive is the maximum output voltage. However, from the working principle (theory) and structure of two-phase inverter drives, the maximum output voltage reduces compared to the conventional three-phase inverter drives. The reduction in maximum output voltage has a negative effect on the performance of the two-phase inverter drive, especially in the high-speed region.

Up till date, most of the literature focused on the performance characteristics of the two-phase inverter-fed motor drive in the low-speed region. However, most of the applications where vector-controlled inverter-fed motor drives are utilized require good dynamic performance in its entire operating region. Thus, there is a need to investigate and evaluate the performance of the two-phase inverter-fed induction motor drive in its entire operating region by experiment. Proper evaluation of the performance of the two-phase inverter drive, will enable determination of the kinds of applications where two-phase inverter can be utilized as an emergency strategy.

1.7.3 Performance optimization in the high-speed region

In the conventional three-phase inverter-fed motor drives, the output voltage reaches its maximum value (voltage saturation) at a certain speed called the base speed. Above the base speed, in order to maintain current control and optimize the performance of the drive in the high-speed region, a field weakening control strategy is usually applied as shown in Fig.1.21. Over the years, many field weakening strategies have been proposed for the conventional three-phase inverter-fed induction motor drive. However, due to the reduction in the maximum output voltage (base speed) of the two-phase inverter drives compared to the conventional three-phase inverter drives, these field weakening control strategies cannot be directly applied to two-phase inverter drives.

Consequently, in this dissertation a novel field weakening control strategy is proposed to optimize the performance of two-phase inverter-fed induction motor drives in the high-speed region.

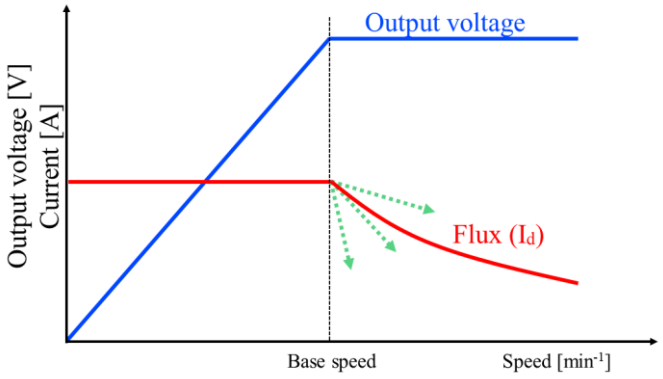

Fig. 1.21 Conventional field weakening control method

1.8 Organization of dissertation

This dissertation consists of five chapters. In this section, the contents of each chapter are briefly described.

In Chapter 1, background and the basics of inverter-fed AC motor drives are explained, followed by an explanation of inverter failure and emergency strategies for inverter-fed AC motor drives. The two-phase inverter is then introduced as an emergency strategy for the conventional three-phase inverter-fed induction motor drive. A review of reported literature on two-phase inverter-fed motor drives is conducted. Finally, the problem statements and the objectives of this research are explained in detail.

In Chapter 2, a new transformation matrix is proposed to enable instantaneous derivation of voltage references V_A^* and V_B^* , instantaneous speed control and easy implementation of the vector controlled two-phase inverter drive as an emergency strategy. The procedure of deriving the transformation matrix is described in detail. The ability of the proposed transformation to retain the same power before and after the transformation is verified.

In Chapter 3, the effectiveness of the proposed transformation matrix is verified by simulation and validated from the experimental results. A comparison between the performance of vector-controlled two-phase and three-phase inverter-fed induction motor drives is performed. Furthermore, a comparison of the vector-controlled two-phase inverter-fed induction motors drive using the proposed transformation matrix and the previous method in literature is performed by experiment.

In Chapter 4, a field weakening control strategy is proposed to improve the performance characteristics of the vector controlled two-phase inverter in the high-speed region. The proposed method enables precise and adequate control of the stator currents to achieve better performance in the high-speed region. The effectiveness of the proposed strategy is verified by simulation and experiment.

In Chapter 5, works done in this dissertation are summarized.

References

1. 森本雅之：「よくわかるパワーエレクトロニクス」、森北株式会社、pp.146-158(2016)
2. 堀孝正：「新インターユニバーシティ パワーエレクトロニクス」、オーム社、pp.14-18(2008)
3. 山村昌　大野栄一：「パワーエレクトロニクス入門」、オーム社、pp.234-240 (1991)
4. ABB, (drives and motors for improving energy efficiency), 15125, ABB drives and motors energy efficiency, EN Rev A23.9 lowres, pp.2-12(2010)
5. ABB “Saving energy with Variable speed drives” (http://www.abb.com/cawp/seitp202/c253ae5e6abf5817c1256feb0053baf7.aspx)
6. F. Steyn: “Motors and drives for improving energy efficiency”, *Southern African Energy Efficiency Convention (SAEEC)*, pp.1-7(2011)
7. 電気学会・センサレスベクトル制御の整理に関する調査専門委員会：「AC ドライブシステムのセンサレスベクトル制御」、オーム社、pp.234(2016)
8. B.K. Bose: “Power electronics and motor drive recent progress and perspective”, *IEEE Trans. Ind. Electron*., Vol.56, No.2, pp.581-588(2009)
9. 森本雅之：「よく分かるパワーエレクトロニクス」、森北出版株式会社、pp.153-156(2016)
10. 百目鬼英雄：「電動モータドライブの基礎と応用」、技術評論社、pp.110-113(2010)
11. 森本雅之：「入門モータ工学」、森北出版株式会社、pp.1-2(2013)
12. T. Sawa and T.Kume: “Motor drive technology- history and vision for the future”, *IEEE Ann.Power Elect. Specialists Conf.(PESC)*, Vol.1, pp.2-9(2004)
13. S. Hussain and M.A. Bazaz: “Review of vector control strategies for three phase induction motor drive”, *Int.Conf. on recent developments in control, automation and power eng.(RDCAPE)*, pp.96-101(2015)
14. K. Ni, Y. Hu, Y. Liu, and C. Gan: “Overview on fault-tolerant four-switch three-phase voltage source converters”, *Chinese Journal of Electrical Engineering*, Vol.3, No.2, pp.87-101(2017)
15. M. Yamato and Y. Sato: “An investigation of a control method for fault-mode inverters to drive induction motors”, *IEE Japan Trans.Industry Appl.*, Vol.123, No.12, pp.1430-1437(2003) *(In Japanese)*
16. K. Matsuse and D. Matsuhashi: “New technical trends on adjustable speed AC motor drives”, *Chinese Journal of Electrical Engineering*, Vol.3, No.1, pp.1-9(2017)
17. W. Zhang, D. Xu, P.N. Enjeti, H. Li, J.T. Hawke, and H.S. Krishnamoorthy: “Survey of fault-tolerant techniques for power electronic converters”, *IEEE Trans. Power Electronics*, Vol.29, No.12, pp.6319-6331(2014)
18. S. Ceballos, J. Pou, J. Zaragoza, J. L. Martin, E. Robles, I. Gabiola, and P. Ibanez: “Efficient modulation technique for a four-leg fault-tolerant neutral-point-clamped inverter”, *IEEE Trans. Ind. Electronics*, Vol.55, No. 3, pp.1067–1074(2008)
19. Y. Song and B. Wang: “A hybrid electric vehicle powertrain with fault- tolerant capability”, *Proc. IEEE 27th Annu. Appl.Power Electron. Conf. Expo(APEC)*, pp.951-956(2012)
20. S. Ceballos, J. Pou, J. Zaragoza, E. Robles, J.L.Villate, and J.L. Martin: “Fault-tolerant neutral-point-clamped converter solutions based on including a fourth resonant leg”, *IEEE Trans. Ind. Electronics*, Vol.58, No.6, pp.2293-2303(2011)
21. J. Song-Manguelle, T. Thurnherr, S. Schroder, A.Rufer, and J. M.Nyobe-Yome: “Re-generative asymmetrical multi-level converter for multi- megawatt variable speed drives”, *Proc. IEEE Energy Convers. Cong. Expo. (ECCE)*, pp.3683-3690(2010)
22. K. Shen, B. Xiao, J. Mei, L.M. Tolbert, J. Wang, X. Cai, and Y. Ji: “A modulation reconfiguration based fault-tolerant control scheme for modular multilevel converters”, in *Proc. IEEE Annu. Appl. Power Electron. Conf.(APEC)*, pp.3251-3255(2013)
23. X. Sun, L.-K. Wong, Y.-S. Lee, and D. Xu: “Design and analysis of an optimal controller for parallel multi-inverter systems”, *IEEE Trans. Circuits Syst. II, Exp. Briefs*, Vol. 53, No.1, pp.56-61(2006)
24. A. L. Julian and G. Oriti: “A comparison of redundant inverter topologies to improve voltage source inverter reliability”, *IEEE Trans. Ind. Appl*., Vol.43, No.5, pp.1371-1378(2007)
25. S.Wei, B.Wu, S. Rizzo, and N. Zargari: “Comparison of control schemes for multilevel inverter with faulty cells”, *IEEE Annu. Conf. Ind. Electron. Soc.(IECON)*, Vol.2, pp.1817-1822(2004)

26. B.Mirafzal: “Survey of fault-tolerance techniques for three-phase voltage source inverters”, *IEEE Trans. Ind. Electronics*, Vol.61, No.10, pp.5192-5202(2014)
27. D. Kastha and B.K. Bose: “Investigation of fault modes of voltage-fed inverter system for induction motor drive”, *IEEE Trans. Industry Appl.*, Vol.30, No.4, pp.1028-1038(1994)
28. B.Liu and S.K.Sharma: “A literature review of IGBT fault diagnostic and protection methods for power inverters” , *IEEE Trans. Industry Appl.*, Vol.45, No.5, pp.1770-1777(2009)
29. Y.Song and B.Wang: “Survey on reliability of power electronic systems”, *IEEE Trans. Power Electronics*, Vol.28, No.1, pp.591-604(2014)
30. 森本雅之：「入門インバータ工学」、森北出版株式会社、 pp.95-96(2011)
31. Mitsubishi Electric, “Semiconductor device reliability” (http://www.mitsubishielectric.com/cn/semiconductors/files/manuals/reliability.pdf) pp.1-2(1998)
32. S. Li and L. Xu: “Strategies of fault tolerant operation for three-level PWM inverters”, *IEEE Trans. Power Electronics*, Vol.21, No.4, pp.933-940(2006)
33. P. Lezana, J. Pou, T. A. Meynard, J. Rodriguez, S. Ceballos, and F. Richardeau: “Survey on fault operation on multilevel inverters”, *IEEE Trans. Ind. Electronics*, Vol.57, No.7, pp.2207-2218(2010)
34. S. Wei, B. Wu, S. Rizzo, and N. Zargari: “Comparison of control schemes for multilevel inverter with faulty cells”, *IEEE Annu. Conf. Ind. Electron. Soc.(IECON)*, Vol. 2, pp.1817-1822(2004)
35. P. Correa and J. Rodrıguez: “Control strategy reconfiguration for a multilevel inverter operating with bypassed cells”, *IEEE Int. Symp. Ind. Electronics*, pp.3162-3167(2007)
36. A. Chen, Lei Hu, L. Chen, Y. Deng, and X. He: “A multilevel converter topology with fault-tolerant ability”, *IEEE Trans. Power Electronics*, Vol.20, No.2, pp.405-415(2005)
37. B.A. Welchko, T.A. Lipo, T.M. Jahns and S. E. Schulz: “Fault tolerant three-phase AC motor drive topologies: a comparison of features, cost, and limitations”, *IEEE Trans. Power Electronics*, Vol.19, No.4, pp.1108-1116(2004)
38. T.H. Liu, J.R. Fu and T.A. Lipo: “A strategy for improving reliability of field-oriented controlled induction motor drives”, *IEEE Trans. Ind. Appl.*, Vol.29, No.5, pp.910-918(1993)
39. R. Wang, J.Zhao, and Y. Liu: “A comprehensive investigation of four-switch three phase voltage source inverter based on double fourier integral analysis”, *IEEE Trans. On Power Electronics*, Vol.26, No.10, pp. 2774-2787(2011)
40. M. S. Zaky and M. K. Metwaly: “A performance investigation of a four-switch three-phase inverter-fed IM drives at low speeds using fuzzy logic and PI controllers”, *IEEE Trans. on Power Electronics*, Vol.32, No.5, pp.3741-3753(2017)
41. L. Julian and G. Oriti: “A comparison of redundant inverter topologies to improve voltage source inverter reliability”, *IEEE Trans. Ind. Appl*., Vol.43, No.5, pp.1371-1378(2007)
42. J. Flack, C. Felgemacher, A. Rojiko, M. Liserre, and P. Zacharias: “Reliability of power electronic systems: An industry perspective”, *IEEE Industrial Electronics Magazine*, Vol.12, No.2, pp.24-35(2018)
43. Yaskawa America “Variable Frequency Drives Control Methods” (2014) (https://www.yaskawa.com/delegate/getAttachment?documentId=WP.AFD.13)
44. 河村篤男：「パワーエレクトロニクス学入門―基礎から実用例まで」、コロナ社、pp.127-128(2009)
45. M. Kazmierkowski, L. Franquelo, J. Rodriguez, M. Perez, and J. Leon: “High-performance motor drives”, *IEEE Industrial Electronics Magazine*, Vol.5, No.3, pp.6-26(2011)
46. H.W.V.D. Broeck and J.D.V. Wyk: “A comparative investigation of a three-phase induction machine drive with a component minimized voltage-fed inverter under different control options”, *IEEE Trans. Industry Appl*, Vol.IA-20, No.2, pp.309-320(1984)
47. J. Kim, J. Hong, and K.Nam: “A current distortion compensation scheme for four-switch inverter”, *IEEE Trans. Power Electronics*, Vol.24, No.4, pp.1032-1040(2009)
48. W. Ma and Masayuki Morimoto: “Emergency drive method for EV at the inverter fault”, *IEEE Int. Conf. on Elec. Machines and Syst.(ICEMS)*, pp.2008-2011(2010)
49. T. Ishikawa and M. Morimoto: “EV traction at inverter faulty condition” *Proceedings of the school of engineering, Tokai University*, Vol.49, No.1, pp.37-42(2009)

50. A.M.S. Mendes, X.M. Lopez-Fernandez, and A.J.M. Cardoso: “Thermal performance of a three-phase induction motor under fault tolerant operating strategies”, *IEEE Trans. Power Electronics*, Vol.23, No.3, pp.1537-1544(2008)
51. H.H. Lee, P.Q. Dzung, L.D. Khoa, and L.M. Phuong: “Dynamic adaptive space vector PWM for four switch three phase inverter fed induction motor with compensation of DC-link voltage ripple”, *IEEE Int. Conf. on Power Electron and Drive systems(PEDS)*, pp.399-404(2009)
52. F. Blaabjerg, S. Freysson, H.H. Hansen, and S. Hansen: “A new optimized space-vector modulation strategy for a component-minimized voltage source inverter”, *IEEE Trans. Power Electronics*, Vol.12, No.4, pp.704-714(1997)
53. G.A. Covic and G.L. Peters: “DC link imbalance compensation in four- switch inverter AC motor drives”, *IET Electronic Letters*, Vol.33, No.13, pp.1101-1102(1997)
54. S. Kazemlou and M.R. Zolghadri: “Direct torque control of four switch three phase fed induction motor using a modified SVM to compensate DC-Link voltage imbalance”, *Proc.Int. Conf. on Power and Energy Conversion Systems(EPECS)*, pp.1-6(2009)
55. F. Blaabjerg, D. O. Neacsu, and J. K. Pedersen: “Adaptive SVM to compensate DC-link voltage ripple for four switch three phase voltage source inverters”, *IEEE Trans. Power Electronics*, Vol.14, No.4, pp.743-752(1999)
56. R. Wang, J. Zhao, and Y. Liu: “A comprehensive investigation of four-switch three phase voltage source inverter based on double fourier integral analysis”, *IEEE Trans. Power Electronics*, Vol.26, No.10, pp.2774-2787(2011)
57. M. B. de R. Correa, C. B. Jacobina, E. R. C. da Silva, and A.M.N. Lima: “A general PWM strategy for four-switch three phase inverters”, *IEEE Trans. Power Electronics*, Vol.21, No.6, pp.1618-1627(2006)
58. P. Q. Dzung, L.M. Phoung,and P.Q. Vinh: “A new switching for direct torque control of induction motor using four-switch three-phase inverter”, *IEEE Int. Conf. Power Electron and Drive Syst*, pp.1331-1336(2007)
59. Q.T.An, L.Sun, K.Zhao, and T.M. Jahns: “Scalar PWM algorithms for four-switch three-phase inverters”, *IET Electronics Letters*, Vol.46, pp.900-902(2010)
60. Y.Liu, X.Ge, J. Zhang and X.Feng: “General SVPWM strategy for three different four switch three phase inverters”, *IET Electronics Letters*, Vol.51, No.4, pp.357-359(2015)
61. M. Yamato, A. Jaya, and Y. Sato: “An investigation of a control method for fault mode inverters to drive Induction Motors”, *IEE Japan National Conventional Record*, Vol.1, No.4-143, pp.233-234(2002) (*In Japanese*)
62. G. Kim and T.A. Lipo: “VSI-PWM Rectifier/Inverter System with a Reduced Switch Count”, *IEEE Trans. Industry Appl.*, Vol.32, No.6, pp.1331-1337(1996)
63. H. Tanaka, S. Saito, and K. Matsuse: “Improved performance of independent two induction motor drives fed by a four leg inverter with vector control method”, *IEEE Int. Conf. Elec. Machines and Syst.(ICEMS)*, pp.1-6(2012)
64. T. Liu, J. Fu, and T.A. Lipo: “A strategy for improving reliability of field-oriented controlled induction motor drives”, *IEEE Trans. Ind. Appl.*, Vol.29, No.5, pp.910-918(1993)
65. A. Katagiri, B. Kezuka, C. Tanaka, and K. Matsuse: “Improved performance of independent two induction motor drives fed by four-leg inverter”, *Int. Conf. on Power elect. (ECCE Asia)*, pp.2498-2505(2011)
66. T. Ishikawa and M. Morimoto: “EV traction method for inverter faulty condition” *IEEJ Industry Applications Division Annual Conference (JIASC)*, No.2-45, pp.419-422(2009) (*In Japanese*)
67. W. Ma and M. Morimoto: “Emergency drive method for EV at the inverter fault”, *IEEE Int. Conf. on Elec. Machines and Syst.(ICEMS)*, pp.2008-2011(2010)
68. 金東海：「パワースイッチング工学―パワーエレクトロニクスの基礎理論」、オーム社、pp.203-204(2003)
69. 正田英介、深尾正、島田隆一、河村篤男：「パワーエレクトロニクスのすべて」、オーム社、pp.60-64(1995)
70. D.W. Novotny, T.A.Lipo, Vector control and dynamics of AC Drives, Oxford: pp.1-5(1996)
71. 山村昌：「交流モータの解析と制御」、オーム社、pp.9-10(1988)
72. 野中作太郎、岡田英彦、小山純、伊藤良三：「パワーエレクトロニクス入門」、朝倉書店、pp.102-103(1999)

73. 堀孝正：「パワーエレクトロニクス」、オーム社、pp.121-122(2002)
74. 小山純、伊藤良三、花本剛士、山田洋明：「最新パワーエレクトロニクス入門」、朝倉書店、pp.116-119(2012)
75. J.A. Santisteban and R.M. Stephan: “Vector control methods for induction machines: an overview”, *IEEE Trans. On Education*, Vol.44, No.2, pp.170-175(2001)
76. N. Mohan, T.M. Undeland, W.P.Robbins, Power Electronics: Converters, Applications and Design, John Wiley & Sons : pp.286-289(1989)
77. B.K. Bose, Modern Power Electronics and AC Drives, Prentice Hall: pp.356-384(2001)
78. 河村篤男、松井景樹、西條隆繁、木方靖二：「基礎パワーエレクトロニクス」、コロナ社、pp.231-232(1988)
79. 赤津観：「モータ技術のすべてがわかる本」、ナツメ社、pp.226-227(2012)
80. 正田英介、楠本一幸：「パワーエレクトロニクス」、オーム社、pp.184-185(1995)
81. 西田克美：「インバータ制御技術と実践」、科学情報出版株式会社、pp.85-90(2016)
82. 前川佐里、長谷川幸之：「家電用モータのベクトル制御と高効率運転法」、科学情報出版株式会社、pp.243-244(2014)
83. 大野榮一、小山正人：「パワーエレクトロニクス入門改訂 5 版」オーム社、pp.160-161(2014)
84. I. Boldea, S.A. Nasar, Vector Control of AC Drives, CRCpress: pp.73-87(1992)
85. K.Kondo, H.Kubota: “Innovative application technologies of AC motor drive systems”, *IEE Japan Trans. of Ind.Appl.*, Vol.1, No.3, pp.132-140(2012)

Chapter 2

Derivation of transformation matrix for instantaneous vector control of two-phase inverter-fed AC motor drives

2.1 Introduction

As explained in Chapter 1, in order to ease the implementation of the vector-controlled two-phase inverter as an emergency strategy, a transformation matrix that can generate output voltage references irrespective of the damaged inverter phase *U*, *V*, or *W* is required. In this chapter, a transformation matrix to generate output voltage references that have a phase difference of $\pi/3$ for vector control of two-phase inverter-fed three-phase AC motor drives is proposed.

In section 2.2, the disadvantages of the previous methods of deriving output voltage references for two-phase inverters is explained. The conditions and procedure of creating a transformation matrix for vector control of two-phase inverter are described in section 2.3.

In section 2.4, first, an indirect transformation is achieved by creating a transformation matrix from the $\alpha\beta$ axis to the *AB* axis. Next, a transformation matrix that can transform the output voltage references from the *dq* axis to the *AB* axis is derived in section 2.5. The most important characteristic of the transformation matrix is that the power before and after the transformation is constant, which is called power invariance. In this regard, the power invariance of the instantaneous transformation matrix is verified in section 2.6.

2.2 Previous methods and their disadvantages

In section 1.6.4 of Chapter 1, the previous method of deriving voltage references V_A^* and V_B that have a phase difference of $\pi/3$ for sinusoidal PWM was explained. Also, a brief review of its disadvantages and the need to create a more efficient method to derive the output voltage references were described.

In the conventional three-phase inverter-fed motor drive, there are several PWM methods. The two most widely used methods are the sinusoidal PWM and space vector PWM method [(1)]. Space vector PWM can utilize more of the DC source voltage compared to sinusoidal PWM and other PWM methods [(2)]. However, the sinusoidal PWM method is popular/widely used because of simplicity, low switching losses and ease in implementation [(3)].

In the previous literature both the sinusoidal PWM and space vector PWM methods have been applied to two-phase inverter-fed motor drives. An *et al.* implemented both the space vector and sinusoidal PWM methods on the two-phase inverter and they reported that space vector PWM-fed two-phase inverters require more complex algorithms [(4)]. Regarding complexity, they explained that more complicated vector algorithms are required because two-phase inverters outputs only four nonzero voltage vectors and have fewer control degrees of freedom compared to three-phase inverters. Furthermore, these complex algorithms result in heavy calculations which requires a high-performance controller [(4)].

Another literature that utilized space vector PWM on two-phase inverters reported that depending on the inverter phase *U, V,* or *W* that fails a different strategy is required [(5)]. This implies that three different space vector PWM softwares must be installed, which takes up lots of memory space in the controller and increases the complexity of the control strategy [(5)].

As explained in Chapter 1, there are two criteria that must be considered in order to apply two-phase inverters as an emergency strategy for three-phase inverter-fed induction motor drives. These criteria are easy implementation and no additional component. These two criteria cannot be achieved using the space vector PWM method. Therefore, in this dissertation, the sinusoidal PWM method is adopted.

The previous method of deriving voltage references for sinusoidal PWM for two-phase inverters was explained in Chapter 1. In the previous method, the output voltage references V_A^* and V_B^* are derived by subtraction from V_u^*, V_v^*, and V_w^* of the three-phase inverter as shown in Fig. 1.20. The previous method has one similar disadvantage with the space vector PWM method, which is depending on the inverter phase *U, V,* or *W* that fails, the process of generating the output voltage references is different.

Hence, in this dissertation, in order to apply two-phase inverters as an emergency strategy, an instantaneous transformation matrix that can generate the output voltage references V_A^* and V_B^*, irrespective of the damaged inverter phase *U, V,* or *W* is proposed.

2.3 Conditions and procedure for derivation of a transformation matrix for two-phase inverter

In section 1.6.3 of Chapter 1, the transformation procedure to derive the output voltage references V_u^*, V_v^*, and V_w^* for the conventional three-phase inverter was explained in detail. As shown in Fig. 2.1 (a), the voltage references $V_d^*$and V_q^* in rotating coordinates are first transformed to V_α^* and V_β^* in stationary coordinates and finally three-phase voltage references V_u^*, V_v^*, and V_w^*.

The previous method for two-phase inverter as shown in Fig. 2.1 (b) involves a similar transformation procedure to the three-phase inverter; however, the output voltage references V_A^* and V_B^* is derived by subtraction from voltage references V_u^*, V_v^*, and V_w^*. The objective in this chapter is to create a coordinate transformation for vector control of two-phase inverters by deriving an instantaneous transformation matrix that can generate output voltage references V_A^* and V_B^* as shown in Fig. 2.1(c).

The following three conditions must be taken into account before creating the transformation matrix for the two-phase inverter that will be utilized as an emergency strategy. (i) The transformation matrix must be applicable, irrespective of the damaged inverter phase *U, V,* or *W*. (ii) The transformation matrix must be power invariant. (iii) The transformation matrix must be capable of instantaneous speed control and response in different load conditions.

The procedure for creating the instantaneous transformation for the two-phase inverter is principal because the output voltage references V_d^* and V_q^* are in rotating coordinates and the required output voltage references V_A^* and V_B^* are in stationary coordinates.

In order to input changes to fulfill the earlier stated three conditions, an indirect transformation is first created. In the indirect transformation, voltage references are transformed from *dq* axis to *αβ* axis using inverse Park transformation, a matrix is then created to transform voltage references from *αβ* axis to *AB* axis as shown in Fig. 2.2 (a). Here, the two matrices are denoted as C_1 and C_2.

Once C_2 is created, the instantaneous transformation matrix C_3 can be derived from the product of C_1 and C_2, as shown in Fig. 2.2 (b). The instantaneous transformation matrix C_3 must fulfill the three conditions earlier stated in this section.

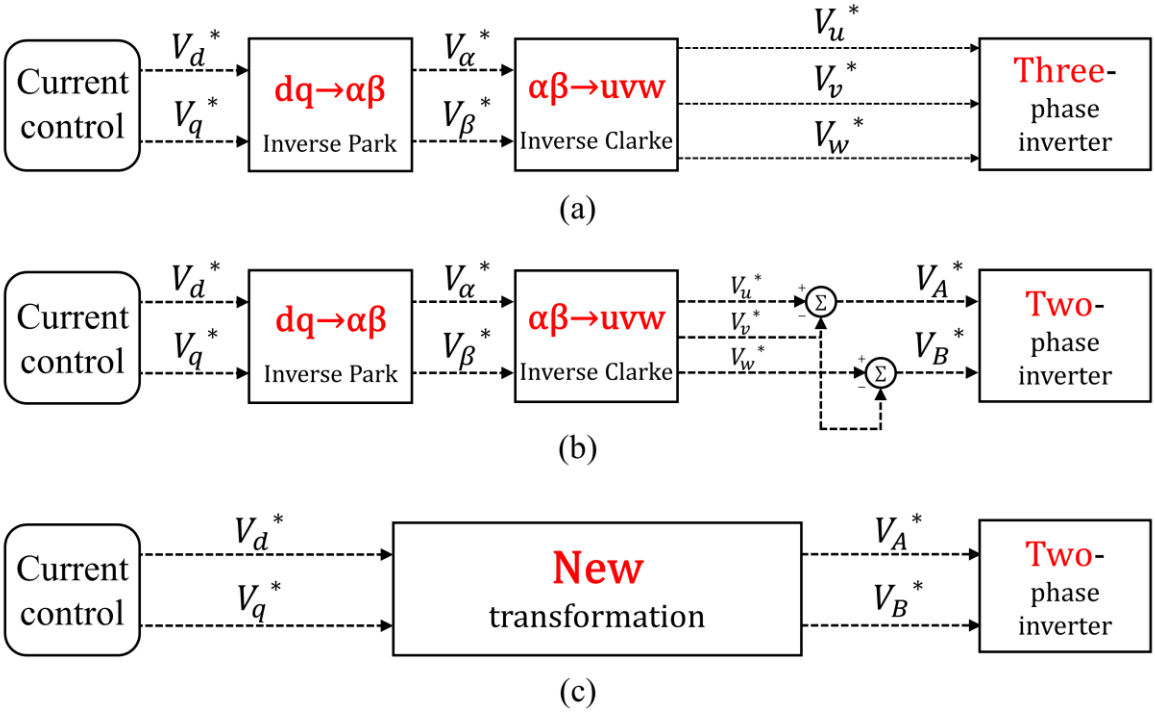

(a) Three-phase inverter (b) Two-phase inverter (Previous method) (c) Two-phase inverter (Instantaneous transformation)

Fig. 2.1 Derivation procedure for output voltage references

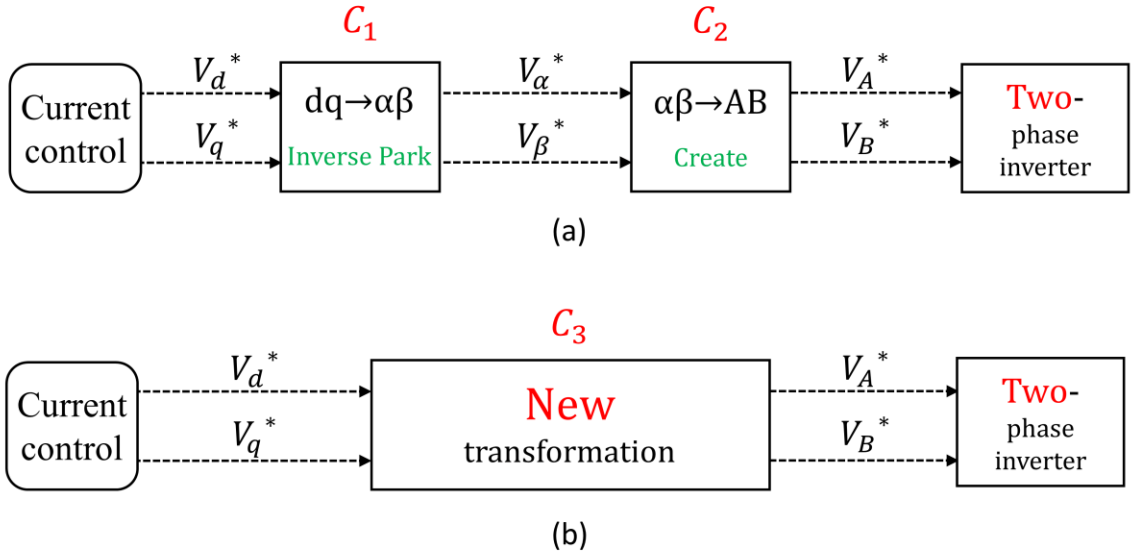

(a) Indirect transformation (b) Instantaneous transformation

Fig. 2.2 Procedure for creating instantaneous transformation

2.4 Indirect transformation for two-phase inverter (*dq→αβ→AB*)

In this section, an indirect transformation to derive voltage references V_A^* and V_B^* for two-phase inverters is created. In the indirect transformation, first, the output voltage references V_d^* and V_q^* are transformed into voltage references V_α^* and V_β^* using inverse Park transformation as mentioned in Chapter 1 (section 1.6.3-3). The voltage references V_α^* and V_β^* are then transformed to voltage references V_A^* and V_B^* by creating a transformation matrix. The block diagram of the indirect transformation is shown in Fig. 2.3.

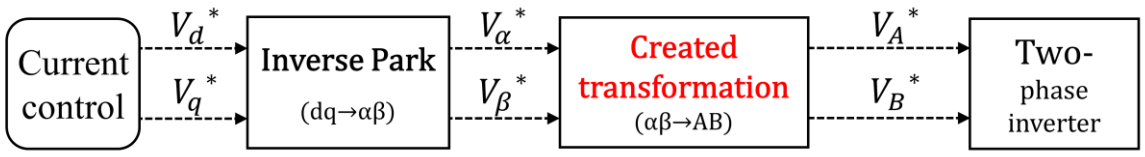

Fig. 2.3 Indirect transformation for two-phase inverter

The transformation from voltage references V_d^* and V_q^* in rotating coordinates to voltage references V_α^* and V_β^* in stationary coordinate by inverse Park transformation is shown in equation (2.1).

$$\begin{bmatrix} V_\alpha^* \\ V_\beta^* \end{bmatrix} = \begin{bmatrix} \cos\theta & -\sin\theta \\ \sin\theta & \cos\theta \end{bmatrix} \begin{bmatrix} V_d^* \\ V_q^* \end{bmatrix} \tag{2.1}$$

Assuming $\theta = \omega t$, $V_d^* = \sqrt{3}V_m$, and $V_q^* = 0$, $V_\alpha{}^*$ and $V_\beta{}^*$ can be expressed by equations (2.2) and(2.3).

$$V_\alpha{}^* = \sqrt{3}V_m \cos\omega t \tag{2.2}$$

$$V_\beta{}^* = \sqrt{3}V_m \sin\omega t \tag{2.3}$$

In order to transform voltage references $V_\alpha{}^*$ and $V_\beta{}^*$ that have a phase difference of π/2 to voltage references $V_A{}^*$ and $V_B{}^*$ that have a phase difference of π/3, a transformation matrix that fulfills the earlier stated three conditions was created. The created transformation matrix is expressed as equation (2.4).

$$\begin{bmatrix} V_A^* \\ V_B^* \end{bmatrix} = \sqrt{\frac{2}{3}} \begin{bmatrix} 1 & 0 \\ \frac{1}{2} & -\frac{\sqrt{3}}{2} \end{bmatrix} \begin{bmatrix} V_\alpha^* \\ V_\beta^* \end{bmatrix} \tag{2.4}$$

Substituting equations (2.2) and (2.3) into equation (2.4) yields equations (2.5) and (2.6).

$$V_A{}^* = \sqrt{2}V_m \cos\omega t \tag{2.5}$$

$$V_B{}^* = \sqrt{2}V_m \cos\left(\omega t + \frac{\pi}{3}\right) \tag{2.6}$$

As shown in equations (2.5) and (2.6), voltage references $V_A{}^*$ and $V_B{}^*$ that have a phase difference of π/3 can be derived from voltage references $V_\alpha{}^*$ and $V_\beta{}^*$ using the created the transformation matrix in equation (2.4) [(11)-(14)].

2.5 Instantaneous transformation matrix for two-phase inverter (*dq→AB*)

In the previous section, the indirect transformation (*dq→αβ→AB*) was created. In this section, the instantaneous transformation matrix is proposed to derive output voltage references V_A^* and V_B^* from the output voltage references V_d^* and V_q^* of vector control. A block diagram of the proposed instantaneous transformation is shown in Fig. 2.4.

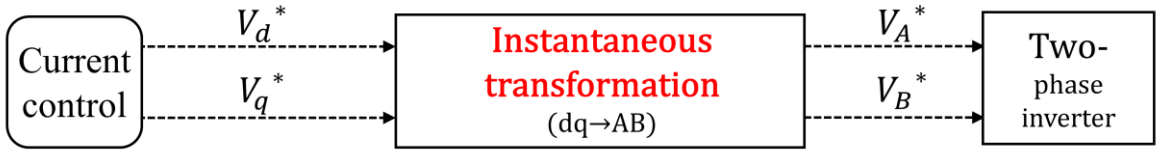

Fig. 2.4 Instantaneous transformation matrix for two-phase inverter

2.5.1 Derivation procedure of the instantaneous transformation matrix

In this section, the procedure to derive the instantaneous transformation matrix is explained. The procedure requires the inverse Park transformation and the indirect transformation as given in equations (2.1) and (2.4).

The transformation matrix of equation (2.1) is denoted as $[C_1]$, and the transformation matrix in equation (2.4) is denoted as $[C_2]$. The matrices are expressed as in equations (2.7) and (2.8).

$$[C_1]=\begin{bmatrix}\cos\theta & -\sin\theta\\ \sin\theta & \cos\theta\end{bmatrix} \tag{2.7}$$

$$[C_2]=\sqrt{\frac{2}{3}}\begin{bmatrix}1 & 0\\ \frac{1}{2} & -\frac{\sqrt{3}}{2}\end{bmatrix} \tag{2.8}$$

The instantaneous transformation from voltage references V_d^* and V_q^* to V_A^* and V_B^* can be derived by the product of transformation matrices $[C_1]$ and $[C_2]$ as shown in equation (2.9).

$$\begin{bmatrix}V_A^*\\ V_B^*\end{bmatrix}=[C_2][C_1]\begin{bmatrix}V_d^*\\ V_q^*\end{bmatrix} \tag{2.9}$$

The instantaneous transformation matrix from voltage references V_d^* and V_q^* to voltage references V_A^* and V_B^* can be expressed as one matrix $[C_3]$ as in equation (2.10).

$$
\begin{aligned}
[C_3] &= [C_2][C_1] \\
&= \sqrt{\frac{2}{3}}\begin{bmatrix} \cos\theta & -\sin\theta \\ \cos\left(\theta+\frac{\pi}{3}\right) & \sin\left(\theta-\frac{2}{3}\pi\right) \end{bmatrix}
\end{aligned}
\tag{2.10}
$$

Equation (2.10) is the proposed instantaneous transformation matrix.

2.5.2 Derivation of voltage references from the proposed instantaneous transformation matrix

In this section, the derivation of voltage references V_A^* and V_B^* that have a phase difference of π/3 using the instantaneous transformation matrix [C_3] is shown in detail. From equations (2.9) and (2.10), the instantaneous transformation from voltage references V_d^* and V_q^* to voltage references V_A^* and V_B^* can be expressed as in equation (2.11).

$$
\begin{bmatrix} V_A^* \\ V_B^* \end{bmatrix} = [C_3]\begin{bmatrix} V_d^* \\ V_q^* \end{bmatrix} \tag{2.11}
$$

Equation (2.12) is given by substituting equation (2.10) into equation (2.11). Assuming $\theta = \omega t$, $V_d^* = \sqrt{3}V_m$, and $V_q^* = 0$, V_A^* and V_B^* can be expressed by equations (2.13) and (2.14).

$$
\begin{bmatrix} V_A^* \\ V_B^* \end{bmatrix} = \sqrt{\frac{2}{3}}\begin{bmatrix} \cos\theta & -\sin\theta \\ \cos\left(\theta+\frac{\pi}{3}\right) & \sin\left(\theta-\frac{2}{3}\pi\right) \end{bmatrix}\begin{bmatrix} V_d^* \\ V_q^* \end{bmatrix} \tag{2.12}
$$

$$
\begin{aligned}
V_A^* &= \sqrt{\frac{2}{3}}\left(V_d^*\cos\theta - V_q^*\sin\theta\right) \\
&= \sqrt{2}V_m\cos\omega t
\end{aligned}
\tag{2.13}
$$

$$
\begin{aligned}
V_B^* &= \sqrt{\frac{2}{3}}\left\{V_d^*\cos\left(\theta+\frac{\pi}{3}\right) + V_q^*\sin\left(\theta-\frac{2}{3}\pi\right)\right\} \\
&= \sqrt{2}V_m\cos\left(\omega t+\frac{\pi}{3}\right)
\end{aligned}
\tag{2.14}
$$

As shown in equations (2.13) and (2.14), voltage references V_A^* and V_B^* that have a phase difference of π/3 can be derived using the proposed instantaneous transformation matrix [C_3].

2.6 Verification of power invariance

In order to use the instantaneous transformation matrices in motor control, the power before and after the transformation must be constant. In this section, the power invariance of the proposed instantaneous transformation matrix is verified.

2.6.1 Absolute transformation

An absolute transformation is a coordinate transformation where using a transformation matrix[*C*], the power before and after the transformation is invariant [6]. If the transformation matrix [*C*] satisfies the relationship in equations (2.15), where the inverse matrix $[C]^{-1}$ is equal to the transposed matrix $[C]^t$, it is an absolute transformation [6]-[10].

$$[C]^{-1} = [C]^t \tag{2.15}$$

A transformation matrix that satisfies the condition of equation (2.15) is called a unitary matrix [6]-[10].

2.6.2 Verification of power invariance of the instantaneous transformation matrix (*dq→AB*)

In this section, the power invariance of the proposed instantaneous transformation matrix is verified. In order to verify the power invariance of the proposed transformation matrix, the relationship in equation (2.15) must be satisfied.

To calculate the inverse matrix, the transformation matrix must be a three-row and three-column matrix. Therefore, zero-phase sequence component voltage V_0 is added to the proposed instantaneous transformation matrix given in equation (2.10). The transformation matrix is then expressed as in equation (2.16).

$$\begin{bmatrix} V_A^* \\ V_B^* \\ V_0 \end{bmatrix} = \sqrt{\frac{2}{3}} \begin{bmatrix} \cos\theta & -\sin\theta & \frac{1}{\sqrt{2}} \\ \cos\left(\theta + \frac{\pi}{3}\right) & \sin\left(\theta - \frac{2}{3}\pi\right) & -\frac{1}{\sqrt{2}} \\ \cos\left(\theta - \frac{\pi}{3}\right) & \sin\left(\theta + \frac{2}{3}\pi\right) & -\frac{1}{\sqrt{2}} \end{bmatrix} \begin{bmatrix} V_d^* \\ V_q^* \\ V_0 \end{bmatrix} \tag{2.16}$$

The proposed instantaneous transformation matrix is denoted as $[C_{dq\text{-}AB}]$ and expressed as equation (2.17).

$$\left[C_{dq-AB}\right]=\sqrt{\frac{2}{3}}\begin{bmatrix}\cos\theta & -\sin\theta & \frac{1}{\sqrt{2}}\\ \cos\left(\theta+\frac{\pi}{3}\right) & \sin\left(\theta-\frac{2}{3}\pi\right) & -\frac{1}{\sqrt{2}}\\ \cos\left(\theta-\frac{\pi}{3}\right) & \sin\left(\theta+\frac{2}{3}\pi\right) & -\frac{1}{\sqrt{2}}\end{bmatrix} \tag{2.17}$$

The inverse matrix $[C_{dq\text{-}AB}]^{-1}$ is given by equation (2.18).

$$\left[C_{dq-AB}\right]^{-1}=\sqrt{\frac{2}{3}}\begin{bmatrix}\cos\theta & \cos\left(\theta+\frac{\pi}{3}\right) & \cos\left(\theta-\frac{\pi}{3}\right)\\ -\sin\theta & \sin\left(\theta-\frac{2}{3}\pi\right) & \sin\left(\theta+\frac{2}{3}\pi\right)\\ \frac{1}{\sqrt{2}} & -\frac{1}{\sqrt{2}} & -\frac{1}{\sqrt{2}}\end{bmatrix} \tag{2.18}$$

The transposed matrix $[C_{dq\text{-}AB}]^{t}$ can be expressed in equation (2.19).

$$\left[C_{dq-AB}\right]^{t}=\sqrt{\frac{2}{3}}\begin{bmatrix}\cos\theta & \cos\left(\theta+\frac{\pi}{3}\right) & \cos\left(\theta-\frac{\pi}{3}\right)\\ -\sin\theta & \sin\left(\theta-\frac{2}{3}\pi\right) & \sin\left(\theta+\frac{2}{3}\pi\right)\\ \frac{1}{\sqrt{2}} & -\frac{1}{\sqrt{2}} & -\frac{1}{\sqrt{2}}\end{bmatrix} \tag{2.19}$$

From the equations (2.18) and (2.19), it can be seen that the inverse matrix is identical to the transposed matrix and the condition for power invariance given in equation (2.15) is satisfied. Therefore, the proposed instantaneous transformation matrix is a unitary matrix. The transformation is an absolute transformation.

2.7 Conclusion

In this chapter, an instantaneous transformation matrix for vector control of two-phase inverter-fed AC motor drives was proposed. The derivation procedure of the proposed transformation was explained in detail. The proposed transformation matrix can instantaneously transform the output voltage references of vector control V_d^* and V_q^* in rotating coordinates to voltage references $V_A^*$and V_B^* in stationary coordinates that have a phase difference of $\pi/3$.

Furthermore, the power invariance of the proposed instantaneous transformation matrix was verified. This verification indicates that the proposed transformation matrix can be used in motor control. The effectiveness of the proposed instantaneous transformation matrix is verified by simulation and experiment in the next chapter.

References

1. B. Hua, Z. Zhengming, M. Shuo, L. Jianzheng, and S. Xiaoying: “Comparison of three PWM strategies – SPWM, SVPWM & one-cycle control”, *IEEE Int. Conf. on Power Electronics and Drive Systems (PEDS)*, Vol.2, pp.1313-1316(2003)
2. J. Sabarad and G.H. Kulkarni: “Comparative analysis of SVPWM and SPWM techniques for multilevel inverter”, *IEEE International Conference on Power and Advanced Control Engineering (ICPACE)*, pp.232-237(2015)
3. J.Pradeep and R. Devanathan: “Comparative analysis and simulation of PWM and SVPWM inverter fed permanent magnet synchronous motor”, *IEEE Int. Conf. on Emerg.Trends in Elec.Eng. and Energy Manag. (ICETEEEM)*, pp.299-305(2012)
4. Q.T. An, L. Sun, K. Zhao, and T.M. Jahns: “Scalar PWM algorithms for four-switch three-phase inverters”, *IET Electronics Letters*, Vol.46, pp.900-902(2010)
5. Y. Liu, X. Ge, J. Zhang, and X. Feng: “General SVPWM strategy for three different four switch three phase inverters”, *IET Electronics Letters*, Vol.51, No.4, pp.357-359(2015)
6. 電気学会・センサレスベクトル制御の整理に関する調査専門委員会：「AC ドライブシステムのセンサレスベクトル制御」、オーム社、pp.49-50(2016)
7. 電気学会大学講座執：「基礎電気機器学」、オーム社、pp.88-90(2006)
8. 宮入庄太：「電気・機械エネルギー変換工学」、丸善株式会社、pp.135-145(1976)
9. 松瀬貢規：「電動機制御工学―可変ドライブの基礎」、オーム社、pp.20-29(2007)
10. 森本茂雄、真田雅之：「省エネモータの原理と設計法」、科学技術出版株式会社、pp.35-40(2013)
11. U. U. Ekong, M. Inamori, and M. Morimoto: “Field Oriented Control of Two Phase Inverter to drive a Three Phase Induction Motor” *IEEE International Conference on Electrical Machines and Systems (ICEMS)*, pp.125-128(2015)
12. U.U. Ekong, M. Inamori, and M. Morimoto: “Field Oriented Control of Two Phase Inverter to drive a Three Phase Induction Motor”, *IEEJ Industry Applications Division Annual Convention (JIASC)*, Y-132(2015) *(In Japanese)*
13. U.U. Ekong, M. Inamori, and M. Morimoto: “Instantaneous Vector Control of Four Switch Three Phase Inverter fed Induction motor drive”, *IEEE International Conference on Electrical Machines and Systems (ICEMS)*, pp.125-128(2016)
14. U.U. Ekong, T. Shiraishi, M. Inamori, and M. Morimoto: “Derivation of Transformation Matrix for 3 phase vector control of a 2 phase Inverter” *IEEJ National Annual Convention*, Vol.4, pp.46-47(2017) *(In Japanese)*
15. T. Shiraishi, U.U. Ekong, M. Inamori, and M. Morimoto: “Instantaneous Co-ordinate Transformation of a vector controlled 2 Phase Inverter fed 3 Phase Induction Motor Drive”, *IEEJ Industry Applications Division Annual Conference (JIASC)*, Y-106(2017) *(In Japanese)*
16. U.U. Ekong, M. Inamori, and M. Morimoto: “Instantaneous Vector Control of Four Switch Three Phase Inverter fed Induction motor drive” *IEE Japan Trans.* of *Industry Applications*, Vol.6, No.6, pp.429-434(2017)

Chapter 3

Evaluation of proposed transformation matrix for vector control of two-phase inverter

3.1 Introduction

In this chapter, the proposed transformation matrix is verified by simulation and experiment. The conventional indirect vector control method is used for the verification of the proposed transformation matrix. Furthermore, the performance of the two-phase inverter-fed induction motor drive is evaluated by experiment.

Vector control of inverter-fed AC motor drives is well known to have instantaneous dynamic control of speed and torque [(1)-(3)]. Hence, both by simulation and experiment, the dynamic performance of the motor driven by the two-phase inverter with the proposed transformation matrix is examined at various speeds and load conditions.

Most of the reported literature on two-phase inverters focused on the VVVF control method and literature on the vector control method are rarely seen [(4)(5)]. For this reason, the difference between the performance characteristics of vector-controlled two-phase and three-phase inverters are yet to be reported in detail. In this chapter, a comparison of vector-controlled two-phase and three-phase inverter-fed induction motor drives is performed. The experiment focuses on the maximum output voltage, torque-speed characteristics, and motor efficiency. Subsequently, a comparison between the motor characteristics of the vector-controlled and the VVVF-controlled two-phase inverter-fed induction motor drives is performed.

Finally, a comparison of the proposed method in this dissertation and the previous method in literature for vector control of two-phase inverter-fed induction motor drives is performed by experiment.

3.2 Verification by simulation

In this section, the effectiveness of the proposed transformation matrix for vector control of two-phase inverter-fed AC motor drives is verified by simulation. A simulation model of the indirect vector control method with the proposed transformation matrix is implemented.

3.2.1 Simulation model

The block diagram of the circuit for simulation is shown in Fig. 3.1. The diagram includes the proposed transformation matrix from *dq* axis to *AB* axis. The basic equations of the indirect vector control method are shown from equations (3.1) to (3.3). Where, Ψ is the rated flux, L_m is the

magnetizing inductance, L'_2 is the rotor leakage inductance, R'_2 is the rotor resistance, T^* is the electromagnetic torque command, and P is the number of pair poles.

$$I_d^* = \frac{\psi}{L_m} \tag{3.1}$$

$$I_q^* = \frac{4}{3}\frac{L'_2 T^*}{PL_m\psi} \tag{3.2}$$

$$\omega_s^* = \frac{L_m R'_2}{L'_2 \psi} I_q^* \tag{3.3}$$

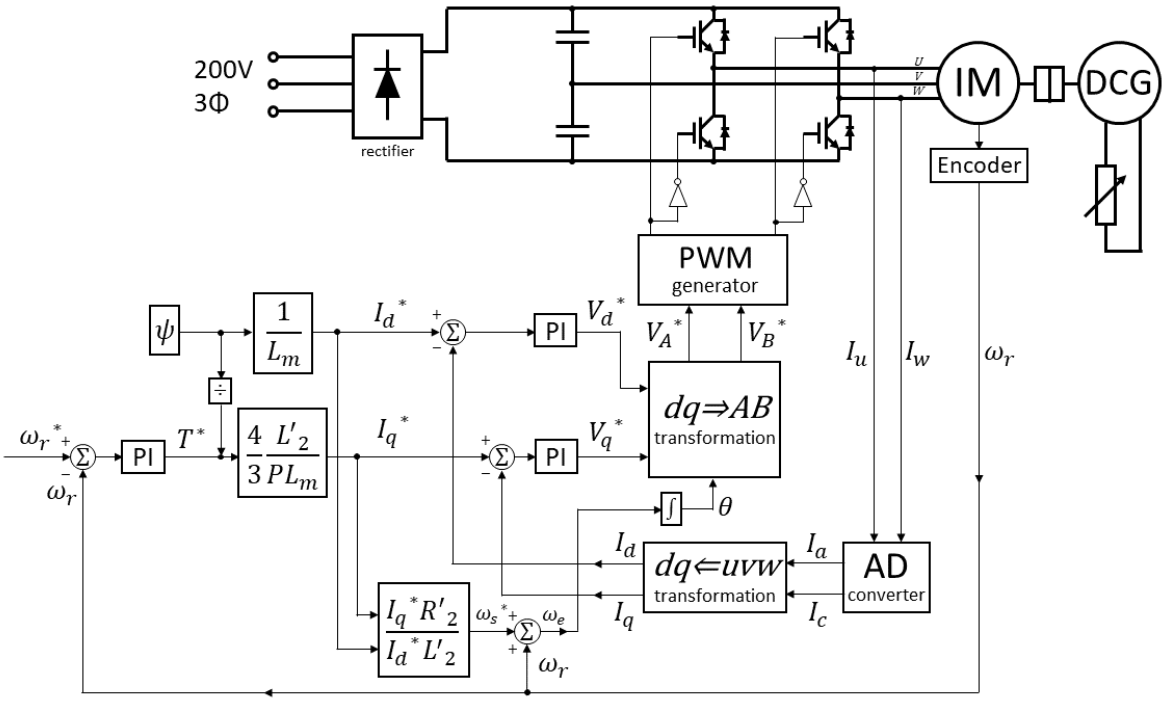

Fig. 3.1 Block diagram of simulation model

The simulation was conducted using PSIM software. PSIM is an electric circuit simulation software developed for power electronics and motor control. PSIM is used for power electronics analysis, control system circuit design, inverter, motor drive research, and so on. Compared to other simulation softwares, PSIM can perform high-speed simulations with a simple user interface.

Vector control accomplishes instantaneous commutation with velocity feedback signal ω_r from the motor and feedforward slip command ω_s. The motor currents are decomposed into the magnetizing flux component current (d-axis) I_d and torque component current (q-axis) I_q. As shown in Fig. 3.1, the speed

reference ω_r^*, d-axis reference I_d^*, and q-axis reference I_q^* are compared to their feedback values, and their errors are processesed through a PI(Proportional Integral) controller. The output voltage references V_d^* and V_q^* are transformed to voltage references V_A^* and V_B^* using the proposed transformation matrix. The voltage references V_A^* and V_B^* are used to generate PWM signals that are transmitted to the inverter. In this indirect vector control method, the d-axis reference I_d^* is kept constant.

In the simulation, it was assumed that the *V*-phase switches of the inverter were short-circuited, and the wiring to the *V*-phase of the motor was reconnected to the midpoint of the DC source. The main circuit consists of four IGBT switches which were considered as ideal switches.

3.2.2 Simulation parameters

The simulation parameters are shown in Table 3.1. The equivalent circuit of the induction motor used in the simulation is shown in Fig. 3.2. Table 3.2 shows the equivalent circuit constants.

Table 3.1 Simulation conditions

Parameter	Symbol	Value
Reference Speed	N[min^{-1}]	100 – 2000
Carrier Frequency	f_c[Hz]	5000
Dead Time	T_d[μs]	4
Power Supply Voltage	V[V]	200
Power Supply frequency	f[Hz]	50
Capacitors	C[μF]	8200
Encoder	[p/r]	1000

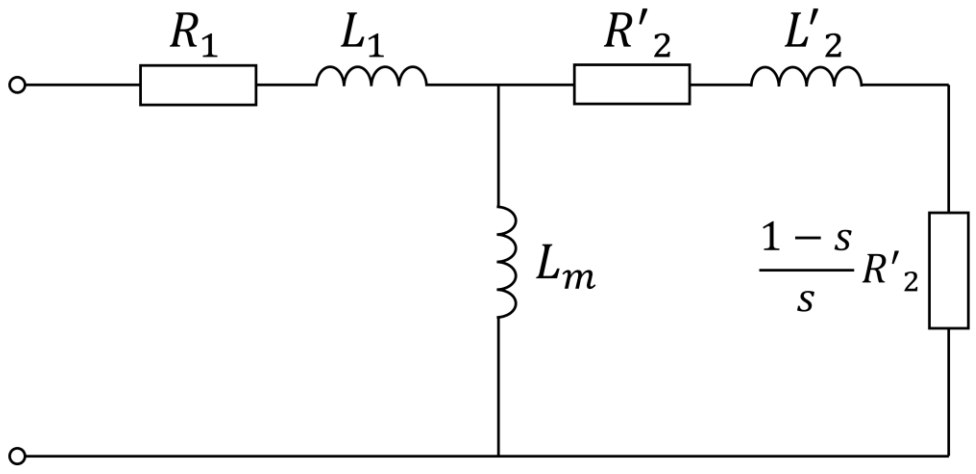

Fig. 3.2 Equivalent circuit of induction motor

Table 3.2 Equivalent circuit constants of the motor

Name	Symbol	Value
Stator resistance	$R_1[\Omega]$	12.8
Stator Leakage Inductance	L_1[H]	0.033645354
Rotor resistance	$R'_2[\Omega]$	10.17
Rotor Leakage Inductance	L'_2[H]	0.033645354
Magnetizing Inductance	L_m[H]	0.553222582
Poles	P	4
Moment of Inertia	J[Kg.m^2]	0.0004

3.2.3 Simulation results

The simulation was conducted in the speed control mode. The speed reference was set from 100 min^{-1} to 2000 min^{-1} and the load torque was set from 0 Nm – 1.49 Nm (0 % to 100% of the rated torque).

3.2.3-1 Voltage references

The output voltage references V_A^* and V_B^* for the two-phase inverter during operation at motor speed 400 min^{-1} and load torque 1.49 Nm are shown in Fig. 3.3. The results show that the proposed transformation matrix can generate the voltage references V_A^* and V_B^* that have a phase difference of $\pi/3$.

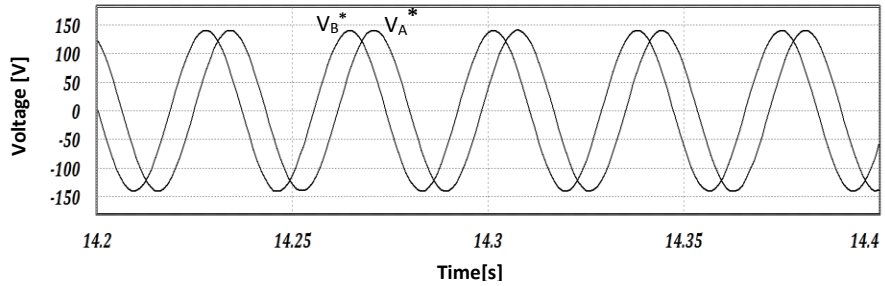

Fig. 3.3 Voltage references (simulation)

3.2.3-2 Motor current waveforms

The current waveforms at 400 min^{-1} and 1.49 Nm are shown in Fig. 3.4. From the results, it can be seen that the balanced three-phase motor currents waveforms can be obtained using the proposed transformation matrix.

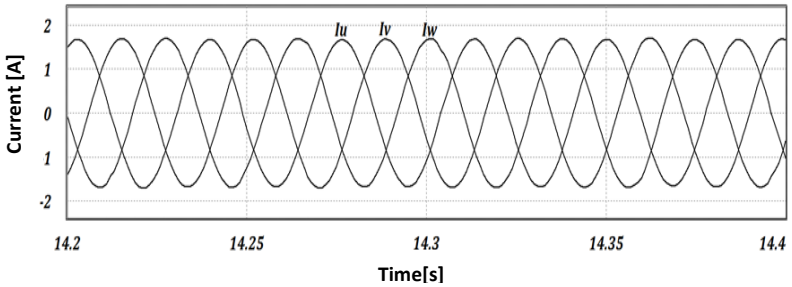

Fig. 3.4 Motor current waveforms (simulation)

3.2.3-3 Response characteristics

The response characteristics of the drive in various speed and load conditions are examined. Figure 3.5 shows speed response to a step change in speed reference. The speed reference was increased after 3 seconds from 500 min^{-1} to 1000 min^{-1} at full load condition. The result shows the motor speed reaches its reference speed in less than 0.5 seconds with negligible oscillations.

The speed response to a step increase in load torque is also examined as shown in Fig. 3.6. At start-up operation, the motor speed reference is set at 400 min^{-1} and load torque at 0 Nm. After 4 seconds, the load torque was stepped up from 0 Nm to 1.49 Nm (rated torque). From the result, it can be seen that the speed slightly falls but recovers in few seconds when load torque is increased. Furthermore, the three-phase motor current amplitude increased in order to handle the increase in load torque. These results demonstrate the drive has the fast speed response characteristics in different load conditions.

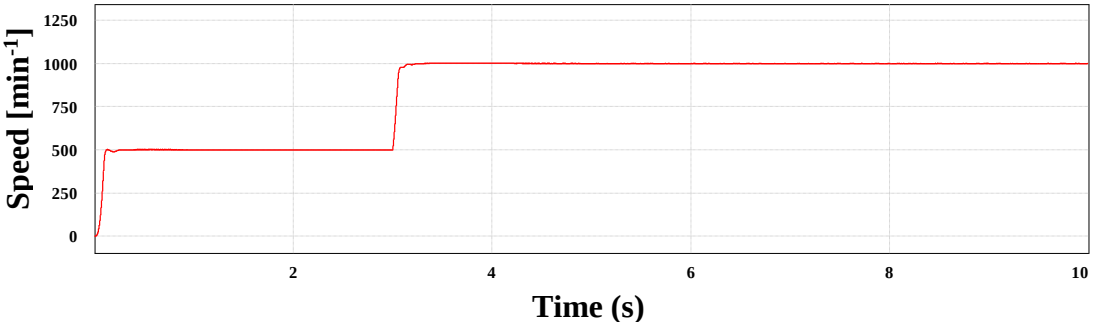

Fig. 3.5 Speed response to step change in speed reference (simulation)

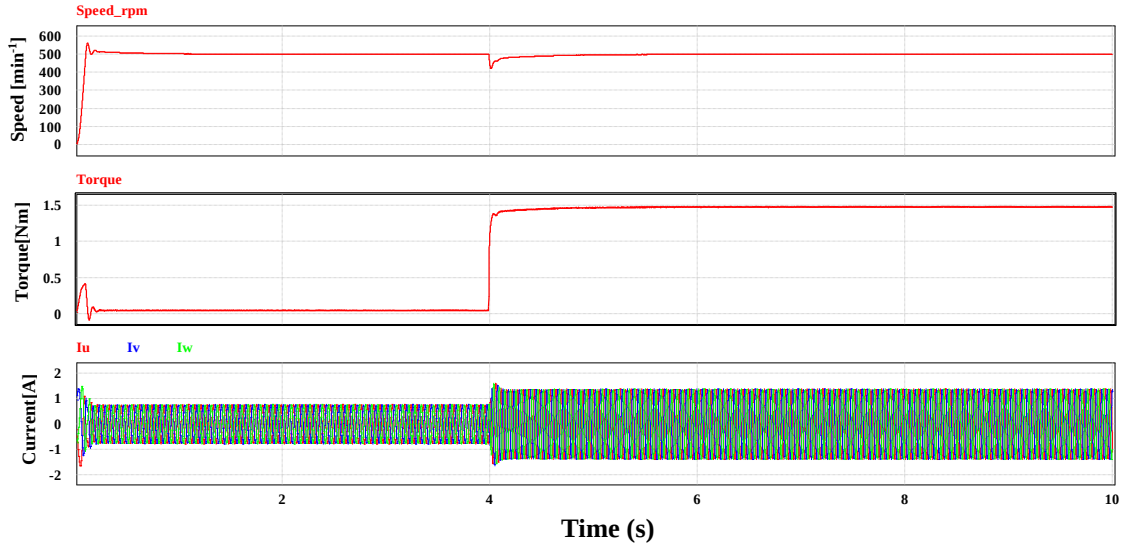

Fig. 3.6 Speed response to step increase in load (simulation)

3.2.3-4 Torque-speed characteristics

The torque-speed characteristics of the vector controlled two-phase and three-phase inverter-fed induction motor drives are shown in Fig. 3.7. In the simulation, the speed reference was increased from 100 min^{-1} to 2000 min^{-1} by steps of 100 min^{-1} and the maximum attainable torque at each speed was measured.

The results indicate that both the two-phase and three-phase inverter drives can produce full torque in the low-speed region (100 min^{-1} to 600 min^{-1}). However, from the middle-speed region approximately 700 min^{-1} and above, the maximum attainable torque of the two-phase inverter drive reduces compared to the three-phase inverter drive.

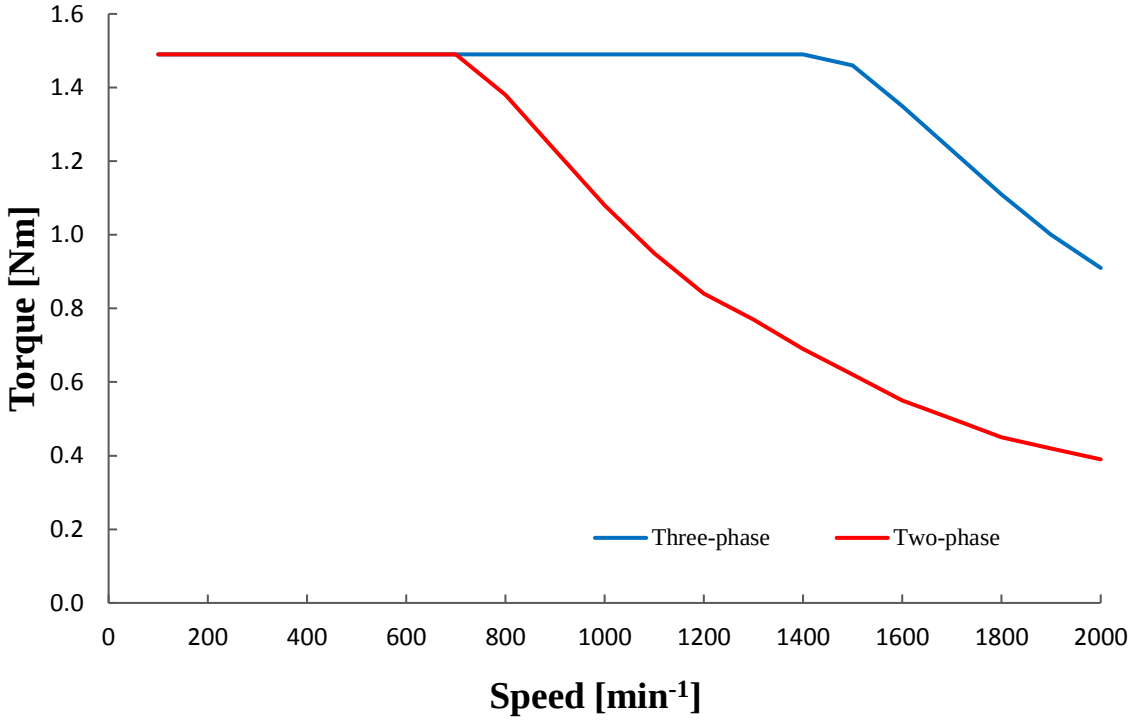

Fig. 3.7 Torque-speed characteristics (simulation)

3.2.4 Summary of simulation results

The simulation results show that;

i. Instantaneous derivation of the voltage references V_A^* and V_B^* that have a phase difference of $\pi/3$ is achievable.
ii. Instantaneous speed control and response are achievable irrespective of a step change in load.
iii. In the two-phase inverter drive, the maximum speed at which the rated torque can be produced reduces by approximately 50% compared to the three-phase inverter drive.

3.3 Validation by experiment

In the previous section, the effectiveness of the proposed transformation matrix was verified by simulation. In this section, the simulation results are validated by experiment.

3.3.1 Experimental setup

In the experiment, the *V*-phase of the motor was connected to the midpoint of the DC source. The specification of the induction motor and the inverter parameters are shown in Table 3.3. The same inverter parameters were used for both the two-phase and three-phase inverter experiments.

The block diagram of the experiment system is shown in Fig. 3.8. PE-Expert 3 is a digital system that is equipped with a Digital Signal Processor (DSP) which has an Analog Digital (AD) converter and PWM function. The program signals are transmitted from the host computer to the DSP of the PE-Expert3. A DC generator was used as the load.

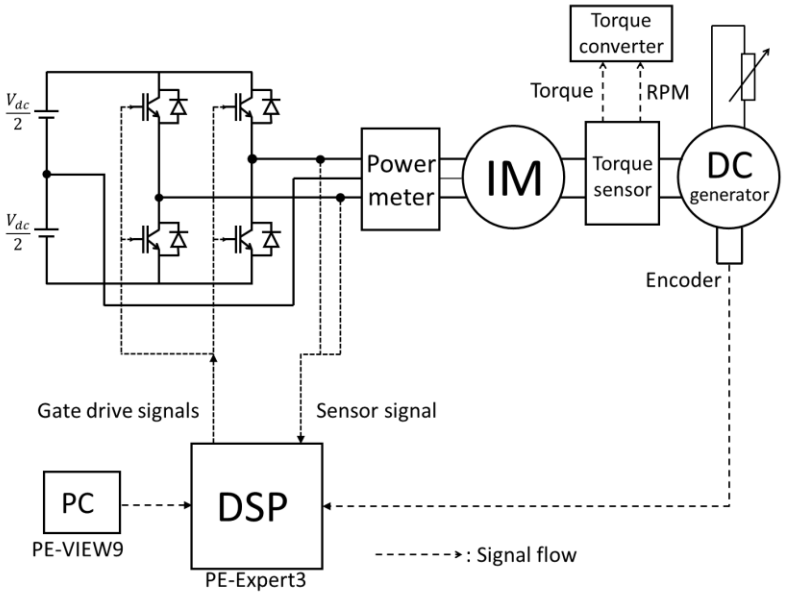

Fig. 3.8 Experiment system

Table 3.3. Motor and inverter parameters

Induction Motor	Rated power	p	200	[W]
	Rated frequency	f	50	[Hz]
	Rated speed	n	1250	[min^{-1}]
	Rated torque	T	1.49	[Nm]
	Rated voltage	V	200	[V]
	Rated current	I	1.1	[A]
	Number of poles	P	4	[poles]
Inverter	DC link voltage	V	283	[V]
	Filter capacitor	C	8200	[μF]
	Carrier frequency	f_c	10	[kHz]
	Dead time	DT	3.5	[μs]

3.3.2 Experimental results

3.3.2-1 Voltage references

Figure 3.9 shows the waveforms of the voltage references V_A^* and V_B^* at a motor speed 500 min^{-1} and a rated torque 1.49 Nm. The results illustrates that voltage references V_A^* and V_B^* that have a phase difference of $\pi/3$ can be generated using the proposed transformation matrix.

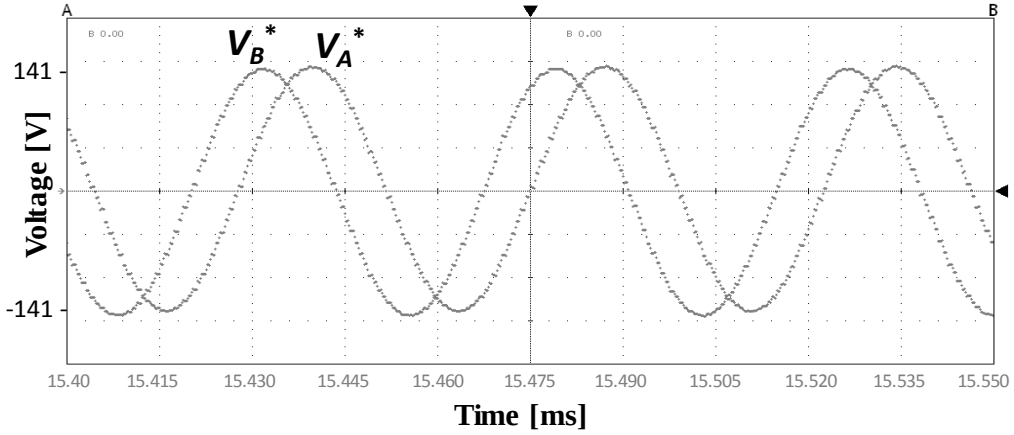

Fig. 3.9 Voltage references (experiment)

3.3.2-2 Motor current waveforms

The waveforms of the three-phase motor currents at 500 min^{-1} and 1.49 Nm are shown in Fig. 3.10. As seen in Fig. 3.10, balanced three-phase motor currents can be obtained using the proposed transformation matrix.

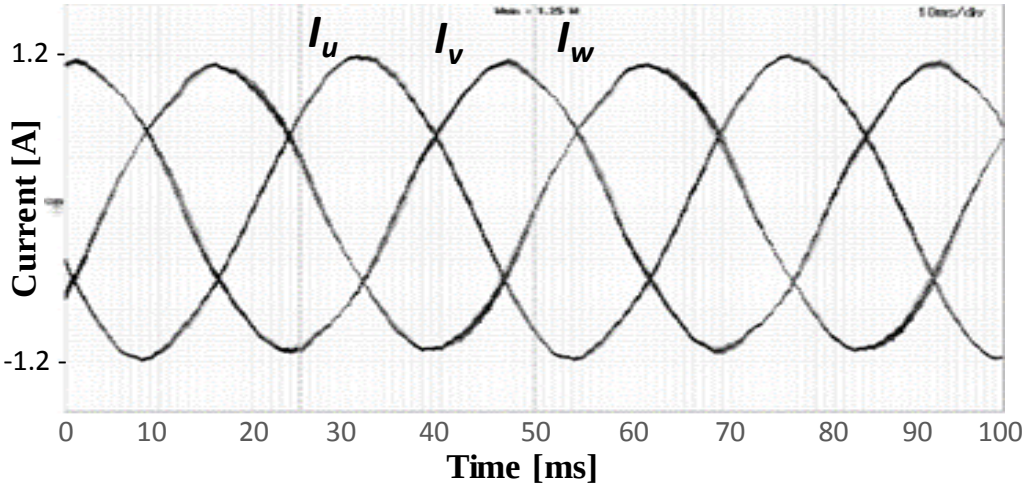

Fig. 3.10 Motor current waveforms (experiment)

3.3.2-3 Response characteristics

The response characteristics of the two-phase inverter-fed induction motor drive system are evaluated in different load conditions. The speed reference was set at a constant 500 min^{-1}, and the load torque was varied from no load to 1.49 Nm (0% to 100%). The speed response to a step change in load is shown in Fig. 3.11. Due to a mechanical loss in the experiment system, in a no-load condition, a torque of 0.17 Nm is generated.

At startup condition, the load was set at 0%, after 6 seconds, the load torque is increased from 0% to 100% as shown in Fig. 3.11. The results illustrate that the motor speed slightly falls below the speed reference but recovers instantaneously as the load torque increases. The load torque was also reduced from 100% to 0% and increased from 0% to 100% repeatedly. The result shows that when the load torque reduces, the speed slightly increases above its reference (500 min^{-1}) and returned to its reference in less than 1 second.

From these results, it is clear that instantaneous speed response is achievable in different load conditions using the proposed transformation matrix.

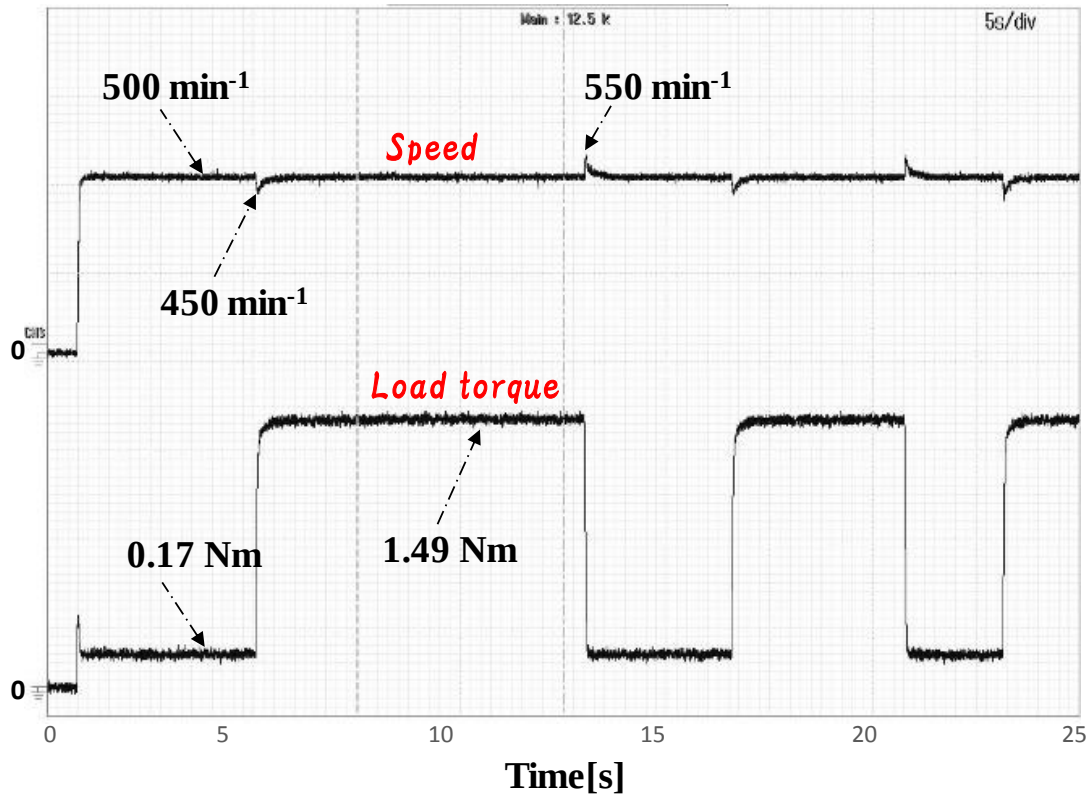

Fig. 3.11 Speed response of two-phase inverter drive

3.3.2-4 Torque-speed characteristics

The torque-speed characteristics of the two-phase inverter-fed induction motor drive are shown in Fig. 3.12. For comparison purposes, the result of the conventional three-phase inverter drive is also shown in Fig. 3.12. The maximum torque was set at 1.49 Nm (rated torque). The experiment results show that;

1. From zero speed region to middle-speed region (approx. 700 min^{-1}) in both the two-phase inverter and three-phase inverter drives, the same torque can be obtained.
2. In the two-phase inverter drive, the maximum speed at which the maximum torque (1.49 Nm) can be produced is approximately 700 min^{-1}. However, in the three-phase inverter drive, maximum torque can be produced up to approximately 1400 min^{-1}. Compared to the three-phase inverter drive, the maximum torque attainable speed of the two-phase inverter drive reduces. This reduction is because the maximum output voltage of two-phase inverter drives compared to three-phase inverter drives reduces by a factor of $1/\sqrt{3}$.
3. Compared to the simulation results, both the two-phase and three-phase inverter drives cannot produce the maximum torque from 0 min^{-1} to approximately 350 min^{-1}. The reason for the low-torque production below 350 min^{-1} will be explained later in this chapter.

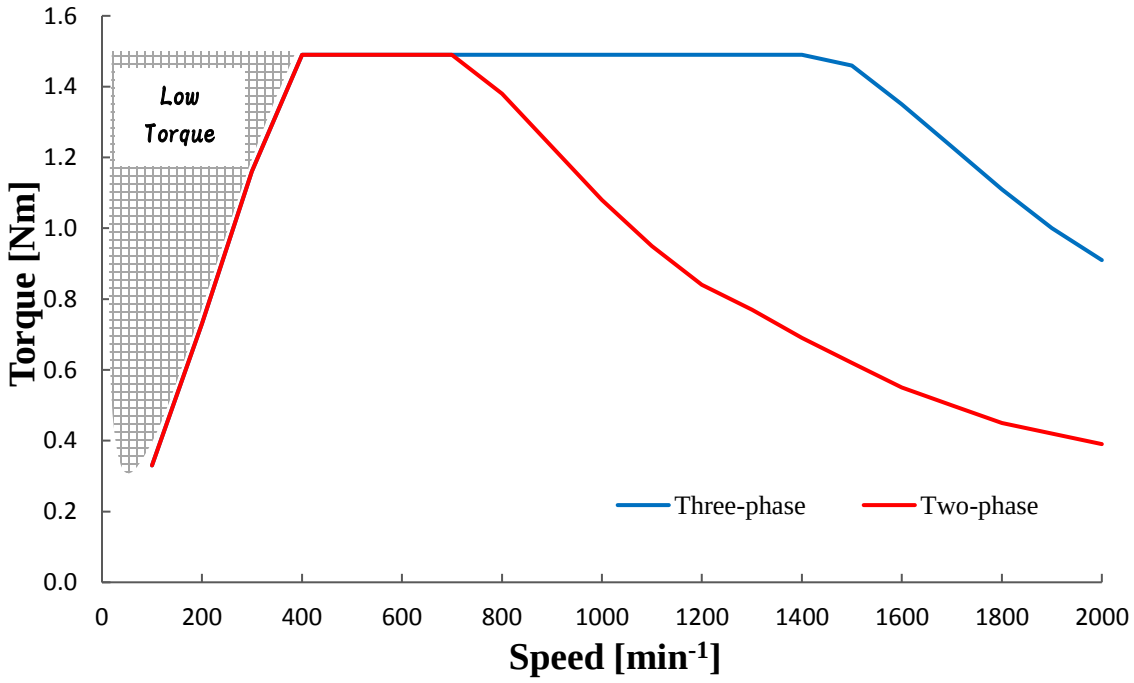

Fig. 3.12 Torque-speed characteristics (experiment)

3.3.2-5 Maximum output voltage

The output line voltage of both the two-phase and the three-phase inverter drives at the maximum attainable torque (Fig. 3.12) of each speed from 0 min^{-1} to 2000 min^{-1} was measured. As shown in Fig. 3.13, from the low-speed region to approximately 700 min^{-1}, the output line voltage of both the two-phase and three-phase inverter drives are the same. The maximum output voltage of the two-phase inverter drive is attained at a lower speed compared to the three-phase inverter drive.

The maximum line output voltages (fundamental value) of the two-phase and three-phase inverters are 98.1V and 171V, respectively. From this result, it can be said that the maximum output voltage of two-phase inverter drives reduces by a factor of $1/\sqrt{3}$, compared to the three-phase inverter drives.

The output voltage results agree with the working principle (theory) of two-phase inverters explained in Chapter 1.

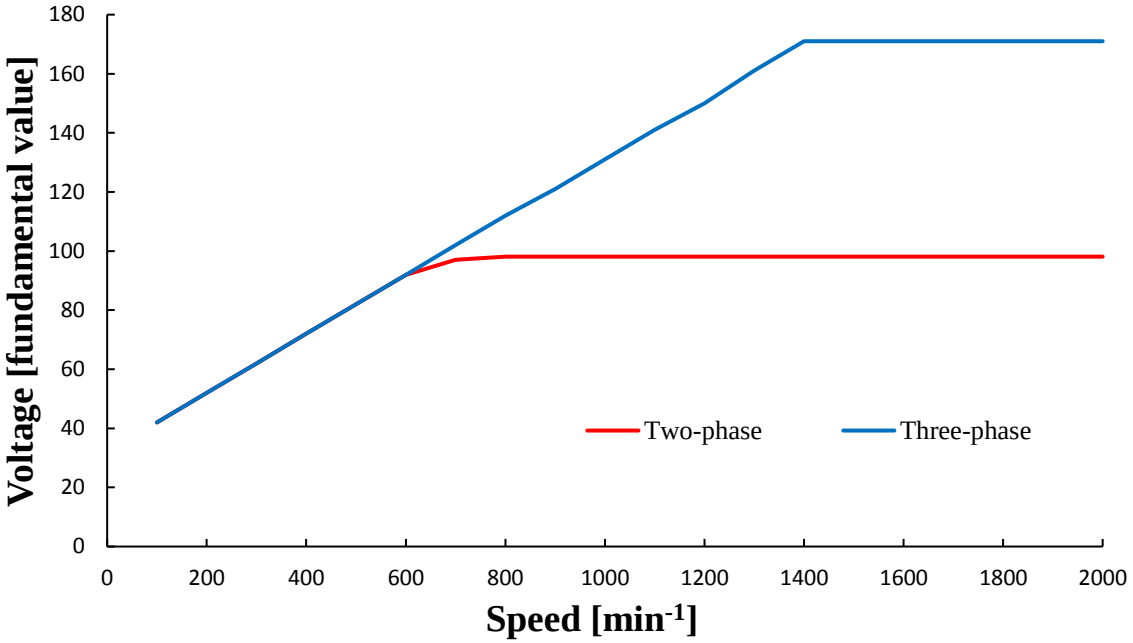

Fig. 3.13 Output voltage of two-phase and three-phase inverter drives

3.3.2-6 Motor efficiency

The efficiency of the motor driven by the two-phase inverter and the three-phase inverter is examined. The motor efficiency formula is shown below in equation (3.5). The input power was read from the power meter used in the experiment. The output power was calculated from the speed and torque of the motor as shown in equation (3.6). The maximum torque was set to 1.49 Nm which is the rated torque of the induction motor. In the experiment, the torque was increased by steps of 0.1 Nm from 0 Nm to the maximum attainable torque at each speed, and all data points were recorded.

$$Motor\ Efficiency\ \ [\%] = \frac{Power\ Out}{Power\ In} \times 100 \tag{3.5}$$

$$Power\ Out\ [W] = Speed\left[\frac{rad}{s}\right] \times Torque\,[Nm] \tag{3.6}$$

The motor efficiency was evaluated using a motor efficiency map. An efficiency map is a 2-D plot of the efficiency and torque of the motor versus its rotation speed which facilitates easier evaluation of all possible operating points of the motor.

From the experimental results, the motor efficiency maps of both the two-phase and three-phase inverter drives were plotted using MATLAB as shown in Figs. 3.14 and 3.15, respectively. A comparison of the results shows that both the two-phase and the three-phase inverter drives have similar motor efficiency from 0 min^{-1} to approximately 550 min^{-1}. However, above 550 min^{-1}, the three-phase inverter drive can achieve higher motor efficiency over a wider speed range. The motor efficiency in the entire low-speed region was not measurable because of the inadequacy of the experimental apparatus.

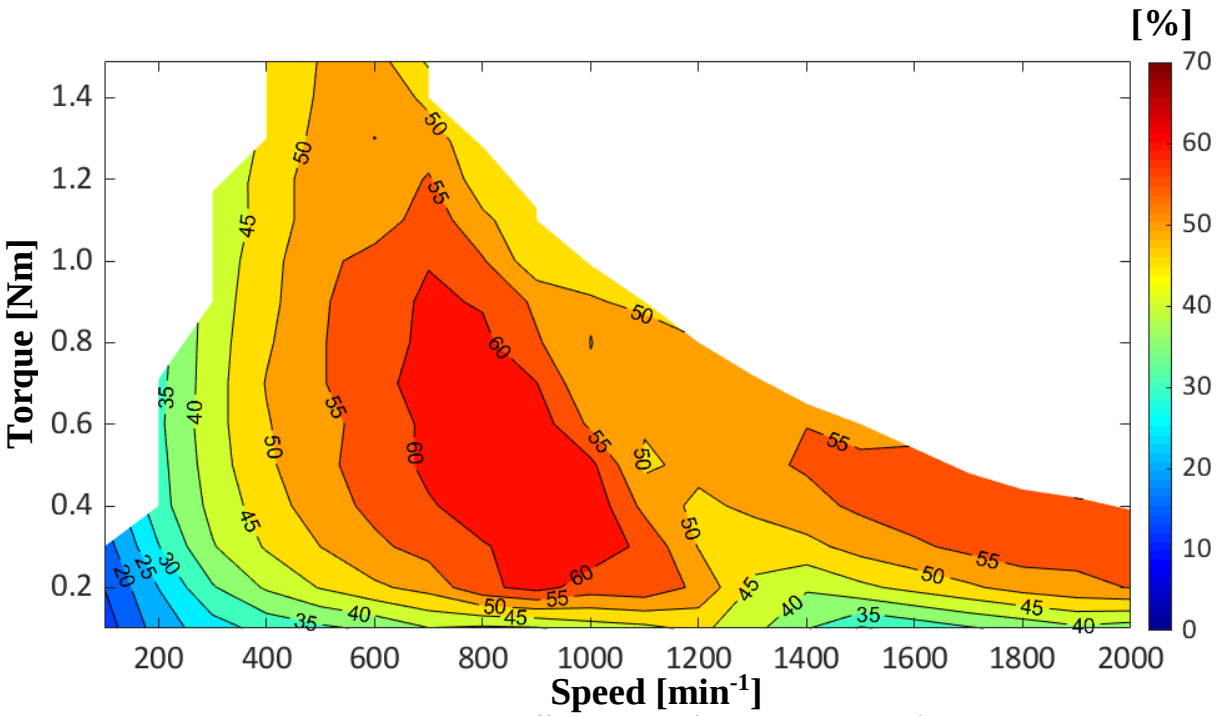

Fig. 3.14 Motor efficiency map (two-phase inverter)

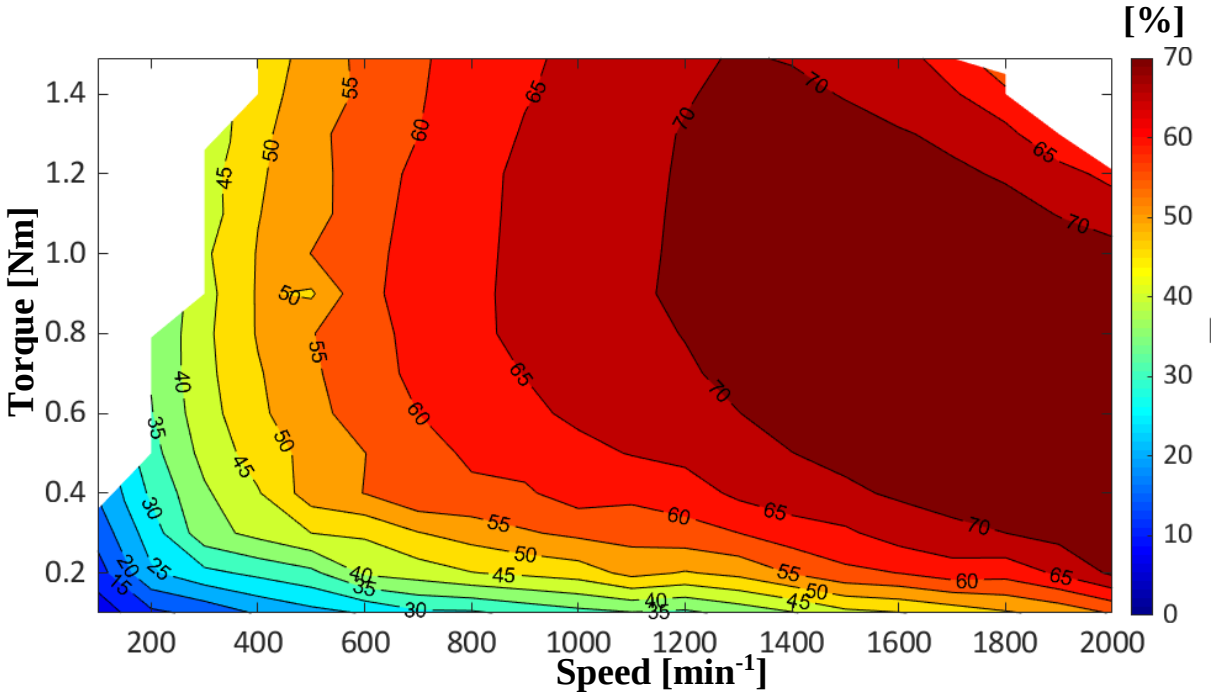

Fig. 3.15 Motor efficiency map (three-phase inverter)

3.4 Load torque measurement system improvement

The experimental results in section 3.3 showed an inadequacy of torque from zero speed to approximately 350 min^{-1}. Due to this inadequacy, the torque-speed characteristics and the motor efficiency in the entire low-speed region could not be examined.

As explained in Chapter 1, vector-controlled inverter-fed AC motor drives can produce full torque from zero speed. In order to utilize the two-phase inverter as an emergency strategy for electric vehicles, the torque-speed characteristics of the entire operating region must be evaluated. Therefore, it was necessary to investigate the reasons for the inadequacy of torque in the low-speed region.

The low torque production problem could have been from the software (control) or hardware (experimental apparatus) used in the experiment. The experimental system had to be investigated. As a result, it was discovered that the reason for low torque in the low-speed region was the load of the experimental apparatus. Thus, the load system was improved.

3.4.1 Load system

In order to evaluate the performance of inverter-fed motor drives, the load system must be accurately picked. Under-sizing and over-sizing of the load system have a significant impact on the torque characteristics and efficiency of the driving motor which is the IM in this dissertation.

As explained in section 3.2.1, in indirect vector control, an encoder is used to measure the speed at which the driving motor is running, and the speed is fed back to the control circuit. Figure 3.16 shows an IM with a DC generator load. Here, the encoder can be attached to either the back of the IM or the DC generator, because the shaft is rotating at the same angle and velocity. From the experimental results in Figs. 3.12, 3.14 and 3.15, this load system cannot provide adequate torque and efficiency measurement in the low-speed region because of the characteristics of the DC generator (Load machine).

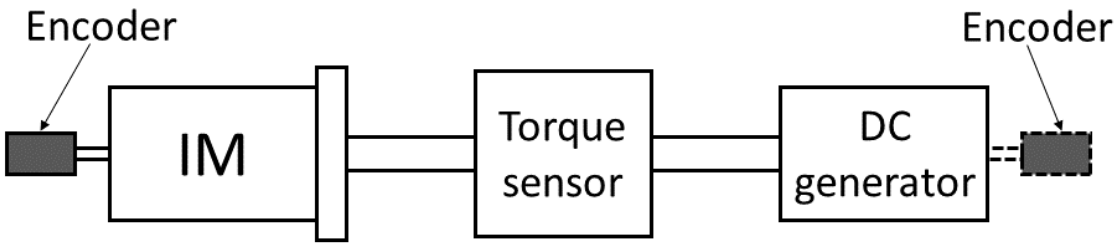

Fig. 3.16 Induction motor with a DC generator load

3.4.2 Improved load system

In this section, the load system for the vector-controlled inverter-fed induction motor drive is improved. The load system is improved by adding a gear to the DC generator. Generally, gears take the driving motor power, reduces its speed, and magnifies its torque. In this application, the encoder must be connected to the IM (driving motor) because the speed at the shaft of the IM and the load machine (DC generator) is different.

In order to choose a reduction gear that is appropriate for this experiment, the gear ratio was considered. From calculations, a gear ratio of 1:5 is appropriate for the drive. A gear that is suitable for the drive was selected, and its specification is shown in Table 3.4. The gear is connected to the DC generator as shown in Fig. 3.17 (a). A photo of the improved load system is shown in Fig. 3.17 (b), where a Torque Sensor (TS) is connected in between the IM and the improved load system.

It is important to note that, if the improved experiment load system in Fig. 3.17 is proposed for a VVVF controlled two-phase inverter drive, the torque-speed characteristics in the low-speed region will be the same as the results in Fig. 3.12. This is because only the voltage and frequency can be controlled in the VVVF control method. Thus, motor currents that lead to increase in torque production cannot be controlled.

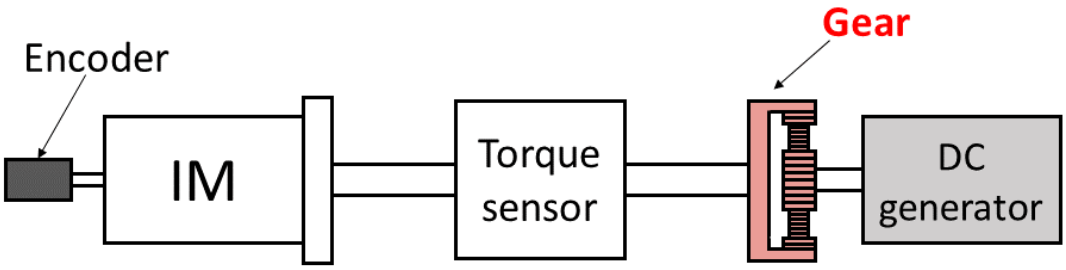

(a) Geared DC generator load

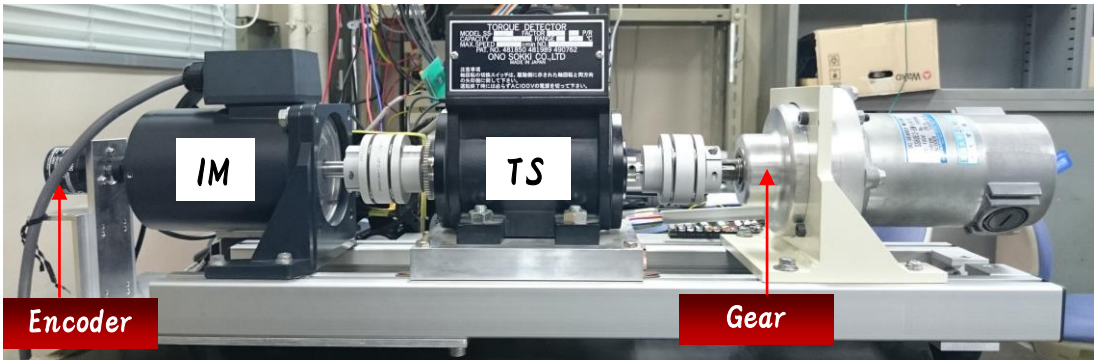

(b) Photo of geared DC generator load

Fig. 3.17 Improved experiment load system

3.4.3 Experimental setup with improved load system

In this section, the effectiveness of the improved load system is verified by experiment. In the experiment, the *V*-phase of the inverter was assumed to be broken down, and its wiring was reconnected to the center potential of the DC source. The specification of the induction motor and inverter parameters are the same as shown in Table 3.3. The configuration of the experiment system with the improved load system is shown in Fig. 3.18. The differences in the experiment systems are the position of the encoder and the proposed load system.

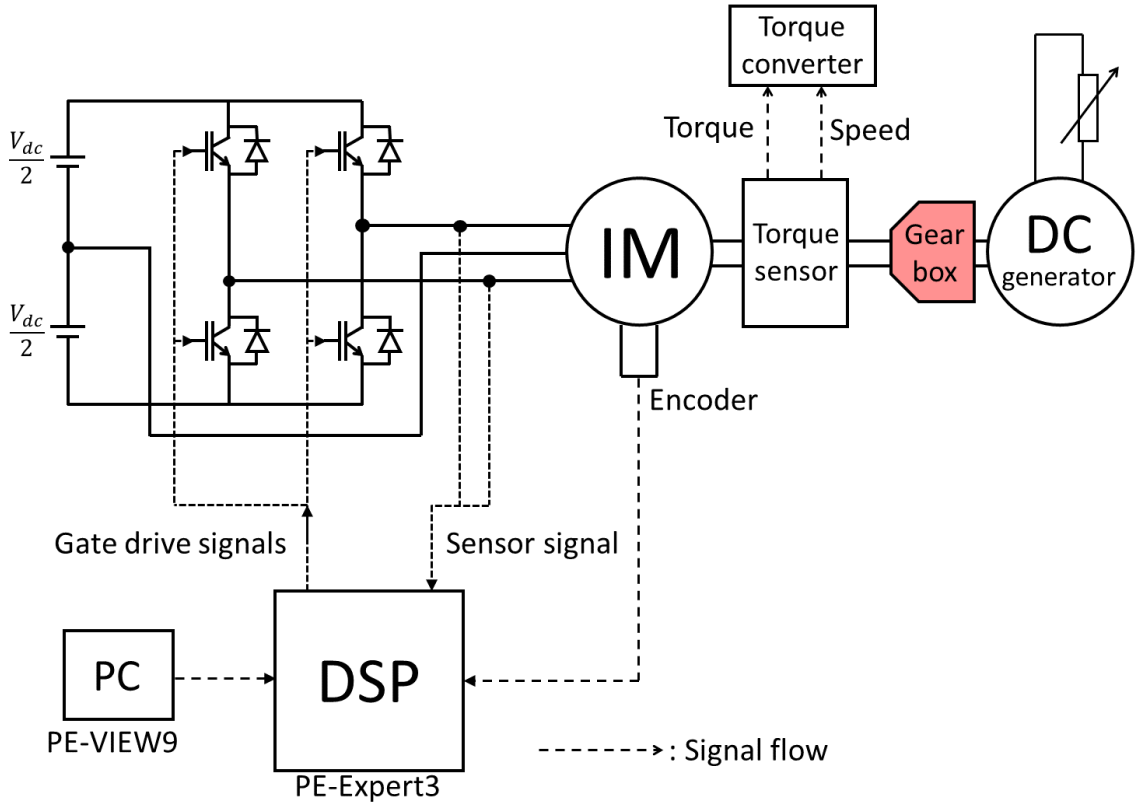

Fig. 3.18 Experiment system (improved load system)

Table 3.4. Specification of geared DC motor

Gear	Gear ratio	*GR*	1:5	[mG]
DC Motor	Rated speed	*n*	2500	[min^{-1}]
	Rated voltage	*V*	100	[V]
	Armature current	*I*	4.8	[A]
	Armature resistance	*R*	2.4	[Ω]

3.4.4 Torque-speed characteristics

3.4.4-1 Comparison of geared DC generator and gearless DC generator

The torque-speed characteristics of the two-phase inverter-fed induction motor drive are evaluated using the improved load system (geared DC generator). The speed range was set from 50 min^{-1} to 500 min^{-1} and the maximum torque at 1.49 Nm (rated torque). The torque-speed characteristics of the improved load system are shown in Fig. 3.19. For comparison purposes, the result of the gearless DC generator load system from 50 min^{-1} to 2000 min^{-1} is also shown in Fig. 3.19.

The results show that the geared DC generator (improved load system) can produce the maximum torque even in the low-speed region from 0 min^{-1} to 400 min^{-1}.

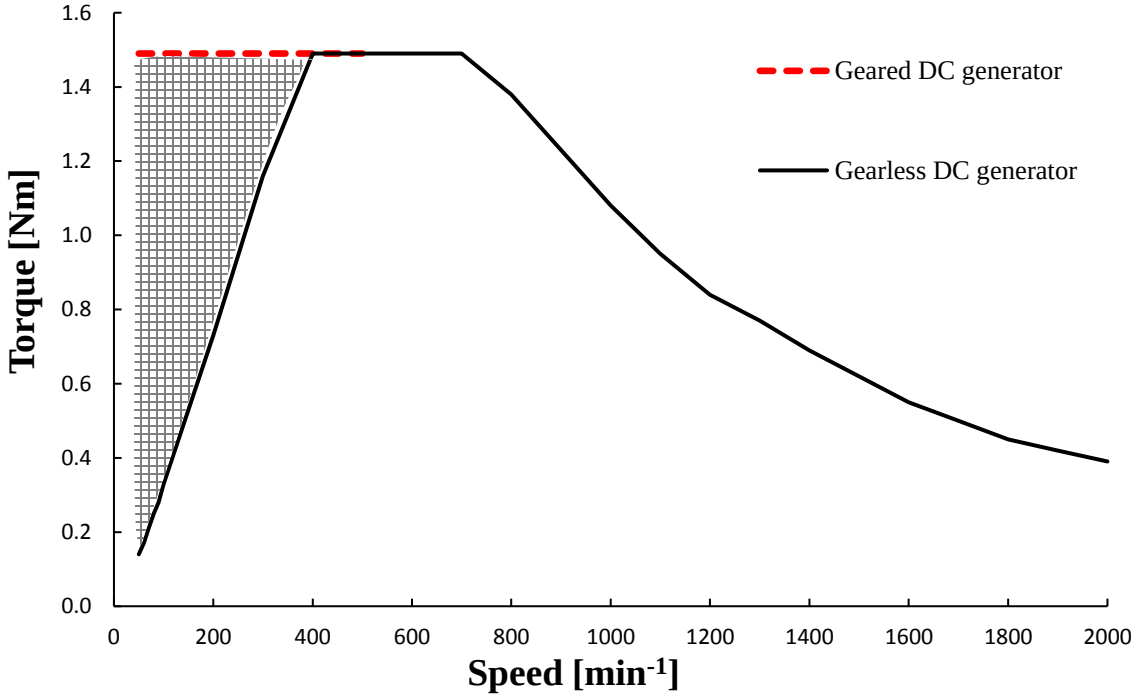

Fig. 3.19 Torque-speed characteristics (improved load system)

3.4.4-2 Comparison of VVVF and vector control

In the previous section, the torque-speed characteristics of the two-phase inverter drive from 100 min^{-1} to 2000 min^{-1} were examined. In this section, the torque-speed characteristics of the vector-controlled and VVVF-controlled two-phase inverter-fed induction motor drive systems are compared as shown in Fig. 3.20.

A comparison of the results shows that the vector-controlled two-phase inverter drive can produce full torque from 100 min^{-1} to 700 min^{-1}. In the high-speed region, the vector control method can produce more torque compared to the VVVF control method.

Generally, the torque-speed characteristics of the vector-controlled three-phase inverter-fed induction motor drives are better than that of the VVVF-controlled drives. The result shown in Fig. 3.20 illustrates that the same tendency can be seen in two-phase inverter-fed induction motor drives.

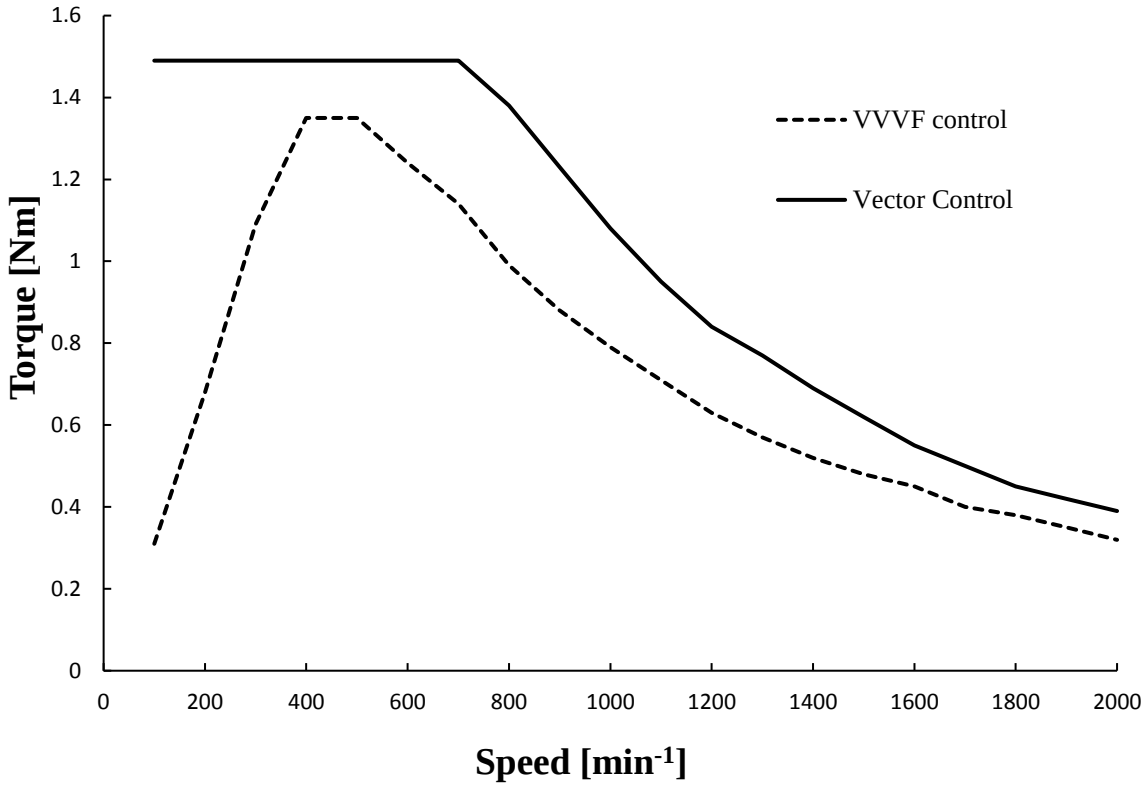

Fig. 3.20 Torque-speed characteristics of VVVF and vector control

3.4.5 Motor efficiency

In section 3.3.2-6, due to the limitation of the experimental apparatus, the motor efficiency of the entire operating region could not be examined. In this section, the motor efficiency in the entire operating region of the vector-controlled two-phase inverter-fed induction motor drive is examined in detail using the improved load system.

3.4.5-1 Motor efficiency per speed

The motor efficiency at each speed from 100 min^{-1} to 2000 min^{-1} of the two-phase and three-phase inverter-fed induction motor drives were calculated from the experimental results. For comparison, the maximum efficiency at each speed of both the two-phase and three-phase inverter drive is shown in Fig. 3.21.

Figure 3.21 shows that as the speed increases from 100 min^{-1} up to 900 min^{-1}, the maximum efficiency of both drives increases. The peak maximum efficiency per speed of the two-phase inverter drive is between 900min^{-1} and 1000 min^{-1}.

However, the results of the three-phase inverter drive illustrate that the maximum efficiency per speed continues increasing up to approximately 1800 min^{-1}. From these results, it can be said that the maximum efficiency per speed of the two-phase inverters also reduces similarly to the torque-speed characteristics and maximum output voltage.

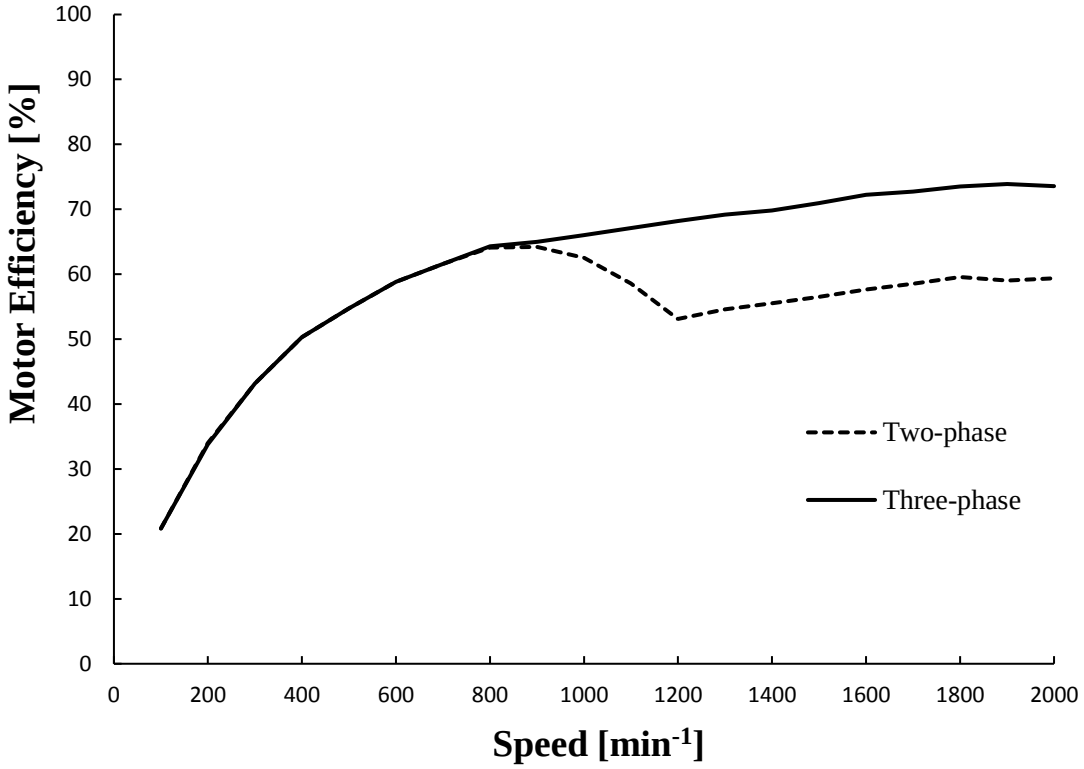

Fig. 3.21 Maximum motor efficiency per speed

3.4.5-2 Motor efficiency map

In section 3.3.2-6, the motor efficiency in the low-speed region could not be examined. In this section, from the experimental results of the improved load system, the motor efficiency is examined. The motor efficiency map of both the two-phase and three-phase inverter-fed induction motor drives are shown in Figs. 3.22 and 3.23, respectively.

Figures 3.22 and 3.23 show that the motor efficiency in the low-speed region is measurable using the geared DC generator load. A comparison of the results shows that the motor efficiency in the low-speed region from 0 min^{-1} to 400 min^{-1} is between 20% and 50% in both the two-phase and three-phase inverter-fed induction motor drive.

From these results, it is clear that the motor efficiency of both the two-phase and three-phase inverter is the same in the low-speed region.

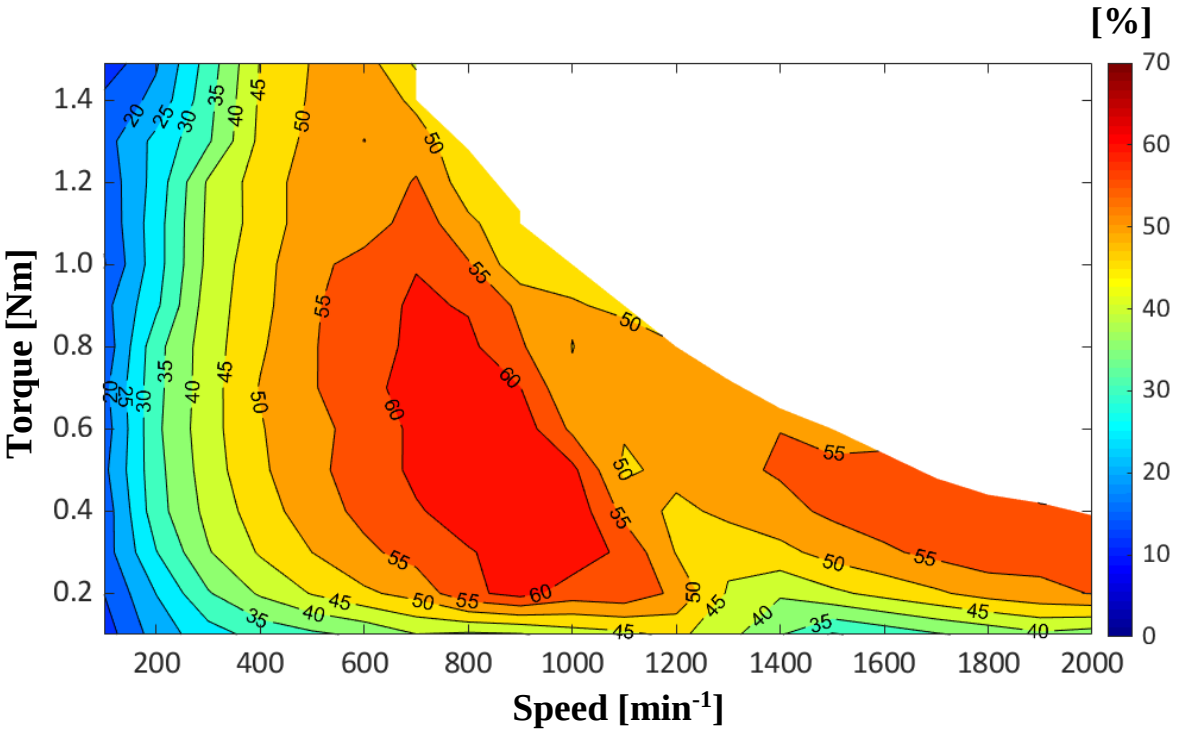

Fig. 3.22. Motor efficiency map (two-phase inverter)

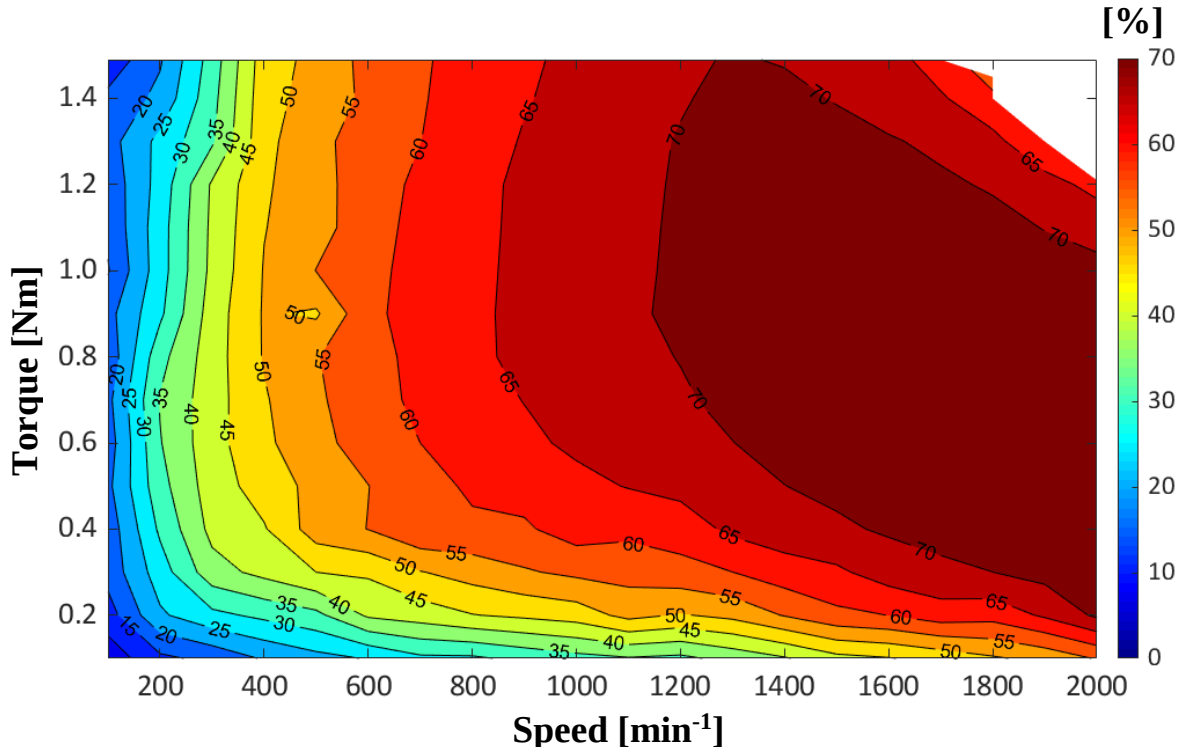

Fig. 3.23. Motor efficiency map (three-phase inverter)

3.5 Comparison of the proposed method and the previous method

From section 3.1 to section 3.4, the effectiveness of the proposed transformation matrix for the vector control of two-phase inverter was verified. In this section, the performance of both the proposed method and the previous method are compared. The vector control method of the two-phase inverter using the proposed transformation matrix in this dissertation is called the proposed method and the reported work in literature is called the previous method [15] [16].

The block diagrams of the proposed method and the previous method are shown in Figs. 3.24 and 3.25, respectively. The comparison is performed from the experimental results of both strategies. The experimental setup is the same as shown in Fig. 3.8. The parameters are the same as shown in Table 3.3. The difference is the software program for the two control strategies.

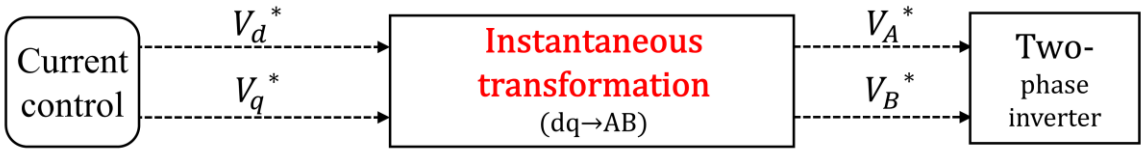

Fig.3.24 Proposed method

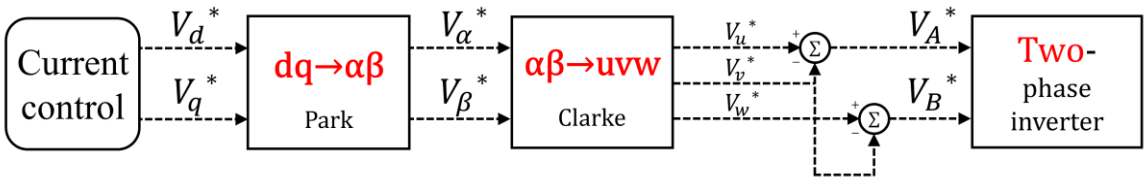

Fig. 3.25 Previous method

3.5.1 Experimental results

3.5.1-1 Voltage references

In the experiment of both control methods, the speed was set at 600 $min^{-1,}$ and the load torque was set at 1.49 Nm. The waveforms of the output voltage references V_A^* and V_B^* using the previous method, and the proposed method are shown in Figs. 3.26 and 3.27, respectively. From the results, it can be seen that in both methods, output voltage references that have a phase difference of $\pi/3$ can be generated.

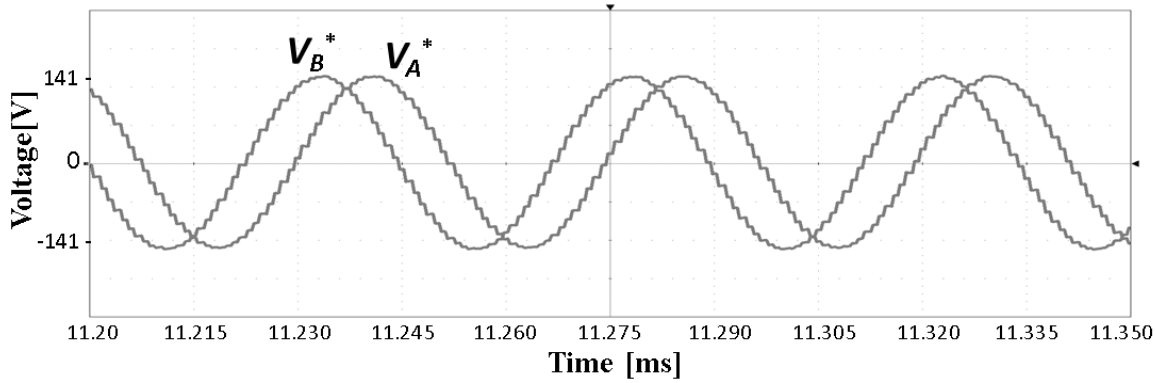

Fig. 3.26 Voltage references with previous method (experiment)

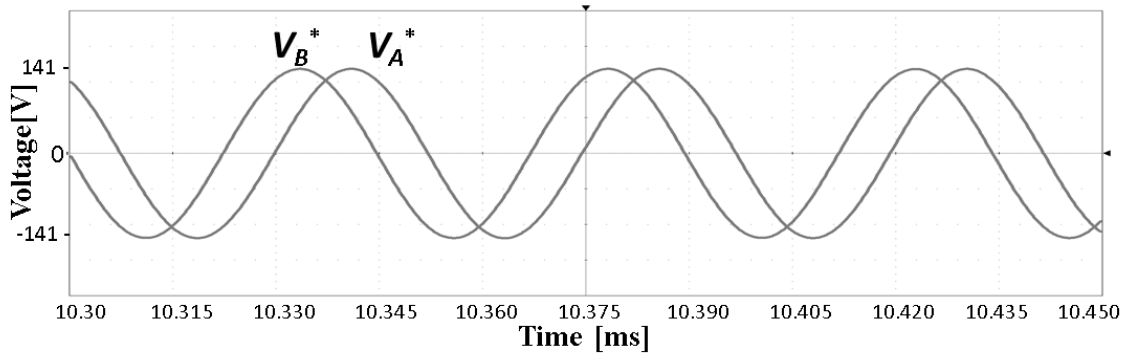

Fig. 3.27 Voltage references with proposed method (experiment)

3.5.1 -2 Three-phase motor current waveforms

Figures 3.28 and 3.29 show the three-phase motor current waveforms of the previous method and the proposed method, respectively. The speed was set at 600 $min^{-1}$and the torque was set at 1.49 Nm. The results show that in the previous method the three-phase motor current was unbalanced. However, by applying the proposed method, better three-phase current can be obtained. Therefore, the proposed method can obtain better motor current waveforms, compared to the previous method.

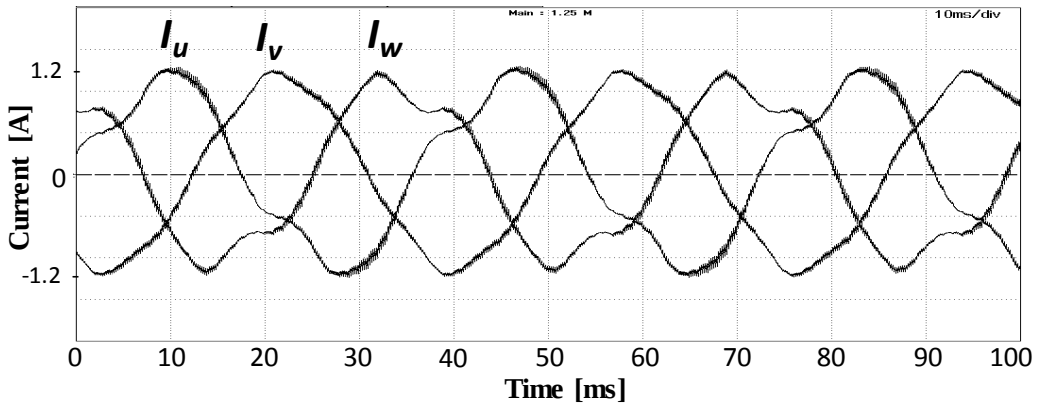

Fig. 3.28 Current waveform with previous method (experiment)

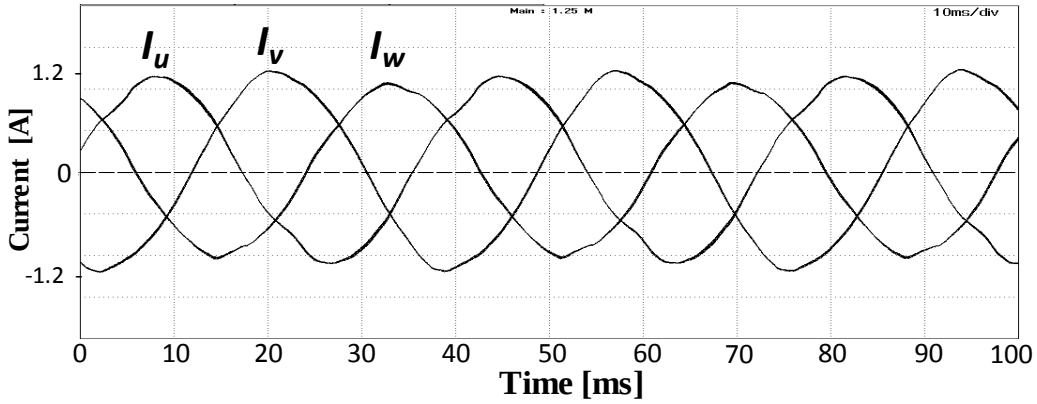

Fig. 3.29 Current waveform with proposed method (experiment)

3.5.1-3 Torque-speed characteristics

The torque-speed characteristics of the two-phase inverter drives using both the proposed and previous methods are shown in Fig. 3.30. The maximum torque was set at 1.49 Nm which is the rated torque of the induction motor used in the experiment. The speed was increased from 0 min^{-1} to 1500 min^{-1} by steps of 100 $min^{-1,}$ and the maximum attainable torque at each speed was measured.

The results show that from 0 min^{-1} to 600 min^{-1} both in the previous method and the proposed method, the maximum attainable torque can be obtained. However, above approximately 650 min^{-1}, the maximum attainable torque of the proposed method is higher compared to that of the previous method.

From the results, it is evident that by applying the proposed method, the torque-speed characteristics of the two-phase inverter-fed induction motor drive improved.

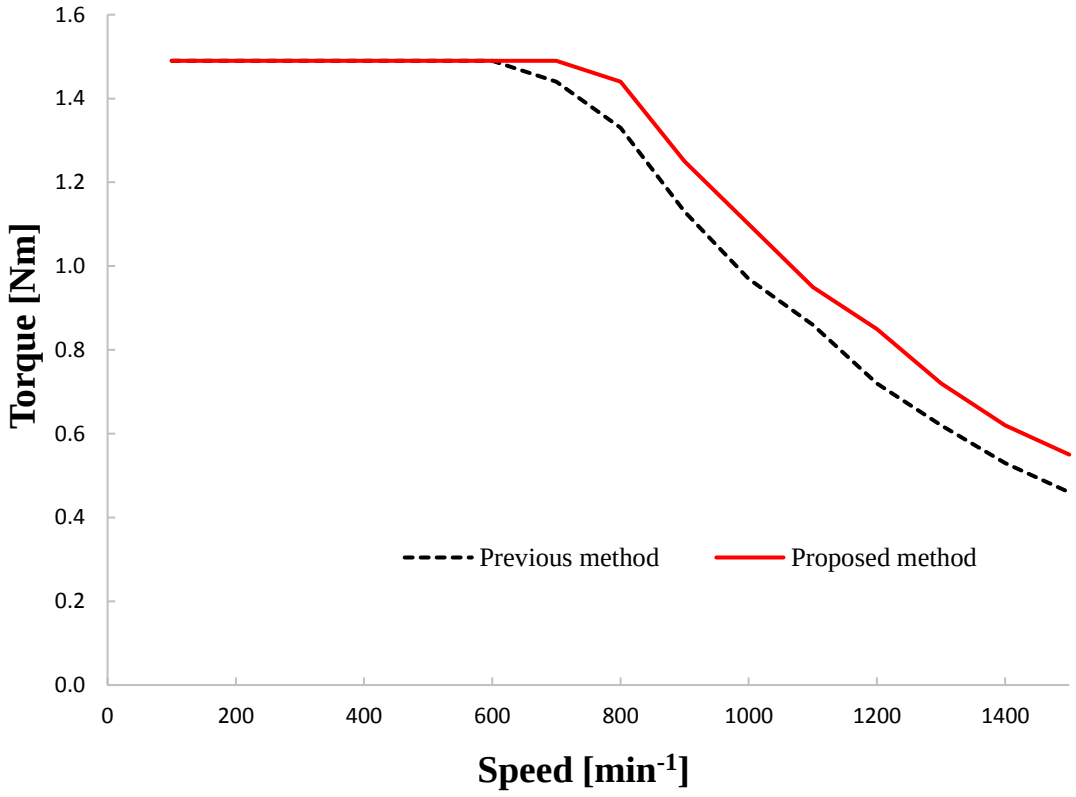

Fig. 3.30 Torque-speed characteristics of previous and proposed method (experiment)

3.5.1-4 Response characteristics

The speed response of both the proposed method and the previous method are shown in Fig. 3.31. At start-up operation, the motor speed reference was set at 600 min^{-1} and load torque at 0 Nm. After a few seconds, the load torque was stepped up from 0 Nm (no load condition) to 1.49 Nm.

The results illustrate that as the load torque increases, the speed reduces below the speed reference but recovers in both methods. However, the recovery time of the proposed method is faster than that of the previous method. The proposed method reaches the steady state or reference speed in 1.2seconds compared to 4.2 seconds of the previous method.

From the results, it is clear that the speed response characteristics of the two-phase inverter-fed induction motor drive improved using the proposed method.

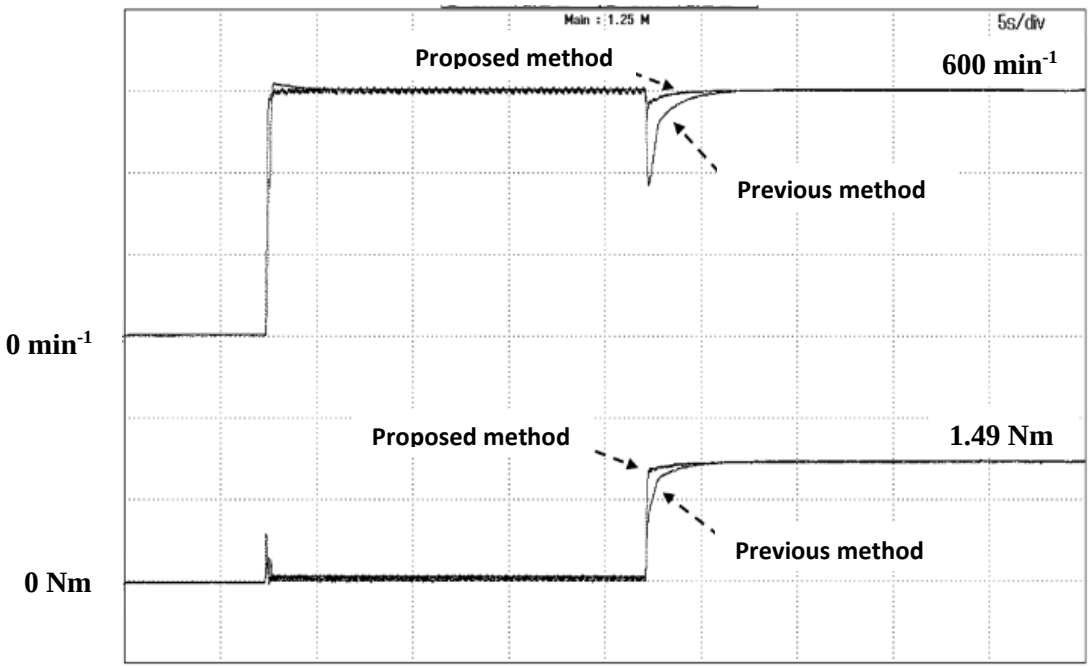

Fig. 3.31 Comparison of speed response (experiment)

3.5.1-5 Motor efficiency

The motor efficiency of the two-phase inverter-fed induction motor drive was examined using the previous method and the proposed method as shown in Figs. 3.32 and 3.33, respectively. The results illustrate that using the proposed method, higher motor efficiency is attainable and the maximum efficiency is higher than that of the previous method, especially in the high-speed region.

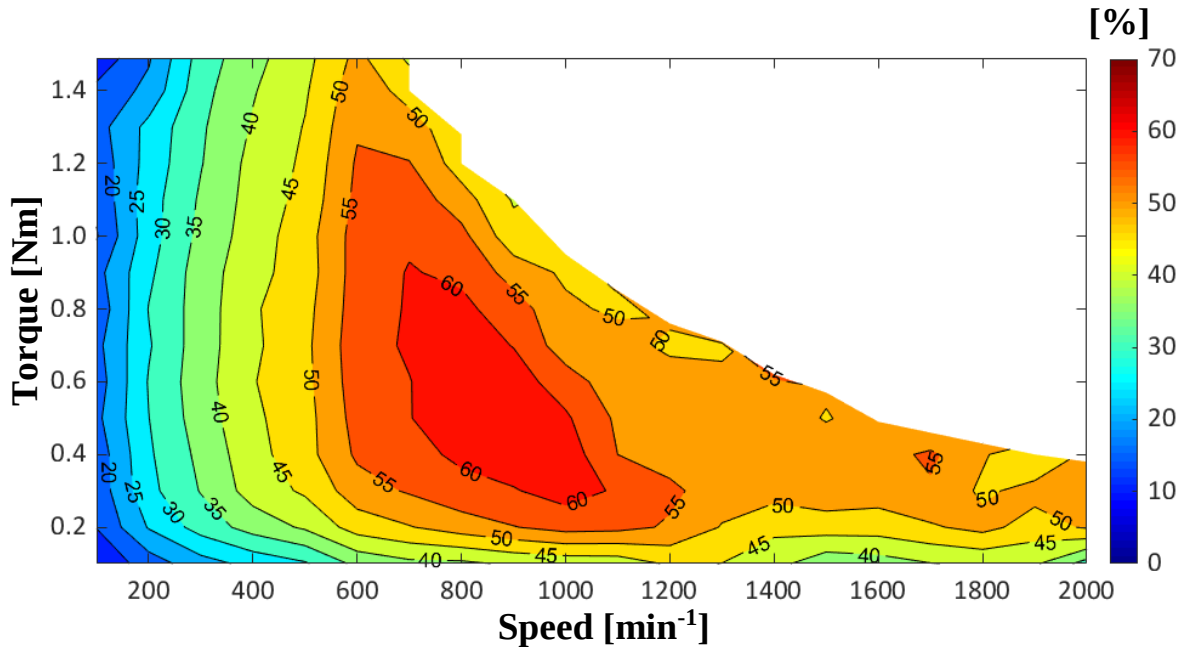

Fig. 3.32 Motor efficiency map with previous method

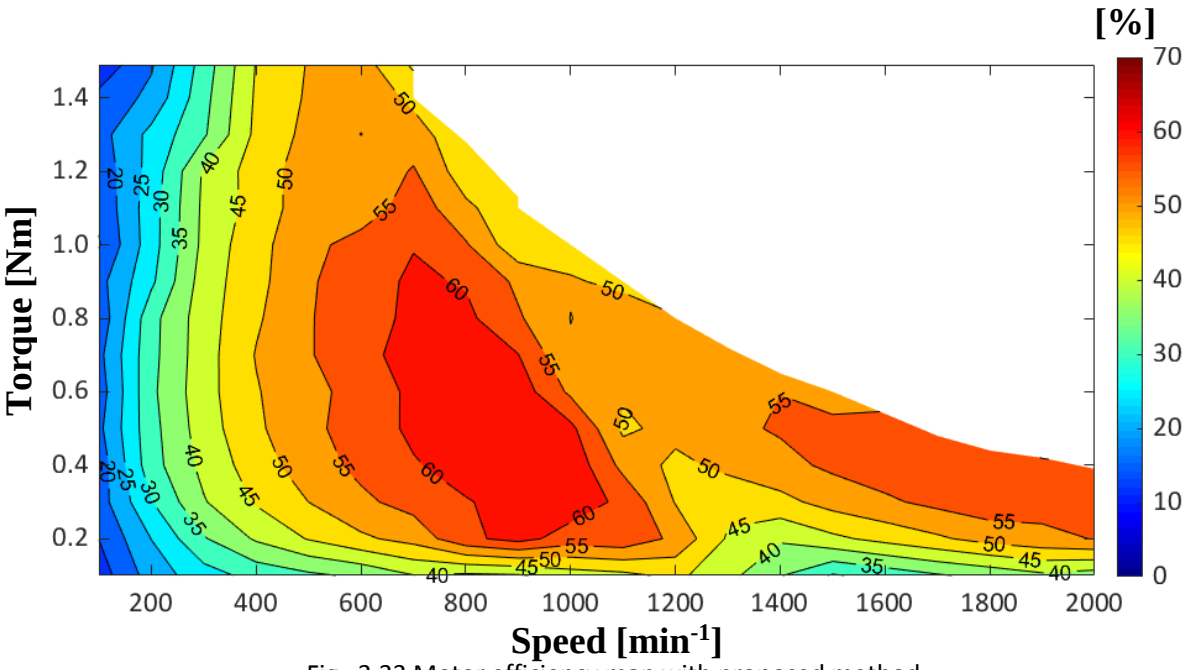

Fig. 3.33 Motor efficiency map with proposed method

3.6 Conclusion

In this chapter, the effectiveness of the proposed transformation matrix was verified by simulation and experiment. Instantaneous generation of voltage references and instantaneous speed response were achieved using the proposed transformation matrix.

In the simulation, the torque-speed characteristics from low-speed to high-speed region were evaluated. However, in the experiment, due to the limitation of the experimental apparatus, the torque-speed characteristics and the motor efficiency in the low-speed region could not be evaluated. Hence, the load system was improved, and evaluation in the whole operating region was performed.

A comparison of the performance characteristics of both the vector-controlled two-phase inverter and the conventional three-phase inverter-fed induction motor drives showed that torque-speed characteristics, maximum output voltage, and motor efficiency of the two-phase inverter reduces.

Finally, a comparison between the experimental results of the vector-controlled two-phase inverter-fed induction motor drive using the proposed and previous methods was performed. From the results, it is clear that although both methods can generate the output voltage references V_A^* and V_B^* that have a phase difference of $\pi/3$, the balanced three-phase motor current, better torque-speed characteristics, and higher motor efficiency were obtained using the proposed method (proposed transformation matrix).

References

1. I. Boldea, S. A. Nasar, Vector control of AC drives, CRC Press, Inc. pp.14-18(1992)
2. N. Mohan, T.M. Undeland, W.P.Robbins, Power Electronics: Converters, Applications and Design, John Wiley & Sons: pp.333-335(1989)
3. F. Giri, AC electric motors control, advanced design techniques and applications, John Wiley & Sons : pp.455-463(2013)
4. H. Tanaka, S. Saito, and K. Matsuse: "Improved performance of independent two induction motor drives fed by a four leg inverter with vector control method", *IEEE Int. Conf. Elec. Machines and Syst.(ICEMS)*, pp.1-6(2012)
5. U. U. Ekong, M. Inamori, and M. Morimoto: "Field Oriented Control of Two Phase Inverter to drive a Three Phase Induction Motor" *IEEE International Conference on Electrical Machines and Systems (ICEMS)*, pp.125-128(2015)
6. U.U. Ekong, M. Inamori, and M. Morimoto : "Field Oriented Control of Two Phase Inverter to drive a Three Phase Induction Motor", *IEEJ Industry Applications Division Annual Convention (JIASC)*, Y-132(2015) *(In Japanese)*
7. U.U. Ekong, M. Inamori, and M. Morimoto: "Instantaneous Field Oriented Control of Two Phase Inverter fed Induction Motor Drive", *IEEJ Industry Applications Division Annual Convention (JIASC)*, Vol.3, pp.121-124(2016) *(In Japanese)*
8. U.U. Ekong, M. Inamori, and M. Morimoto: "Instantaneous Vector Control of Four Switch Three Phase Inverter fed Induction motor drive", *IEEE International Conference on Electrical Machines and Systems (ICEMS)*, pp.125-128(2016)
9. U.U. Ekong, T. Shiraishi, M. Inamori, and M. Morimoto: "Derivation of Transformation Matrix for 3 phase vector control of a 2 phase Inverter" *IEEJ National Annual Convention*, Vol.4, pp.46-47(2017) *(In Japanese)*
10. T. Shiraishi, U.U. Ekong, M. Inamori, and M. Morimoto: "Instantaneous Co-ordinate Transformation of a vector controlled 2 Phase Inverter fed 3 Phase Induction Motor Drive", *IEEJ Industry Applications Division Annual Conference (JIASC)*, Y-106(2017) *(In Japanese)*
11. T. Nakade, U.U. Ekong, M. Inamori, and M. Morimoto: "Flux-Weakening Control of a Vector Controlled Two Phase Inverter", *IEEJ Industry Applications Division Annual Conference (JIASC)*, Vol.3, pp.373-376(2017) *(In Japanese)*
12. O. Sok, U.U. Ekong, M. Inamori, and M. Morimoto: "Evaluation of Motor Efficiency of a vector controlled 2 Phase Inverter fed 3 Phase Induction Motor Drive", *IEEJ Industry Applications Division Annual Conference (JIASC)*, Vol.3, pp.369-372(2017)
13. U.U. Ekong, O. Sok, M. Inamori, and M. Morimoto: "Development of a Load Torque Measurement System for Two Phase Inverter Fed Induction Motor Drive with Vector Control Method", *Proceedings School of Engineering, Tokai University*, Vol.42, pp.9-14(2017)
14. U.U. Ekong, M. Inamori, and M. Morimoto: "Instantaneous Vector Control of Four Switch Three Phase Inverter fed Induction motor drive" *IEE Japan Trans.* of *Industry Applications*, Vol.6, No.6, pp.429-434(2017)
15. G. Kim and T.A. Lipo: "VSI-PWM Rectifier/Inverter System with a Reduced Switch Count", *IEEE Trans. Industry Appl.*, Vol.32, No.6, pp.1331-1337(1996)
16. H. Tanaka, S. Saito, and K. Matsuse: "Improved performance of independent two induction motor drives fed by a four leg inverter with vector control method", *IEEE Int. Conf. Elec. Machines and Syst.(ICEMS)*, pp.1-6(2012)

Chapter 4

Field weakening control of two-phase inverter-fed induction motor drive

4.1 Introduction

In the previous chapter, the characteristics of the two-phase inverter-fed induction motor drive showed that the maximum attainable torque and motor efficiency are low in the high-speed region. In order to apply two-phase inverters as an emergency drive for electric vehicles, the performance in the high-speed region must be improved.

In the conventional three-phase inverter-fed induction motor drive, a method to improve the performance characteristics of the drive in the high-speed region is to apply the field/flux weakening control above the rated speed of the motor, where the output voltage reaches its limit [(1)-(3)]. In field weakening control, the machine flux is weakened in a manner that enables the drive to increase torque production and attain high motor efficiency. Several field weakening control strategies have been proposed for the conventional three-phase inverter-fed induction motor drives [(4)-(15)]. However, these field weakening control strategies cannot be directly applied to two-phase inverter-fed induction motor drives, for reasons that will be explained later in this chapter.

In this chapter, in order to improve the performance characteristics of the vector controlled two-phase inverter-fed induction motor drive in the high-speed region, a novel field weakening control strategy is proposed. The effectiveness of the proposed field weakening control strategy for two-phase inverter drives is verified by simulation and experiment.

4.2 Basics of field weakening control

In inverter-fed induction motor drives, as the speed increases, the output voltage also increases. However, at a certain speed, the output voltage reaches its limit which is called voltage saturation. The speed at which the output voltage reaches its limit is referred to as the base speed (or base frequency) as shown in Fig. 4.1. Generally, the base speed is the rated speed of the motor [(16)].

In inverter-fed induction motor drives, the ability to implement field weakening control depends on the control method either scalar (VVVF) control or vector control. In scalar methods, above the rated speed of the induction motor, where the voltage is saturated, the flux naturally reduces as the speed increases. This reduction is because the flux is proportional to the output voltage and the flux is not controlled independently [(17) (18)]. Furthermore, from the working principle of scalar methods, the torque cannot be controlled independently.

On the other hand, in vector control as earlier explained in Chapter 1, the motor stator current is decoupled into the flux component current I_d and torque component current I_q as shown in Fig. 4.2 (a).

Here, torque control is achieved by keeping the flux component current I_d constant and varying torque component current I_q. Furthermore, in field weakening control, the torque component current I_q can be increased by decreasing the flux component current I_d, taking into account the maximum current I_{smax} on the current limit circle as shown in Fig. 4.2 (b).

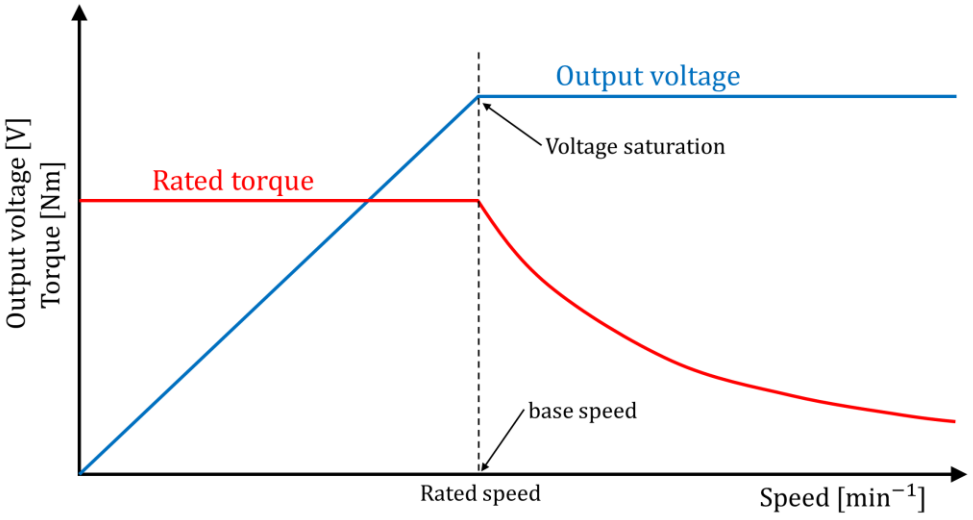

Fig. 4.1 Voltage saturation and base speed

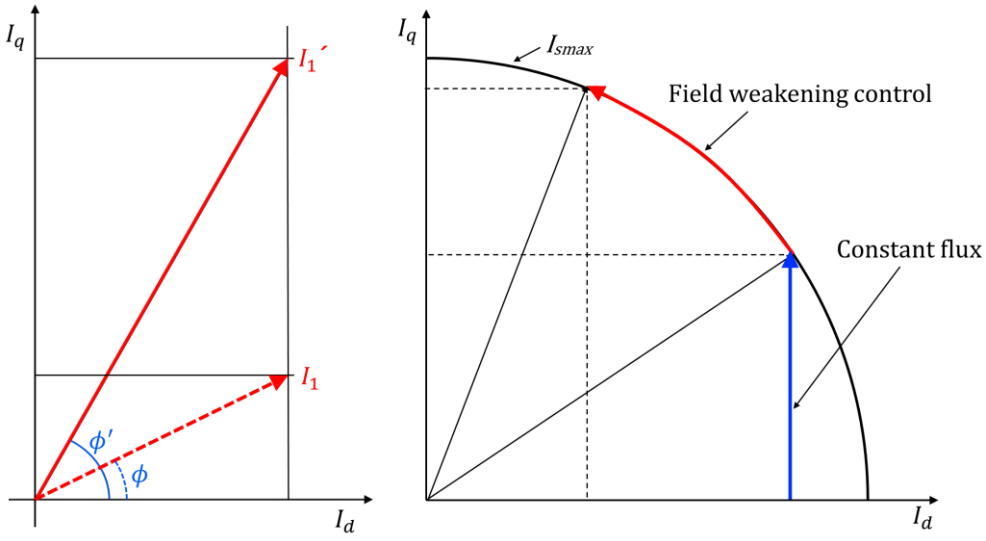

(a) Current vector diagram (b) Current limit circle

Fig. 4.2 Current trajectories in vector control

4.3 Operating constraints in field weakening region

In this section, the operating constraints of inverter-fed induction motor drives in the field weakening region are discussed. In the field weakening region, the performance of the induction motor drive is limited by the maximum output voltage and the inverter current ratings.

4.3.1 Voltage limit

The DC-link voltage and the adopted PWM strategy determine the maximum voltage V_{smax} that the inverter can apply to the induction motor [19][20]. In this dissertation, the sinusoidal PWM strategy is adopted. If over-modulation is not considered, the maximum magnitude of the sinusoidal output voltage is expressed as follows.

$$V_{s\,max} = m \cdot \frac{V_{dc}}{2} \tag{4.1}$$

Here m is the modulation index ($0 \le m \le 1$). The voltage references V_d^* and V_q^* must satisfy the constraints of the voltage limit boundary as shown in equation (4.2).

$$V_d^{*2} + V_q^{*2} \le V_{s\,max}^2 \tag{4.2}$$

4.3.2 Current limit

The motor current is limited to the maximum current I_{smax} which is determined by the thermal rating of the induction motor or the current rating of the inverter. The current references I_d^* and I_q^* must satisfy equation (4.3).

$$I_d^{*2} + I_q^{*2} \le I_{s\,max}^2 \tag{4.3}$$

In order to maintain current control, especially in the high-speed region, the current references I_d^* and I_q^* must be limited to be on the current limit circle as shown in Fig. 4.3.

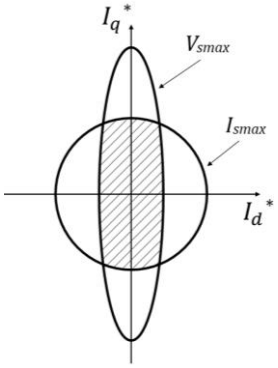

Fig. 4.3 Voltage and current limits

4.4 Field weakening control of three-phase inverter-fed induction motor drive

4.4.1 Field weakening characteristics

The characteristics of an induction motor fed by the conventional three-phase inverter are shown in Fig. 4.4. In three-phase inverter drives, the operating range of the induction motor can be divided into three different regions: i) constant torque region (Base speed region), ii) constant power region (Field Weakening (FW) region 1) and iii) constant slip region (FW region 2) [(1)].

In the base speed region, the d-axis current I_d is constant, and the motor operation is limited by the current. In FW region 1, the motor speed is above the base speed, and the motor operation is limited by both the current and voltage limits because the back electromotive force approaches the maximum inverter voltage.

In FW region 2, the speed becomes so high that the current cannot exceed the maximum inverter current. The slip then increases because it is no more proportional to the torque. These are the basic characteristics of torque, current, voltage, and power in the three-phase inverter drive.

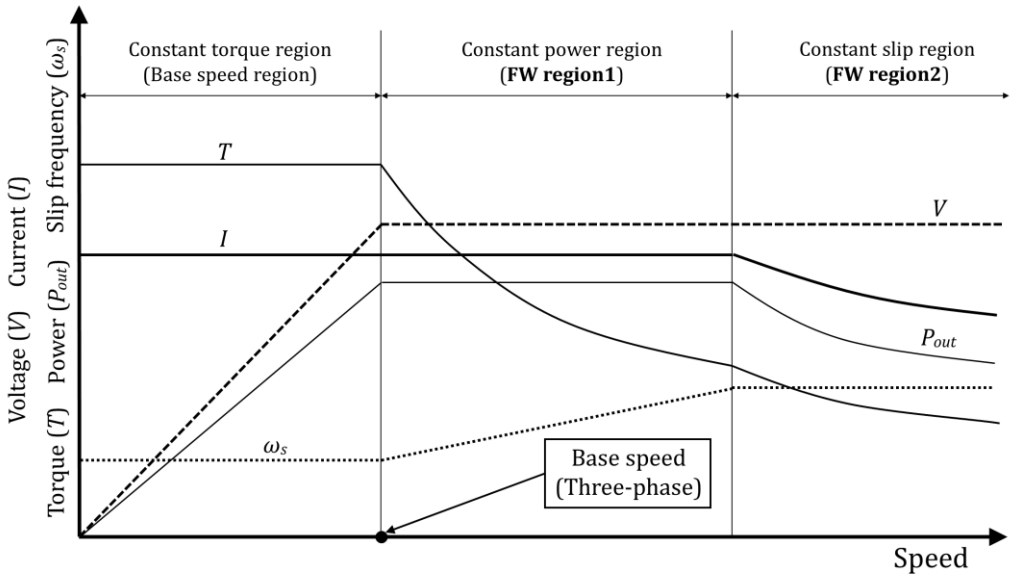

Fig. 4.4 Field weakening characteristics of an induction motor fed by three-phase inverter [(1)]

4.4.2 Field weakening control methods

Field weakening control methods for the conventional three-phase inverter drives have been studied widely and can be classified into three categories [(19)-(26)].

(a) Adjustment of the motor flux in inverse proportion to speed ($1/\omega_r$).
(b) Feedforward control based on simplified motor parameters and motor equations.
(c) Closed loop control of the stator voltage for full utilization of the maximum inverter voltage.

The first method (a) is the conventional and the most frequently used field weakening control method because of its simplicity. In this method, the flux is controlled inversely proportional to the motor speed.

This method has been reported to improve the torque production. However, this method cannot provide the maximum output torque per ampere nor the full utilization of the DC-link voltage [(1) (21)].

The second method (b) is dependent on the voltage and current limitation with respect to the induction motor parameters. This method can achieve good performance in the high-speed region if the accurate motor parameters are known [(22)(23)].

The third method (c) depends on the ability to fully utilize the available inverter voltage, to produce the maximum torque. This method is not dependent on the DC link voltage or motor parameters. However, an extra outer voltage control loop is required [(24)(25)].

In three-phase inverter-fed induction motor drives, the second method (b) which is based on the motor parameters models appears to be the best method in terms of torque production with better-reported results. However, the second and third methods have been reported to have slow response characteristics and dynamic performance [(26)].

In the two-phase inverter drive, since the DC-link voltage and inverter supply voltage cannot be fully utilized, the second and the third method are difficult to implement. Furthermore, the second method (b) is based on the condition that the power source is a three-phase balanced voltage or current supply that is adequately switched by the inverter. This method cannot be implemented in two-phase inverter drives because one phase of the output is connected to the midpoint of the DC source.

Therefore, the first method (a) with some improvements is the most feasible option for two-phase inverter-fed induction motor drives.

4.5 Proposed field weakening control of two-phase inverter-fed induction motor drive

In this section, a field weakening control method is proposed to improve the torque-speed characteristics and motor efficiency of the two-phase inverter-fed induction motor drive.

4.5.1 Maximum output voltage

In Chapter 3, the detailed results of the indirect vector control without field weakening control of both the two-phase inverter and three-phase inverter-fed induction motor drives were investigated. It was clarified that the maximum output voltage and maximum torque attainable speed of the two-phase inverter drive compared to the three-phase inverter drive reduce by approximately 50% as shown in Fig. 4.5[27][28]. In addition, due to the difference of the maximum output voltage of the two-phase inverter and three-phase inverter drives, their base speed is different.

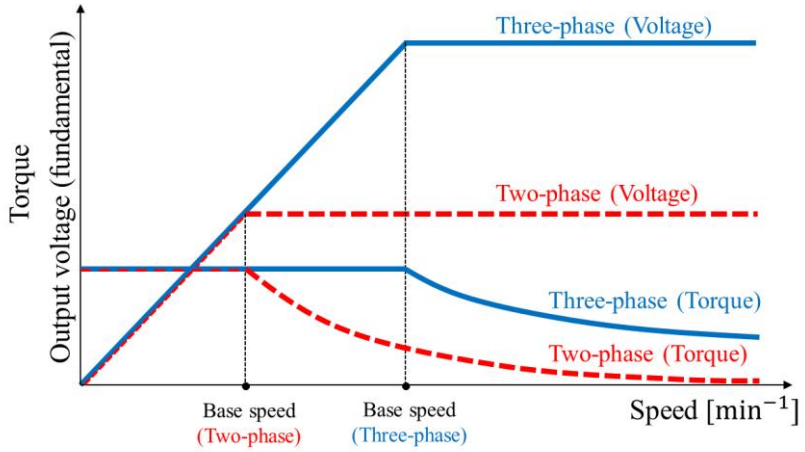

Fig. 4.5 Output voltage and torque vs. speed

4.5.2 d-axis current reference

In the conventional field weakening control strategy of the three-phase inverter drive, the d-axis current reference is kept constant below the base speed ω_{base} and above is inversely proportional to the motor speed as given by equation (4.4).

$$I^*_{d[FW]} = \frac{\omega_{base}}{\omega_r} \times I^*_d \tag{4.4}$$

The constant d-axis current reference I_d^* is calculated by

$$I^*_d = \frac{\psi}{L_m} \quad , \tag{4.5}$$

where ψ is the rated flux and L_m is the magnetizing inductance of the motor.

The base speed ω_{base} also determines the value of the d-axis current reference $I_d^*{}_{[FW]}$ for the field weakening region. If the d-axis current reference is too high, the q-axis current reference cannot be regulated. In the conventional three-phase inverter drive as shown in equation (4.6), the base speed ω_{base} is usually set at the rated speed ω_{rated} of the motor, where the voltage reaches its limit.

$$\omega_{base} = \omega_{rated} \tag{4.6}$$

However, as explained in section 3.3.2-5 and from the working principle of two-phase inverters [28]-[30], the maximum output voltage of two-phase inverters reduces by a factor of $1/\sqrt{3}$. Therefore, in this dissertation, the base speed of the two-phase inverter drive is calculated by

$$\omega_{base[Two-phase]} = \frac{\omega_{rated}}{\sqrt{3}} \ . \tag{4.7}$$

From equations (4.4) and (4.7), the d-axis current reference $I_d^*{}_{[FW]}$ for the field weakening region of the two-phase inverter drive can be derived as follows:

$$I^*_{d[FW]} = \frac{\omega_{base[Two-phase]}}{\omega_r} \times I^*_d \ . \tag{4.8}$$

Figure 4.6 illustrates the d-axis current references of the conventional three-phase inverter drives given in equation (4.4) and the proposed d-axis current reference for two-phase inverter drives given in equation (4.8). In this figure, a significant difference in the two d-axis current reference values is observed. The value of the d-axis current reference is important because if the d-axis reference $I_{d[FW]}{}^*$ is too low or too high, the maximum attainable torque and the motor efficiency are low in the high-speed region.

The conventional field weakening method for three-phase inverter drives cannot fully optimize the performance of two-phase inverter drives in the field weakening region because of the voltage limitation of two-phase inverter drives.

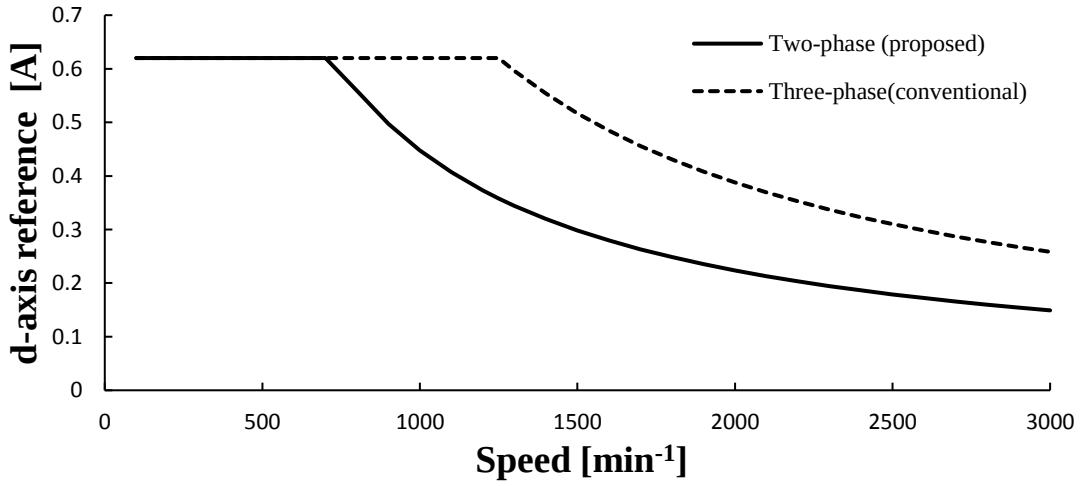

Fig. 4.6 d-axis reference (two-phase and three-phase) vs. speed

4.5.3 q-axis current reference

In the conventional field weakening control of three-phase inverters, the q-axis current reference I_q^* is controlled by limitation in various operating regions. These different limitations are not directly applicable to the two-phase inverter drive because its base speed and maximum output voltage reduce as shown in Fig. 4.5.

In this dissertation, in the base speed region (constant torque region) of the two-phase inverter drive, the q-axis current reference I_q^* is limited as

$$I_q^* \le \sqrt{I_{s\max}{}^2 - I_d^{*2}} \quad . \tag{4.9}$$

Here, I_{smax} is the maximum current of the inverter and is given in equation (4.10). I_{smax} is derived by confirming the maximum current of the inverter and the thermal rating of the induction motor used in the experiment. This maximum current is usually 150% of its rated value [27] [28].

$$I_{s\max} = I_{rated} \times 1.5 \tag{4.10}$$

Up to the base speed $\omega_{base[Two\text{-}phase]}$ in equation (4.7), the d-axis current reference I_d^* is constant. Hence, torque is proportional to the q-axis current. From the base speed $\omega_{base[Two\text{-}phase]}$ up to the rated speed of the motor ω_{rated}, the q-axis current reference is limited by the constraints in equation (4.11). After the base speed region, the d-axis current reference is no longer constant because its value is determined by equation (4.8). This region is called field weakening region 1 (FW region 1) in the two-phase inverter drive, as shown in Fig. 4.7.

$$I_q^* \le \sqrt{I_{s\max}{}^2 - I_{d[FW]}^{*2}} \tag{4.11}$$

In field weakening region 2 of the conventional three-phase inverter-fed drive, in order to maintain the maximum slip ω_{smax} and avoid the loss of current control, the q-axis current reference is reduced by limitation [1] [23]. In the two-phase inverter drive, the voltage that can be utilized in the field weakening region is low; If limitations of the three-phase inverter are applied in FW region 2, it has no positive effect on the output torque or motor efficiency. This is because the q-axis current reference of the two-phase inverter drive will not be as large as that of the three-phase inverter drive.

Furthermore, due to the reduction in maximum output voltage of two-phase inverter drives, the q-axis current reference will be unnecessarily large. In this case, current control is lost and the motor loss increases.

Hence, in this dissertation, a limitation to reduce the q-axis current reference above the rated speed of the motor is proposed. This limitation will enable the two-phase inverter drive to achieve a high motor efficiency and control of the slip linearity to torque in the high-speed region. This region is called the field weakening control region 2.

The proposed limitation for the q-axis current reference is achieved by reducing/limiting the maximum current I_{smax} that the inverter can apply to the motor. The maximum current $I_{smax[FW]}$ for the field weakening region 2 is set at the rated current I_{rated} of the induction motor as in equation (4.12).

$$I_{s\max[FW]} = I_{rated} \tag{4.12}$$

Therefore, the q-axis current reference limitation for the field weakening region 2 can be expressed as

$$I_q^* \le \sqrt{I_{s\,max[FW]}^{\;2} - I_{d[FW]}^{*\;2}} \quad . \tag{4.13}$$

The speed of the motor determines the onset of field weakening region 2. Above the rated speed of the motor ω_{rated}, field weakening region 2 begins. The switching of the q-axis current reference limitations from the base speed region to field weakening region 2 is performed as shown in Fig. 4.8. The first limitation is in the base speed region ($0 < \omega_r < \omega_{base\ [Two\text{-}phase]}$), The second limitation is in the field weakening region 1 ($\omega_{base[Two\text{-}phase]} < \omega_r < \omega_{rated.}$). The third limitation is in the field weakening region 2 ($\omega_{rated} < \omega_r$).

In this section, to improve the performance of the two-phase inverter drive in the high-speed region, a novel method to calculate the optimal d-axis current reference (4.5.2) and limitations for q-axis current reference for the field weakening regions 1 and 2 (4.5.3) has been proposed.

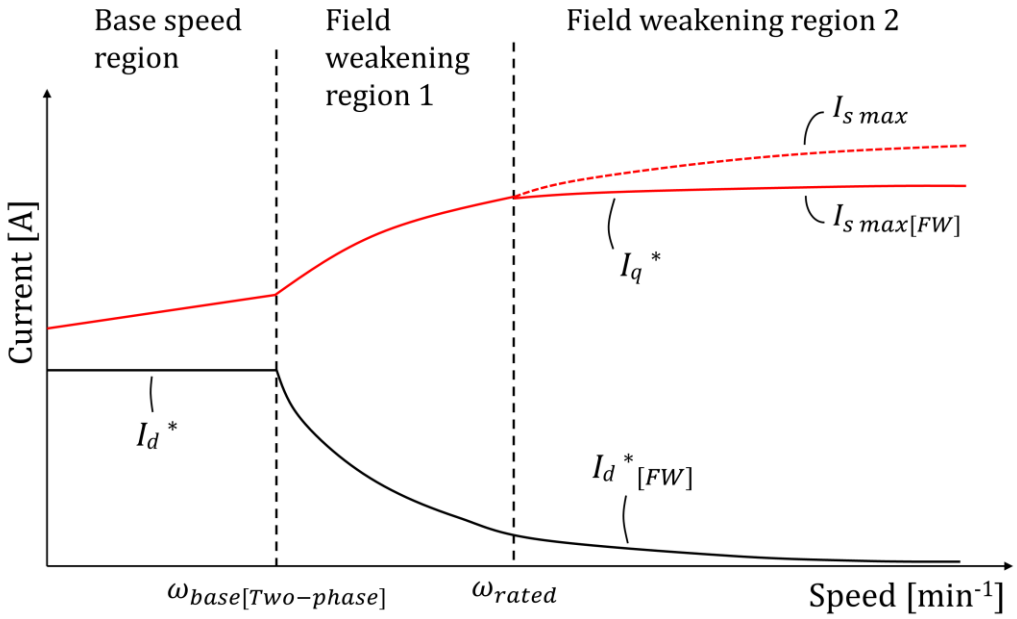

Fig. 4.7 Proposed trajectory of I_d and I_q reference vs. speed

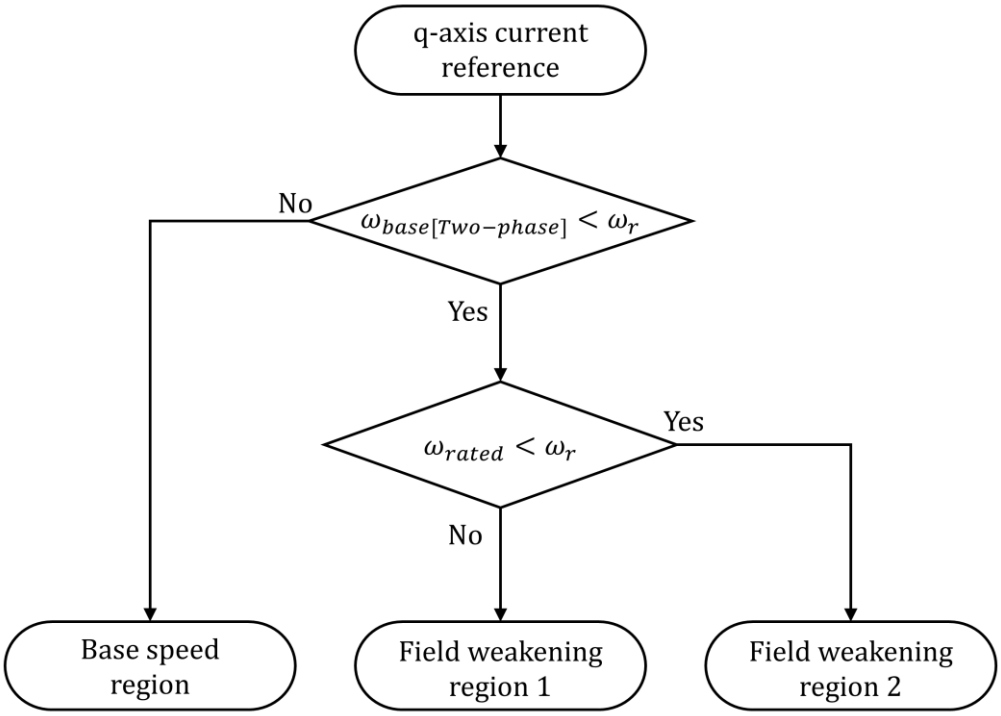

Fig. 4.8 Flow chart of the proposed q-axis current control

4.6 Evaluation by simulation

4.6.1 Simulation model

The simulation model was implemented using PSIM software to verify the proposed field weakening control strategy. The specification of the induction motor and the inverter parameters used in the simulation is shown in Table 3.3. The block diagram of the simulation circuit is shown in Fig. 4.9.

The *V*-phase of the induction motor was assumed to be broken down and was re-connected to the midpoint of the DC source. The speed reference range was set from 50 min^{-1} to 3000 $min^{-1,}$ and the maximum torque was set at 1.49 Nm. For comparison purposes, the same simulation was carried out when using without field weakening control as shown in Fig. 3.1.

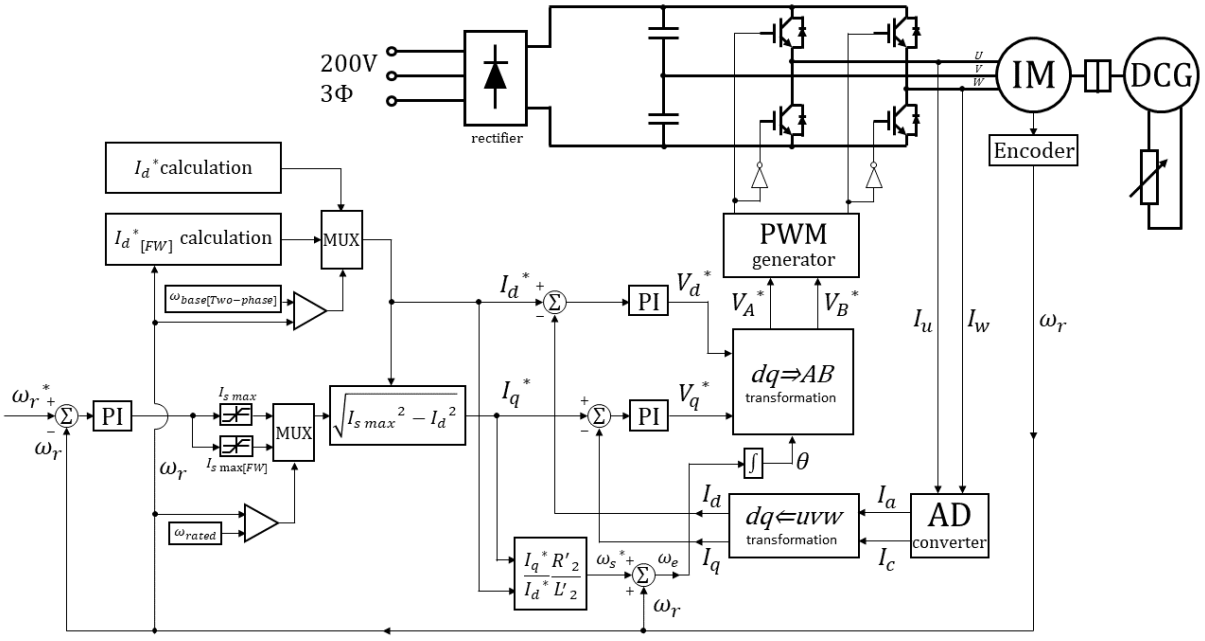

Fig. 4.9 Block diagram of simulation circuit (proposed field weakening control)

4.6.2 Simulation results

4.6.2-1 Currents reference

In the simulation, the trajectory of the d-axis and the q-axis current using the proposed field weakening control strategy is examined. The results in Fig. 4.10 show that the d-axis current is constant in the base speed region and reduces inversely to the speed in the field weakening regions using the proposed field weakening control. Furthermore, the q-axis current increases from the base speed region up till the field weakening region 1 but is limited in the field weakening region 2.

It can be seen that in the control without field weakening, the q-axis current reference suddenly increases in FW region 2. These results show that the q-axis and d-axis current trajectory follow the proposed field weakening control strategy.

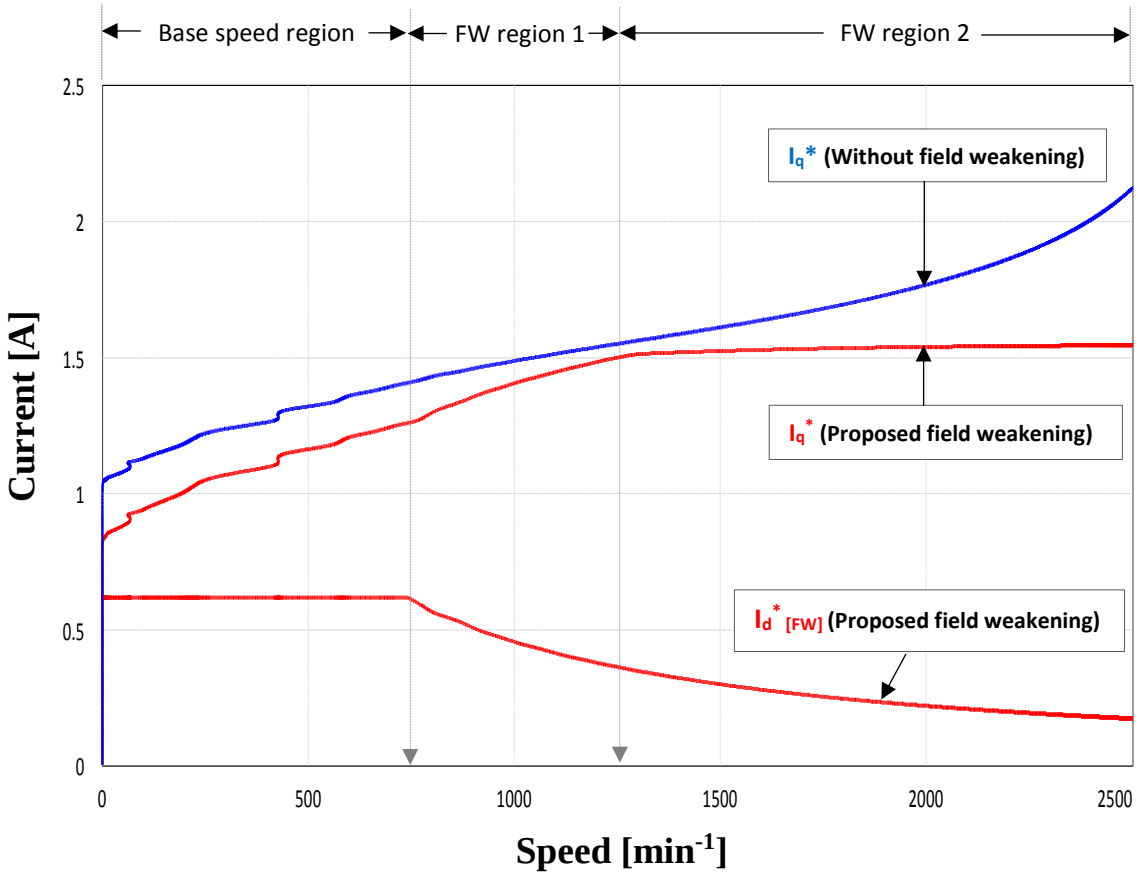

Fig. 4.10 Current trajectory vs. speed (simulation)

4.6.2-2 Slip

In an ideal inverter-fed induction motor drive, in order to maintain current control and stability in the high-speed region, the torque is proportional to q-axis current, and the slip.

The relationship between speed and slip frequency from 0 min^{-1} to 2500 min^{-1} is shown in Fig. 4.11. From the results, it can be seen that the slip frequency in both the proposed field weakening control and the control without field weakening increases in a similar manner from 0 min^{-1} to the base speed. The proposed field weakening control can maintain a linear relationship between the slip frequency and speed in field weakening region 1 and region 2. This indicates that the linear relationship between slip and torque can be maintained using the proposed field weakening control.

In contrast, without field weakening, the slip frequency increases gradually in the field weakening regions, in a nonlinear manner which leads to low torque production in the high-speed region.

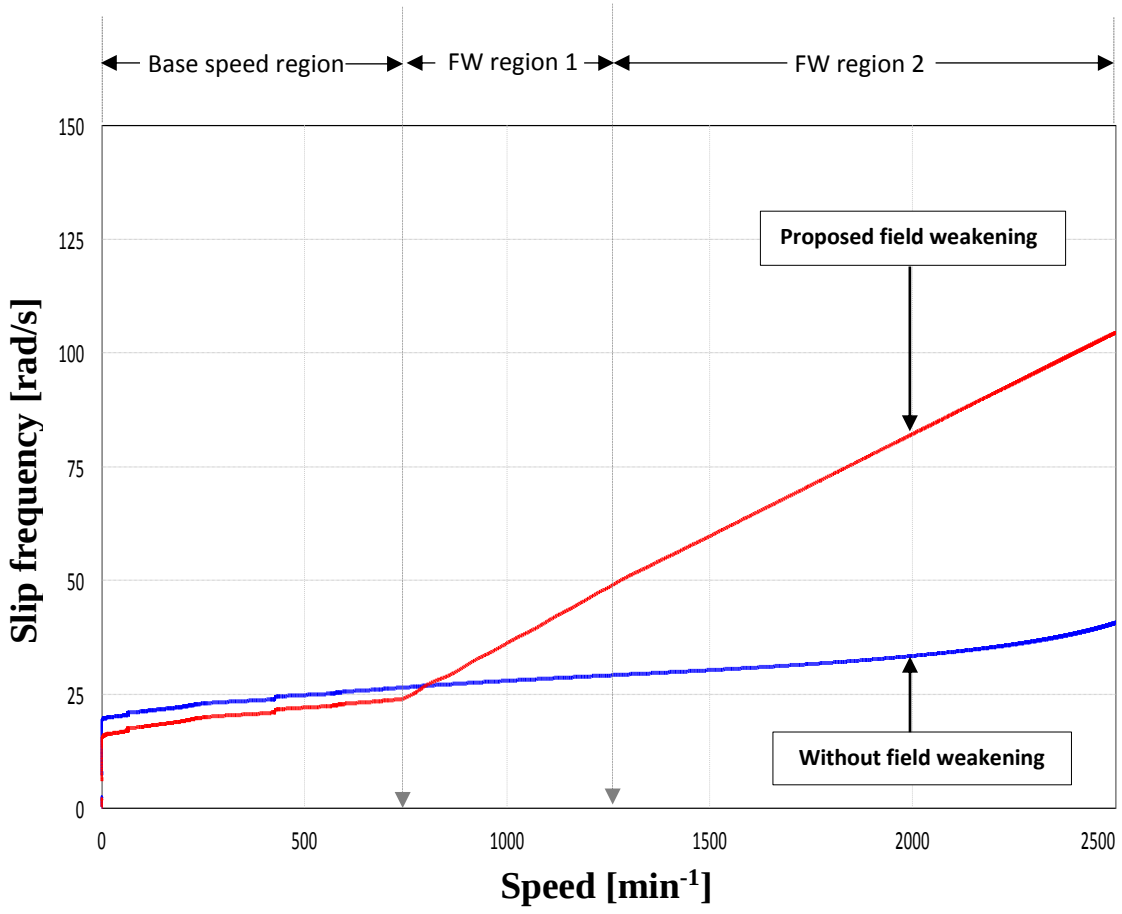

Fig. 4.11 Slip characteristics (simulation)

4.6.2-3 Torque-speed characteristics (simulation)

The maximum attainable torque of both the proposed field weakening control and the control without field weakening was measured, and the results are shown in Fig. 4.12. A comparison of the results show that above the base speed $\omega_{base\ [Two\text{-}phase]}$, the proposed field weakening control strategy can produce more torque of an average of 6% per speed.

The increase in the maximum attainable torque is due to the precise current control achieved using the proposed field weakening control. In the two-phase inverter-fed motor drive, the maximum output voltage is lower than the rating of the motor. Thus, the area where slip and torque are proportional is narrow. In the high-speed region without field weakening, the linear relationship between the q-axis current and torque collapses. For this reason, the torque production is low.

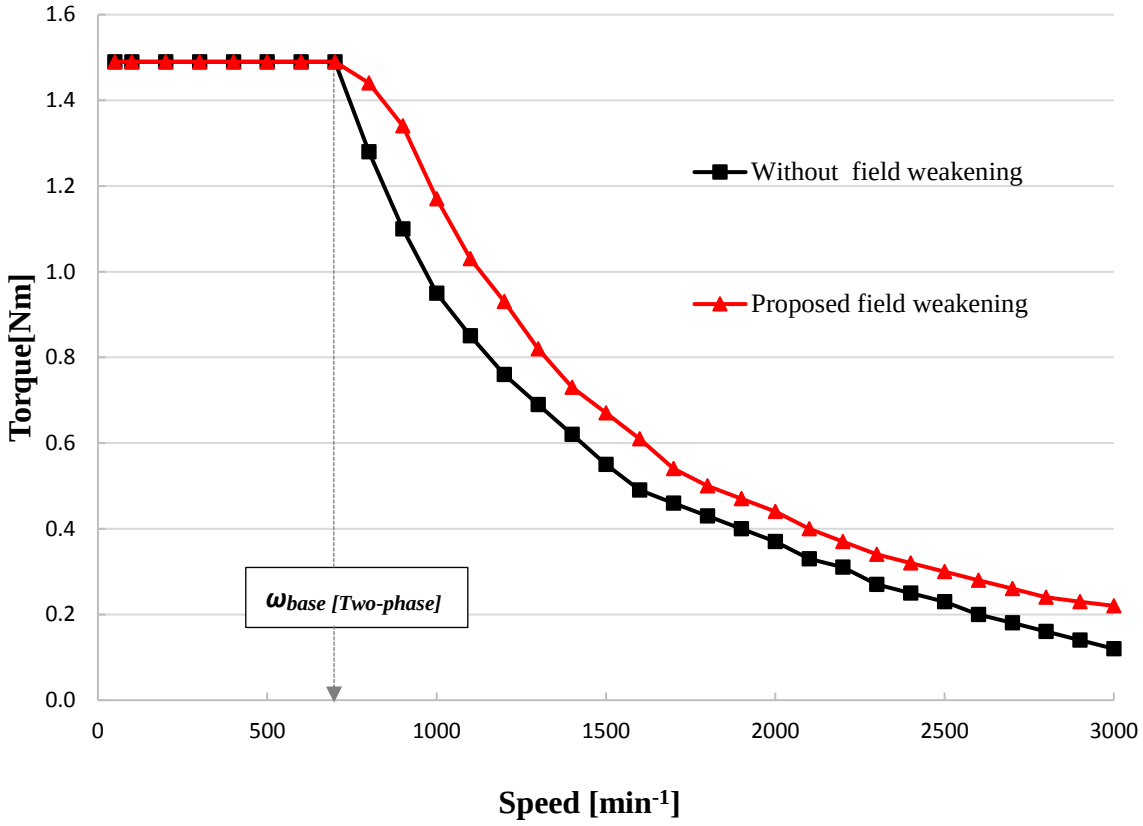

Fig. 4.12 Torque-speed characteristics (simulation)

4.7 Evaluation by experiment

An experiment is carried out to validate the simulation results. The experimental system configuration and inverter parameters are the same as those of Fig. 3.18 and Table 3.3 respectively.

4.7.1 Experimental results

In this section, the experimental results of the torque-speed characteristics and motor efficiency of the entire operating region are evaluated.

4.7.1-1 Torque-speed characteristics (experiment)

In the experiment, the speed reference was set from 50 min^{-1} to 3000 min^{-1} and the maximum torque limit was set at 1.49 Nm (rated torque). The speed was increased by steps of 50 min^{-1}, and the maximum attainable torque at each speed was measured.

The torque-speed characteristics using the proposed field weakening control and control without field weakening are shown in Fig. 4.13. The results show that above the base speed $\omega_{base\ [Two\text{-}phase]}$ (approx. 720 min^{-1}), the maximum attainable torque using the proposed field weakening control is higher compared to the control without field weakening.

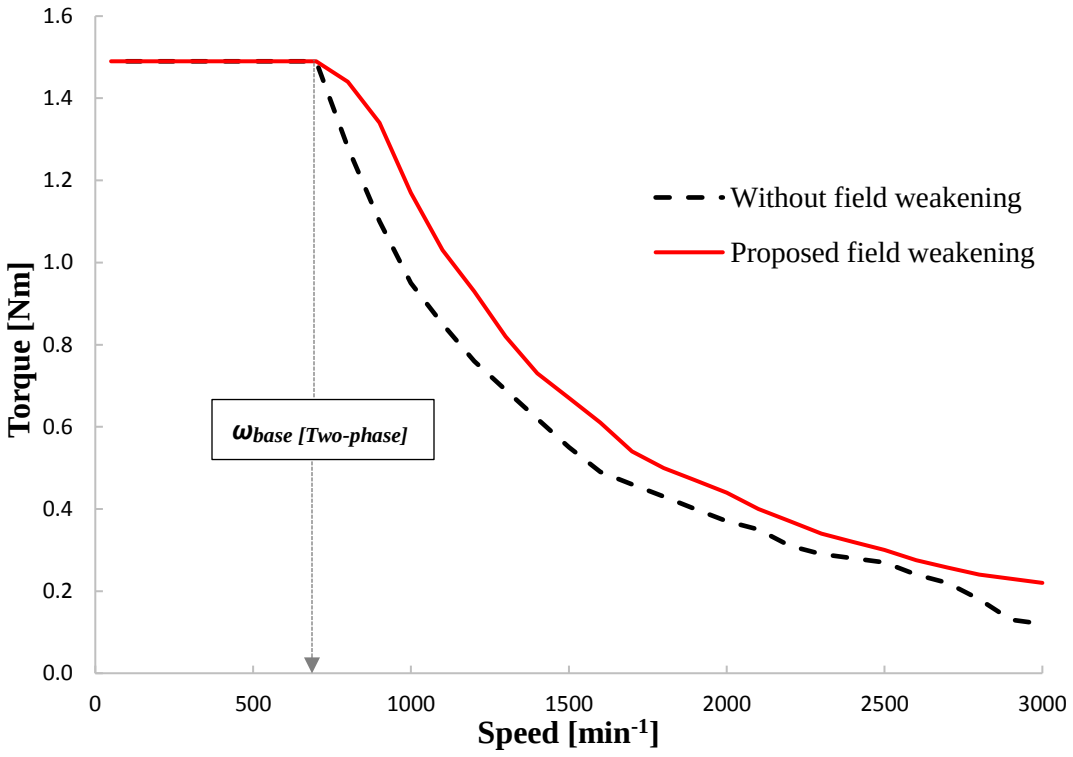

Fig. 4.13 Torque- speed characteristics (experiment)

4.7.1-2 Motor efficiency

The motor efficiency of both the proposed field weakening control and the control without field weakening is examined. The motor efficiency and the output power were calculated by equations (3.5) and (3.6) respectively. The input power is read from a power meter used in the experiment.

In the experiment, the speed range was set from 50 min^{-1} to 3000 min^{-1} and increased in steps of 50 min^{-1}. The maximum torque limit was set at 1.49 Nm, which is the rated torque of the induction motor. In order to increase the data points and enable the accurate evaluation, the torque was increased by steps of 0.1 Nm to the maximum attainable torque of each speed.

The motor efficiency was evaluated using an efficiency map. The results of the proposed field weakening control and the control without field weakening are shown in Figs. 4.14 and 4.15, respectively. The control without field weakening results shows that the maximum efficiency is between 55% and 60% from 650 min^{-1} to 1050 min^{-1}.

It can be seen that the maximum motor efficiency region of the proposed field weakening control is between 60% and 65% from 700 min^{-1} to 3000 min^{-1}. These results show that the proposed field weakening control can achieve a higher efficiency over a wider speed range compared to the control without field weakening.

Furthermore, the motor efficiency maps of both control strategies were plotted in a 3D format to further examine the motor efficiency versus torque and speed. Figure 4.16 shows that the proposed field weakening control can achieve a higher motor efficiency per speed, from low load condition to its maximum attainable torque above base speed.

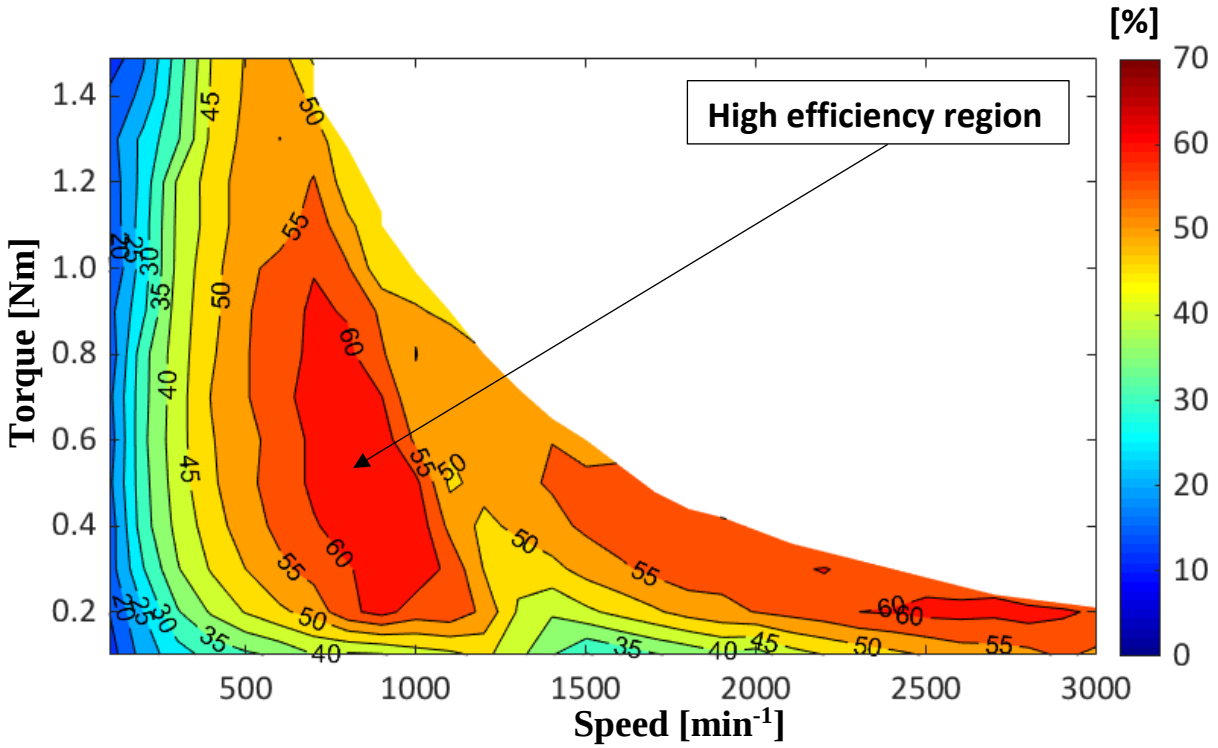

Fig. 4.14 Motor efficiency map (without field weakening control)

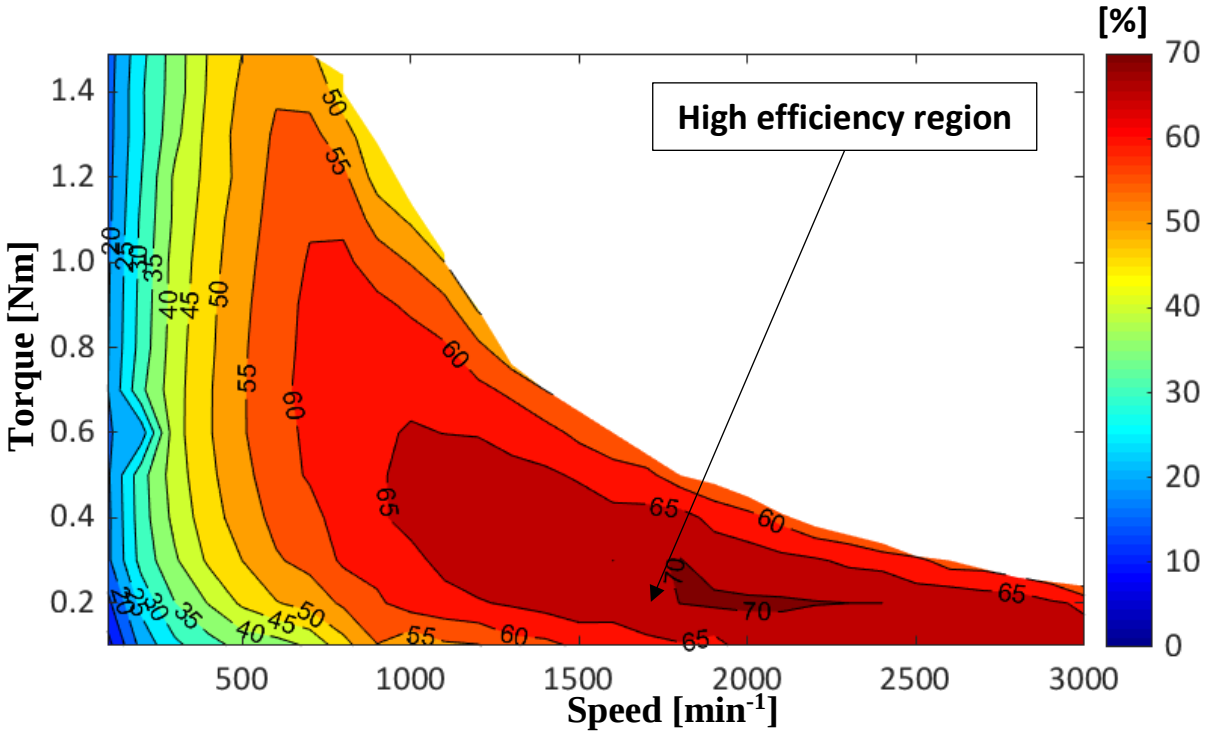

Fig. 4.15 Motor efficiency map (proposed field weakening control)

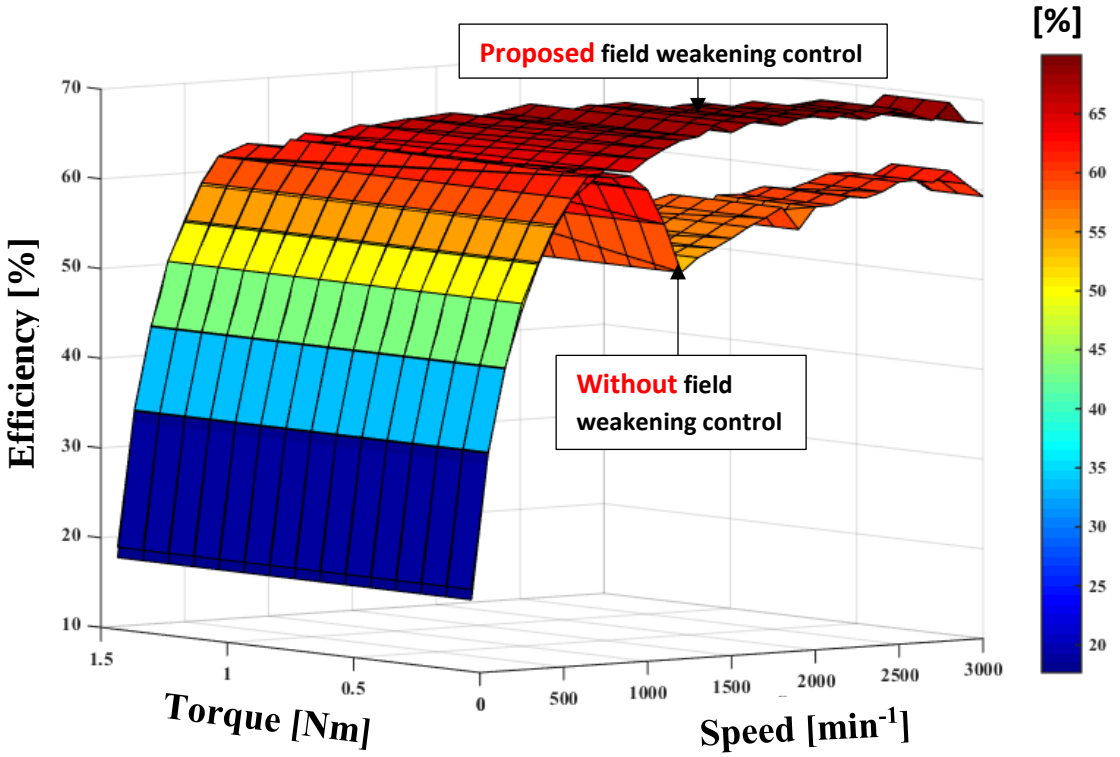

Fig. 4.16 Motor efficiency comparison (3D)

4.8 Conclusion

In this chapter, in order to optimize the performance of the two-phase inverter-fed three-phase induction motor drive, a field weakening control strategy was proposed. In the proposed field weakening control strategy, the d-axis and q-axis current are adequately controlled to enable the drive attain optimal performance in the high-speed region.

The effectiveness of the proposed field weakening control strategy was verified by simulation and validated by the experimental results. The results show that the torque-speed characteristics and motor efficiency are improved in the high-speed region by applying the proposed field weakening control.

The optimization of the motor efficiency in the high-speed region will facilitate the application of vector controlled two-phase inverters as an emergency strategy for three-phase inverter-fed induction motor drives that require high efficiency in the high-speed region. Furthermore, the results in this chapter indicate that field weakening control can also be achieved/applicable in other two-phase inverter-fed AC motor drives.

References

1. D.W. Novotny, T.A. Lipo, Vector control and dynamics of AC Drives, Oxford: pp.413(1996)
2. H. Abu Rub, Iqbal, Atif, Jaroslaw, High Performance Control of AC Drives. Wiley, New York: pp.375-388(2012)
3. S. Sul, Control of Electrical Machine Drive Systems, Wiley, New Jersey: pp.255-267(2011)
4. L. Harnefors, K. Pietilainen, and L. Gertmar: "Torque-maximizing field weakening control: design, analysis, and parameter selection", *IEEE Trans. Ind. Electronics*, Vol.48, No.1, pp.161-168(2001)
5. H. Grotstollen and J. Wiesing: "Torque capability and control of a saturated induction motor over a wide range of flux weakening", *IEEE Trans. Ind. Electronics*, Vol.42, No.4, pp.374-381(1995)
6. G. Gallegos-Lopez, F. Gunawan, and J. Walters: "Current control of induction machines in the field-weakened region", *IEEE Trans. Ind. Appl.*, Vol.43, No.4, pp.981-989(2007)
7. R. Kerkman, T.M. Rowan, and D. Leggate: "Indirect Field-Oriented Control of an Induction Motor in the Field-Weakening Region" *IEEE Trans. Ind. Appl.*, Vol.28, No.4, pp.850-857(1992)
8. F. Briz, A. Diez, M.W. Degner, and R.D. Lorenz: "Current and flux regulation in field-weakening operation", *IEEE Trans., Ind.,Appl.*, Vol.37, No.1, pp.42-50(2001)
9. B.J. Seibel, T. Rowan, and R.J. Kerkman: "Field- Oriented Control of an Induction Machine in the Field-Weakening Region with DC-Link and Load Disturbance Rejection", *IEEE Trans. Ind. Appl.*, Vol.33, No.6, pp.1578-1584(1997)
10. S.K. Sahoo and T. Bhattacharya: "Field Weakening Strategy for a Vector–Controlled Induction Motor Drive Near the Six-Step Mode of Operation", *IEEE Trans. Power Electronics*, Vol.31, No.4, pp.3043-3051(2016)
11. J. Soek and S. Sul: "Optimal flux selection for maximum torque operation of an induction machine in the flux weakening region", *IEEE Power Elec Specialists Conf. (PESC)*, Vol.2, pp.1309-1314(1997)
12. Y. Liu, J. Zhao, R. Wang, and C. Huang: "performance improvement of induction motor current controllers in field-weakening region for electric vehicles", *IEEE Trans. Power Electronics*, Vol.28, No.5, pp.2468-2482(2013)
13. D. Casadei, G. Serra, A. Tani, and L. Zarri: "A robust method for field weakening operation of induction motor drives with maximum torque capability", *IEEE Ind. Appl.Conf, Annual Meeting*, pp.111-117(2006)
14. H. Abu-Rub, H. Schmirgel, and J. Holtz: "Maximum torque production in rotor field oriented control of an induction motor at field weakening", *IEEE Int. Symposium on Ind Electronics*, pp.1159-1164(2007)
15. M. Megone, L. Zarri, A. Tani, G. Serra, and D. Casadei: "Stator flux vector control of induction motor drive in the field weakening region", *IEEE Trans. Power Electronics*, Vol.23, No.2, pp.941-949(2008)
16. 佐藤之彦：「基本を学ぶパワーエレクトロニクス」、オーム社、pp.143(2012)
17. A.M. Trzynadlowski, The field orientation principle in control of induction motors, Kluwer academic publishers: pp.51-52 (1994)
18. 三菱電機株式会社、「インバータ応用マニュアル」pp.79-94 (1985)
19. S.Kim and S. Sul: "Voltage control strategy for maximum torque operation of an induction machine in the field weakening region", *IEEE Trans. Ind. Electronics*, Vol.44, No.4, pp.512-518(1997)
20. F. Yusivar, T. Kihara, M. Sato, S. Wakao, and T. Yamamura: "/Iq/ Added flux weakening strategy for the rotor flux oriented control of a sinusoidal PWM VSI-fed induction motor", *IEEE Ind. Electronics society, Annual conf.*, pp.1160-372(2001)
21. X. Xu and D.W. Novotny: "Selection of the flux reference for induction machine drives in the field weakening region", *IEEE Trans. Ind. Appl.*, Vol.28, No.6, pp.1353-1358(1992)
22. M.H. Shin, D.S. Hyun, and S. Cho: "Maximum torque control of stator-flux oriented induction machine drive in the field-weakening region", *IEEE Trans.Ind. Appl.*, Vol.38, No.1, pp.117-122(2002)
23. S. Kim and S. Sul: "Maximum torque control of an induction machine in the field weakening region", *IEEE Trans.Industry Appl.*, Vol.31, No.4, pp.787-794(1995)
24. A. Bunte, H. Grotstollen, and P. Krafka: "Field weakening of induction motors in a very wide region with regard to parameter uncertainties", *IEEE Power Elec Specialists Conf. (PESC)*, pp.944-950(1996)
25. P. Lin and Y. Lai: "Novel voltage trajectory control for field-weakening operation of induction motor drives", *IEEE Trans. Ind. Appl*., Vol.47, No.1, pp.122-127(2011)

26. M. Megoni, L. Zarri, A. Tani, G. Serra, and D. Casadei: “A comparison of four robust control schemes for field-weakening operation of induction motors”, *IEEE Trans. Power Electronics*, Vol.27, No.1, pp.307-320(2012)
27. U.U. Ekong, M. Inamori, and M. Morimoto: “Field oriented control of two phase inverter to drive a three phase induction motor”, *Int. Conf. on Electrical. Machines and Systems(ICEMS)*, pp.125-128(2015)
28. H.W.V. D Broeck and J.D.V. Wyk: “A comparative investigation of a three-phase induction machine drive with a component minimized voltage-fed inverter under different control options”, *IEEE* Trans. Industry Appl, Vol.IA-20, No.2, pp.309-320(1984)
29. U.U. Ekong, M. Inamori, and M. Morimoto: “Flux weakening control for torque and efficiency optimization of a vector controlled Four Switch Three Phase inverter fed induction motor drive”, *Proc.Int. Conf. on Power and Renewable Energy(ICPRE)*, pp.147-151(2017)
30. U.U. Ekong, M. Inamori, and M. Morimoto: “Instantaneous vector control of four switch three phase inverter fed induction motor drive”, *IEE Japan Trans. Industry Appl*., Vol.6, No.6, pp.429-434(2017)
31. B.J.Charlmers, Electric Motor Handbook, Butterworths: pp.252-254(1988)

Chapter 5

Summary and conclusions

The adoption of inverter-fed induction motor drives in various industries is increasing from home appliances to large industrial equipment. When the inverter failure occurs in industrial motor drive systems like pumps, power generation systems, electric trains and vehicles, the impact on society is enormous. Therefore, there is a need for emergency strategies after the inverter failure occurs in inverter-fed motor drives.

Reported literature and surveys have shown that the semiconductor switches and the leg components of inverters are the weakest links in the drive. This dissertation presents a two-phase inverter as an emergency strategy for switch and leg failure of one-phase of the conventional three-phase inverter-fed AC motor drive.

In this dissertation, vector control was selected as the inverter control method because of its good dynamic performance and its ability to attain precise control of speed and torque. However, in order to effectively implement vector control of two-phase inverter-fed AC motor drives, a few problems have to be resolved as explained in **Chapter 1.**

5.1 Instantaneous vector control of two-phase inverter

In Chapter 1, a review was conducted on the reported literature on the two-phase inverter-fed induction motor drive. This review focused on the challenges, performance and some proposed compensation techniques to improve the characteristics of two-phase inverter-fed motor drives.

Furthermore, vector control of AC drives was introduced by explaining its history, various types, and working principle. The coordinate transformations required to derive the output voltage references for vector control of three-phase inverters were explained in detail. Followed by an explanation of the previous method in literature of deriving the output voltage references for the vector control of two-phase inverters by subtraction from the voltage references V_u^*, V_v^*, and V_w^* of the conventional three-phase inverters. However, this subtraction method has several disadvantages and challenges with instantaneous response characteristics, imbalance three-phase motor currents and implementation of two-phase inverters as an emergency strategy.

In Chapter 2, in order to achieve instantaneous vector control of the two-phase inverters and facilitate easy implementation of the two-phase inverter as an emergency drive, a coordinate transformation method to derive the output voltage references V_A^* and V_B^* was proposed. First, an indirect transformation was created in section.2.4, and finally an instantaneous transformation matrix was proposed in section.2.5. The proposed instantaneous transformation matrix was verified to be power invariant, which gives an absolute transformation suitable for motor control.

In Chapter 3, the effectiveness of the proposed instantaneous transformation matrix to derive the output voltage references V_A^* and V_B^* that have a phase difference of $\pi/3$ was verified by simulation and experiment. The simulation and experimental results show that using the proposed instantaneous transformation matrix the following can be achieved.

(a) Instantaneous derivation of output voltage references V_A^* and V_B^*.
(b) Instantaneous speed control and response.
(c) Better motor current waveforms.
(d) Easy implementation of the two-phase inverter as an emergency strategy.

5.2 Performance evaluation and comparisons

In Chapter 3, in order to evaluate the performance of the vector-controlled two-phase inverter-fed induction motor drive using the proposed instantaneous matrix, the torque-speed characteristics, maximum output voltage and motor efficiency were evaluated from the simulation and experimental results.

For comparison purposes, simulation and experiment were also carried out on the three-phase inverter-fed induction motor drive using the same simulation parameters and experimental apparatus. A comparison of the results shows that the maximum output voltage and maximum (rated) torque attainable speed of the two-phase inverter drive reduces by approximately 50%. Furthermore, from the experiment results, the motor efficiency was calculated and evaluated by plotting motor efficiency maps. The results show that the motor efficiency of both the two-phase and three-phase inverter drives were the same in the low-speed region. However, in the high-speed region, the motor efficiency of the two-phase inverter drive reduced. The results agree with the working principle (theory) of two-phase inverters.

Subsequently, **in Chapter 3**, a comparison between the vector control of two-phase inverter using the proposed transformation matrix in this dissertation and the previous method in literature was performed by experiment. The experimental results show that the proposed method can achieve better torque-speed characteristics, faster response characteristics, and balanced three-phase motor currents.

In addition, a comparison of the experimental results of the two-phase inverter-fed induction motor drives using vector control and the VVVF control was conducted. The results showed that the vector-controlled two-phase inverter drive can produce more torque in the entire operating region.

5.3 Performance optimization of two-phase inverter in high-speed region

In Chapter 4, in order to improve the performance characteristics of the two-phase inverter-fed induction motor drive in the high-speed region, a field weakening control was proposed. The proposed strategy enables precise current control and maintains a linear relationship between torque and slip in the field weakening regions. The proposed strategy was verified by simulation and experiment. The experimental results show that the torque-speed characteristics and motor efficiency improved in the high-speed region. It was clarified that field weakening control could also be applicable in two-phase inverter drives similarly to the conventional three-phase inverter drives.

5.4 Overall conclusion

The explanation in section 5.1 has shown that using the proposed transformation matrix in this dissertation, instantaneous vector control can be achieved in the two-phase inverter drive, similar to the conventional three-phase inverter drive. In section 5.2, performance evaluation and comparisons of the two-phase inverter drive proposed as an emergency strategy and the conventional three-phase inverter drive are discussed. It was observed that the performance characteristics of the two-phase inverter drive such as the torque-speed characteristics and maximum output voltage reduces.

As discussed in Section 5.3, by applying the proposed field weakening strategy, the performance characteristics of the vector controlled two-phase inverter-fed induction motor drive can be optimized in the high-speed region.

In conclusion, the proposed vector control of two-phase inverter-fed induction motor drives in this dissertation is a key technique to achieve the application of the two-phase inverter, which provides an emergency strategy for the conventional three-phase inverter-fed induction motor and other AC motor drives. The progress achieved in this dissertation will facilitate further developments in the practical applications of two-phase inverters.

List of Achievements

Journal Publications

1. **Ufot Ufot Ekong**, Oudam Sok, Mamiko Inamori, Masayuki Morimoto: "Development of a Load Torque Measurement System for Two Phase Inverter Fed Induction Motor Drive with Vector Control Method" ***Proceedings School of Engineering, Tokai University***, Vol.42, pp.9-14, (2017).

2. **Ufot Ufot Ekong**, Mamiko Inamori, Masayuki Morimoto: "Instantaneous Vector Control of Four Switch Three Phase Inverter fed Induction Motor Drive" ***IEEJ Journal of Industry Applications***, Vol.6, No.6, pp.429- 434, (2017).

3. **Ufot Ufot Ekong**, Mamiko Inamori, Masayuki Morimoto: "Field Weakening Control for Torque and Efficiency Optimization of a Four Switch Three Phase Inverter Fed Induction Motor Drive" ***IEEJ Journal of Industry Applications***, Vol.8, No.3, in press (2019).

Proceedings Publication

1. **Ufot Ufot Ekong**, Mamiko Inamori, Masayuki Morimoto: "Flux Weakening Control for Torque and Efficiency Optimization of a Vector Controlled Four Switch Three Phase Inverter Fed Induction Motor Drive" *Proceedings of 2017 2nd International Conference on Power and Renewable Energy (ICPRE),* Vol.1, pp.147-151, *China* (2017).

International Conference Publications

1. **Ufot Ufot Ekong**, Mamiko Inamori, Masayuki Morimoto: "Field Oriented Control of Two Phase Inverter to drive a Three Phase Induction Motor" *IEEE 18th International Conference on Electrical Machines and Systems (ICEMS)* pp.125-128. *Thailan*d (2015).

2. **Ufot Ufot Ekong**, Mamiko Inamori, Masayuki Morimoto: "Instantaneous Vector Control of Four Switch Three Phase Inverter fed Induction motor drive" *IEEE 19th International Conference on Electrical Machines and Systems (ICEMS),* pp. 125-128, *Chiba* (2016).

3. **Ufot Ufot Ekong**, Mamiko Inamori, Masayuki Morimoto: "Flux Weakening Control for Torque and Efficiency Optimization of a Vector Controlled Four Switch Three Phase Inverter Fed Induction Motor Drive" *IEEE 2nd International Conference on Power and Renewable Energy(ICPRE),* Vol.1, Pg.147- 151, *China* (2017).

4. **Ufot Ufot Ekong**, Mamiko Inamori, Masayuki Morimoto: "Improved Torque and Efficiency of a Four Switch Three Phase Inverter fed Induction Motor Drive" *IEEE 12th International Conference on Power Electronics and Drive Systems (PEDS),* pp.919-924, *Hawaii* (2017).

5. Takuya Shiraishi, **Ufot Ufot Ekong**, Mamiko Inamori, Masayuki Morimoto: "Evaluation of Transformation Matrix for Instantaneous Vector Control of Four Switch Three Phase Inverter fed Induction Motor Drive" *IEEE 21st International Conference on Electrical Machines and Systems (ICEMS),* pp.1318-1323, *Korea* (2018).

6. Tomoyuki Nakade, **Ufot Ufot Ekong**, Mamiko Inamori, Masayuki Morimoto: "A Field Weakening Control strategy for Four Switch Three Phase Induction Motor Drive" *IEEE 21st International Conference on Electrical Machines and Systems (ICEMS),* pp.1262-1267, *Korea* (2018).

Domestic Conference Publications

1. **Ufot Ufot Ekong**, Mamiko Inamori, Masayuki Morimoto: "Field Oriented Control of Two Phase Inverter to drive a Three Phase Induction Motor" *IEEJ, Semiconductor Power Conversion Electric Appliances/ Consumer Vehicle Group SPC* – 14- 152, VT- 14-047, pp.43-47, *Kobe* (2014). *(In Japanese)*

2. **Ufot Ufot Ekong**, Mamiko Inamori, Masayuki Morimoto: "Field Oriented Control of Two Phase Inverter to drive a Three Phase Induction Motor" *IEE Japan Industry Applications Division Annual Convention* Y-132, *Ooita* (2015). *(In Japanese)*

3. **Ufot Ufot Ekong**, Mamiko Inamori, Masayuki Morimoto: "Instantaneous Field Oriented Control of Two Phase Inverter fed Induction Motor Drive" *IEE Japan Industry Applications Division Annual Convention*, Vol.3, pp.121- 124, *Gunma* (2016). *(In Japanese)*

4. **Ufot Ufot Ekong**, Takuya Shiraishi, Mamiko Inamori, Masayuki Morimoto: "Derivation of Transformation Matrix for 3 phase vector control of a 2 phase Inverter" *IEE Japan (IEEJ) National Annual Convention*, Vol.4, pp. 46-47, *Toyama* (2017). *(In Japanese)*

5. Takuya Shiraishi, **Ufot Ufot Ekong**, Mamiko Inamori, Masayuki Morimoto: "Instantaneous Co-ordinate Transformation of a vector controlled 2 Phase Inverter fed 3 Phase Induction Motor Drive" *IEEJ Industry Applications Division Annual Conference* Y-106, *Hakodate* (2017). *(In Japanese)*

6. Tomoyuki Nakade, **Ufot Ufot Ekong**, Mamiko Inamori, Masayuki Morimoto: "Flux-Weakening Control of a Vector Controlled Two Phase Inverter" *IEEJ Industry Applications Division Annual Conference,* Vol.3, pp. 373 -376, *Hakodate* (2017). *(In Japanese)*

7. Oudam Sok, **Ufot Ufot Ekong**, Mamiko Inamori, Masayuki Morimoto: "Evaluation of Motor Efficiency of a vector controlled 2 Phase Inverter fed 3 Phase Induction Motor Drive" *IEEJ Industry Applications Division Annual Conference,* Vol.3, pp.369 -372, *Hakodate* (2017).

8. Takuya Shiraishi, **Ufot Ufot Ekong**, Mamiko Inamori, Masayuki Morimoto: "Characteristics of an Instantaneous Vector Controlled Two Phase Inverter" *IEE Japan Industry Applications Division Annual Conference*, Vol.3, pp. 269 -272, *Yokohama* (2018). *(In Japanese)*

9. Tomoyuki Nakade, **Ufot Ufot Ekong**, Mamiko Inamori, Masayuki Morimoto: "A Field Weakening control method for a Four Switch Three Phase Inverter fed Induction Motor Drive" *IEE Japan Industry Applications Division Annual Conference*, Vol.3, pp. 273 -276, *Yokohama (In Japanese)*

10. **Ufot Ufot Ekong**, Mamiko Inamori, Masayuki Morimoto: "Introduction of a 3 Phase Induction Motor Drive driven by a Vector Controlled 2 Phase Inverter" *IEE Japan Industry Applications Division Annual Conference*, Vol.2, pp. 5, *Yokohama* (2018). *(In Japanese)*

Awards

1. **Best Presentation Award**
   "Flux Weakening Control for Torque and Efficiency Optimization of a Vector Controlled Four Switch Three Phase Inverter Fed Induction Motor Drive" (ICPRE 2017)

Appendix

A. Derivation of phase voltage

Here, the derivation of the phase voltage of the three-phase load fed by a two-phase supply is explained.

The basic reason why a two phase power supply that has a phase difference of $\pi/3$ can drive a three phase motor can be explained using Kirchhoff's voltage law.

From the diagram above;

$$\begin{aligned} &-V_A + V_{un} - V_{wn} = 0 \\ &V_{un} = V_A + V_{vn} \end{aligned} \tag{A.1}$$

$$\begin{aligned} &-V_B + V_{wn} - V_{vn} = 0 \\ &V_{wn} = V_B + V_{vn} \end{aligned} \tag{A.2}$$

In a three phase motor, the currents can be expressed as shown below;

$$I_u + I_v + I_w = 0 \tag{A.3}$$

From Ohms law this can be rewritten as shown below;

$$\begin{aligned} &\frac{V_{un}}{R_u} + \frac{V_{vn}}{R_v} + \frac{V_{wn}}{R_w} = 0 \\ &V_{un} + V_{vn} + V_{wn} = 0 \\ &V_{vn} = -(V_{un} + V_{wn}) \end{aligned} \tag{A.4}$$

The phase voltage can be expressed as shown below;

$$\begin{aligned} &V_{un} = V_A + V_{vn} \\ &V_{wn} = V_B + V_{vn} \\ &V_{vn} = -(V_{un} + V_{wn}) \end{aligned} \tag{A.5}$$

By substituting V_{un}, V_{vn} ,V_{wn} in the various phase voltage equations, an expansion of the equation can also be expressed as shown below ;

$$V_{un} = V_A + V_{vn}$$
$$V_{un} = V_A - \left(\frac{V_A + V_B}{3}\right) = \frac{2V_A - V_B}{3} \quad \text{(A.6)}$$

$$V_{wn} = V_B + V_{vn}$$
$$V_{wn} = V_B - \left(\frac{V_A + V_B}{3}\right) = \frac{2V_B - V_A}{3} \quad \text{(A.7)}$$

$$V_{vn} = -(V_{un} + V_{wn})$$
$$V_{vn} = -(V_A + V_{vn} + V_B + V_{vn}) = \frac{-(V_A + V_B)}{3} \quad \text{(A.8)}$$

The phase voltage can be expressed as shown below

$$V_{un} = \frac{2V_A - V_B}{3}$$
$$V_{vn} = \frac{-(V_A + V_B)}{3} \quad \text{(A.9)}$$
$$V_{wn} = \frac{2V_B - V_A}{3}$$

By inserting the power supply V_A and V_B equations shown below in the phase voltage equations above, the phase voltage (V_{un}, V_{vn} ,V_{wn}) can be derived by expansion.

$$V_A = V \cdot \sin \omega t$$
$$V_B = V \cdot \sin\left(\omega t + \frac{\pi}{3}\right) \quad \text{(A.10)}$$

$$
\begin{aligned}
V_{un} &= \frac{2V_A - V_B}{3} \\
&= \frac{2V\cos\omega t - V\cos\left(\omega t + \frac{\pi}{3}\right)}{3} \\
&= \frac{V}{3}\cdot\left\{2\cos\omega t - \cos\left(\omega t + \frac{\pi}{3}\right)\right\} \\
&= \frac{V}{3}\cdot\left\{2\cos\omega t - \cos\omega t\cos\frac{\pi}{3} + \sin\omega t\sin\frac{\pi}{3}\right\} \\
&= \frac{V}{3}\cdot\left\{2\cos\omega t - \frac{1}{2}\cos\omega t + \frac{\sqrt{3}}{2}\sin\omega t\right\} \\
&= \frac{V}{3}\cdot\left\{\frac{3}{2}\cos\omega t + \frac{\sqrt{3}}{2}\sin\omega t\right\} \\
&= \frac{V}{3}\cdot\sqrt{3}\cdot\left\{\frac{\sqrt{3}}{2}\cos\omega t + \frac{1}{2}\sin\omega t\right\} \\
&= \frac{1}{\sqrt{3}}V\cdot\left\{\cos\omega t\cos\frac{\pi}{6} + \sin\omega t\sin\frac{\pi}{6}\right\} \\
&= \frac{1}{\sqrt{3}}V\cos\left(\omega t - \frac{\pi}{6}\right)
\end{aligned}
\qquad \text{(A.11)}
$$

$$
\begin{aligned}
V_{wn} &= \frac{2V_B - V_A}{3} \\
&= \frac{2V\cos\left(\omega t + \frac{\pi}{3}\right) - V\cos\omega t}{3} \\
&= \frac{V}{3}\cdot\left\{2\cos\left(\omega t + \frac{\pi}{3}\right) - \cos\omega t\right\} \\
&= \frac{V}{3}\cdot\left\{2\cdot\cos\omega t\cos\frac{\pi}{3} + 2\cdot\sin\omega t\sin\frac{\pi}{3} - \cos\omega t\right\} \\
&= \frac{V}{3}\cdot\left\{2\cdot\frac{1}{2}\cos\omega t + 2\cdot\frac{\sqrt{3}}{2}\sin\omega t - \cos\omega t\right\} \\
&= \frac{V}{3}\cdot\left\{\cos\omega t + \sqrt{3}\sin\omega t - \cos\omega t\right\} \\
&= \frac{V}{3}\cdot\sqrt{3}\sin\omega t \\
&= \frac{1}{\sqrt{3}}V\sin\omega t \\
&= \frac{1}{\sqrt{3}}V\cos\left(\omega t + \frac{\pi}{2}\right)
\end{aligned}
\qquad \text{(A.12)}
$$

$$
\begin{aligned}
V_{vn} &= \frac{-(V_A + V_B)}{3} \\
&= \frac{-\left\{V\cos\omega t + V\cos\left(\omega t + \frac{\pi}{3}\right)\right\}}{3} \\
&= \frac{V}{3}\cdot\left\{-\cos\omega t - \cos\left(\omega t + \frac{\pi}{3}\right)\right\} \\
&= \frac{V}{3}\cdot\left\{-\cos\omega t - \cos\omega t\cos\frac{\pi}{3} + \sin\omega t\sin\frac{\pi}{3}\right\} \\
&= \frac{V}{3}\cdot\left\{2\cos\omega t - \frac{1}{2}\cos\omega t + \frac{\sqrt{3}}{2}\sin\omega t\right\} \\
&= \frac{V}{3}\cdot\left\{-\frac{3}{2}\cos\omega t + \frac{\sqrt{3}}{2}\sin\omega t\right\} \\
&= \frac{V}{3}\cdot\sqrt{3}\cdot\left\{-\frac{\sqrt{3}}{2}\cos\omega t + \frac{1}{2}\sin\omega t\right\} \\
&= \frac{1}{\sqrt{3}}V\cdot\left\{\cos\omega t\cos\frac{5\pi}{6} + \sin\omega t\sin\frac{5\pi}{6}\right\} \\
&= \frac{1}{\sqrt{3}}V\cos\left(\omega t - \frac{5\pi}{6}\right)
\end{aligned}
\qquad \text{(A.13)}
$$

From the expansions the phase voltage can be expressed as

$$
\begin{aligned}
V_{un} &= \frac{1}{\sqrt{3}}V\cos\left(\omega t - \frac{\pi}{6}\right) \\
V_{vn} &= \frac{1}{\sqrt{3}}V\cos\left(\omega t - \frac{5\pi}{6}\right) \\
V_{wn} &= \frac{1}{\sqrt{3}}V\cos\left(\omega t + \frac{\pi}{2}\right)
\end{aligned}
\qquad \text{(A.14)}
$$

B. Derivation of line voltage

Here, the derivation of the line voltage of the three-phase load fed by a two-phase supply is explained.

$$
\begin{aligned}
V_{uv} &= V_{un} - V_{vn} \\
V_{vw} &= V_{vn} - V_{wn} \\
V_{wu} &= V_{wn} - V_{un}
\end{aligned}
\tag{B.1}
$$

$$
\begin{aligned}
V_{uv} &= V_{un} - V_{vn} \\
&= \frac{1}{\sqrt{3}} V \cos\left(\omega t - \frac{\pi}{6}\right) - \frac{1}{\sqrt{3}} V \cos\left(\omega t - \frac{5\pi}{6}\right) \\
&= \frac{1}{\sqrt{3}} V \cdot \left\{\cos\left(\omega t - \frac{\pi}{6}\right) - \cos\left(\omega t - \frac{5\pi}{6}\right)\right\} \\
&= \frac{1}{\sqrt{3}} V \cdot \left(\cos\omega t \cos\frac{\pi}{6} + \sin\omega t \sin\frac{\pi}{6} - \cos\omega t \cos\frac{5\pi}{6} - \sin\omega t \sin\frac{5\pi}{6}\right) \\
&= \frac{1}{\sqrt{3}} V \cdot \left(\frac{\sqrt{3}}{2}\cos\omega t + \frac{1}{2}\sin\omega t + \frac{\sqrt{3}}{2}\cos\omega t - \frac{1}{2}\sin\omega t\right) \\
&= \frac{1}{\sqrt{3}} V \cdot \sqrt{3}\cos\omega t \\
&= V\cos\omega t
\end{aligned}
\tag{B.2}
$$

$$
\begin{aligned}
V_{vw} &= V_{vn} - V_{wn} \\
&= \frac{1}{\sqrt{3}} V \cos\left(\omega t - \frac{5\pi}{6}\right) - \frac{1}{\sqrt{3}} V \cos\left(\omega t + \frac{\pi}{2}\right) \\
&= \frac{1}{\sqrt{3}} V \cdot \left\{\cos\left(\omega t - \frac{5\pi}{6}\right) - \cos\left(\omega t + \frac{\pi}{2}\right)\right\} \\
&= \frac{1}{\sqrt{3}} V \cdot \left(\cos\omega t \cos\frac{5\pi}{6} + \sin\omega t \sin\frac{5\pi}{6} - \cos\omega t \cos\frac{\pi}{2} + \sin\omega t \sin\frac{\pi}{2}\right) \\
&= \frac{1}{\sqrt{3}} V \cdot \left(-\frac{\sqrt{3}}{2}\cos\omega t + \frac{1}{2}\sin\omega t + 0 \cdot \cos\omega t + 1 \cdot \sin\omega t\right) \\
&= \frac{1}{\sqrt{3}} V \cdot \left(-\frac{\sqrt{3}}{2}\cos\omega t + \frac{1}{2}\sin\omega t + \sin\omega t\right) \\
&= \frac{1}{\sqrt{3}} V \cdot \left(-\frac{\sqrt{3}}{2}\cos\omega t + \frac{3}{2}\sin\omega t\right) \\
&= \frac{1}{\sqrt{3}} V \cdot \sqrt{3} \cdot \left(-\frac{1}{2}\cos\omega t + \frac{\sqrt{3}}{2}\sin\omega t\right) \\
&= V \cdot \left(\cos\omega t \cos\frac{2\pi}{3} + \sin\omega t \sin\frac{2\pi}{3}\right) \\
&= V\cos\left(\omega t - \frac{2\pi}{3}\right)
\end{aligned}
\tag{B.3}
$$

$$
\begin{aligned}
V_{wu} &= V_{wn} - V_{un} \\
&= \frac{1}{\sqrt{3}} V \cos\left(\omega t + \frac{\pi}{2}\right) - \frac{1}{\sqrt{3}} V \cos\left(\omega t - \frac{\pi}{6}\right) \\
&= \frac{1}{\sqrt{3}} V \cdot \left\{ \cos\left(\omega t + \frac{\pi}{2}\right) - \cos\left(\omega t - \frac{\pi}{6}\right) \right\} \\
&= \frac{1}{\sqrt{3}} V \cdot \left(\cos\omega t \cos\frac{\pi}{2} - \sin\omega t \sin\frac{\pi}{2} - \cos\omega t \cos\frac{\pi}{6} - \sin\omega t \sin\frac{\pi}{6} \right) \\
&= \frac{1}{\sqrt{3}} V \cdot \left(0 \cdot \cos\omega t - 1 \cdot \sin\omega t - \frac{\sqrt{3}}{2} \cos\omega t - \frac{1}{2} \sin\omega t \right) \\
&= \frac{1}{\sqrt{3}} V \cdot \left(-\sin\omega t - \frac{\sqrt{3}}{2} \cos\omega t - \frac{1}{2} \sin\omega t \right) \\
&= \frac{1}{\sqrt{3}} V \cdot \left(-\frac{\sqrt{3}}{2} \cos\omega t - \frac{3}{2} \sin\omega t \right) \\
&= \frac{1}{\sqrt{3}} V \cdot \sqrt{3} \cdot \left(-\frac{1}{2} \cos\omega t - \frac{\sqrt{3}}{2} \sin\omega t \right) \\
&= V \cdot \left(\cos\omega t \cos\frac{4\pi}{3} + \sin\omega t \sin\frac{4\pi}{3} \right) \\
&= V \cos\left(\omega t - \frac{4\pi}{3}\right)
\end{aligned}
\tag{B.4}
$$

$$
\begin{aligned}
V_{uv} &= V \cos\omega t \\
V_{vw} &= V \cos\left(\omega t - \frac{2\pi}{3}\right) \\
V_{wu} &= V \cos\left(\omega t - \frac{4\pi}{3}\right)
\end{aligned}
\tag{B.5}
$$

C. Verification of power invariance of the indirect transformation (*dq→αβ→AB*)

Here, the power invariance of the indirect transformation (*dq→αβ→AB*) created in section 2.4 is verified. The indirect transformation consist of the inverse park transformation and the created *αβ→AB* transformation. Inverese Park is widely used and known to be power invariant. Therefore, the power invariance of only the created *αβ→AB* transformation is verified.

In order to verify the power invariance of the indirect transformation matrix, the relationship in equation (2.14) must be satisfied. Therefore, if the created transformation matrix is denoted as $[C_{\alpha\beta\text{-}AB}]$, the inverse matrix $[C_{\alpha\beta\text{-}AB}]^{-1}$ and the transposed matrix $[C_{\alpha\beta\text{-}AB}]^{t}$ must be the same.

In order to calculate the inverse matrix, the transformation matrix must be a three-row and three-column matrix. Therefore, zero-phase-sequence component voltage V_0 is added to the transformation matrix in equation (2.3) as shown in equation (C.1).

$$\begin{bmatrix} V_A^* \\ V_B^* \\ V_0 \end{bmatrix} = \sqrt{\frac{2}{3}} \begin{bmatrix} 1 & 0 & \frac{1}{\sqrt{2}} \\ \frac{1}{2} & -\frac{\sqrt{3}}{2} & -\frac{1}{\sqrt{2}} \\ \frac{1}{2} & \frac{\sqrt{3}}{2} & -\frac{1}{\sqrt{2}} \end{bmatrix} \begin{bmatrix} V_\alpha^* \\ V_\beta^* \\ V_0 \end{bmatrix} \tag{C.1}$$

The transformation matrix is denoted as $[C_{\alpha\beta\text{-}AB}]$ as shown in equation (C.2).

$$\left[C_{\alpha\beta\text{–AB}}\right] = \sqrt{\frac{2}{3}} \begin{bmatrix} 1 & 0 & \frac{1}{\sqrt{2}} \\ \frac{1}{2} & -\frac{\sqrt{3}}{2} & -\frac{1}{\sqrt{2}} \\ \frac{1}{2} & \frac{\sqrt{3}}{2} & -\frac{1}{\sqrt{2}} \end{bmatrix} \tag{C.2}$$

The inverse matrix $[C_{\alpha\beta\text{-}AB}]^{-1}$ is calculated as shown in equation (C.3).

$$\left[C_{\alpha\beta\text{–AB}}\right]^{-1} = \sqrt{\frac{2}{3}} \begin{bmatrix} 1 & \frac{1}{2} & \frac{1}{2} \\ 0 & -\frac{\sqrt{3}}{2} & \frac{\sqrt{3}}{2} \\ \frac{1}{\sqrt{2}} & -\frac{1}{\sqrt{2}} & -\frac{1}{\sqrt{2}} \end{bmatrix} \tag{C.3}$$

The transposed matrix $[C_{\alpha\beta\text{-}AB}]^{t}$ is given by equation (C.4).

$$\left[C_{\alpha\beta-AB}\right]^t = \sqrt{\frac{2}{3}}\begin{bmatrix} 1 & \frac{1}{2} & \frac{1}{2} \\ 0 & -\frac{\sqrt{3}}{2} & \frac{\sqrt{3}}{2} \\ \frac{1}{\sqrt{2}} & -\frac{1}{\sqrt{2}} & -\frac{1}{\sqrt{2}} \end{bmatrix} \tag{C.4}$$

From equations (C.3) and (C.4), the transformation matrix satisfies the condition for power invariance in equation (2.14). Therefore, the indirect transformation is an absolute transformation.